Aus dem Institut für Laboratoriumsmedizin der
Ludwig-Maximilians-Universität München
Vorstand: Prof. Dr. med. D. Teupser

# Role of extracellular vesicles, microvascular fibrin formation and immune surveillance in pancreatic cancer metastasis

Dissertation
zum Erwerb des Doktorgrades der Humanbiologie
an der Medizinischen Fakultät der
Ludwig-Maximilians-Universität zu München

**Urjita Joshi**
from
Pune, India.

2018

Mit Genehmigung der Medizinischen Fakultät

der Universität München

| | |
|---|---|
| Berichterstatter: | Prof. Dr. Bernd Engelmann |
| Mitberichterstatter: | Priv. –Doz. Dr. med. Susanna Müller |
| | Priv. –Doz. Dr. Simon T Schäfer, MHBF |
| Mitbetreuung durch den promovierten Mitarbeiter: | |
| Dekan: | Prof. Dr. med. dent. Reinhard Hickel |
| Tag der mündlichen Prüfung: | 05.07.2018 |

**Abbreviations**

| | |
|---|---|
| Antibody binding cassettes | ABCs |
| Auxin response factors | ARF |
| American type cell culture | ATCC |
| Adenosine triphosphate | ATP |
| Bone marrow derived dendritic cells | BMDCs |
| 8-chloromethyl-4,4-difluoro-1,3,5,7-tetramethyl-4-bora- 3a,4a-diaza-s-indacene | BODIPY |
| Bovine serum albumin | BSA |
| 4-chloromethyl-benzoyl-amino-tetra methyl-rhodamine | CMTMR |
| 4(or 5)(4-(chloromethyl)benzamido)-2-(1,2,2,4,8,10,10,11-octamethyl-1,2,10,11-tetrahydropyrano[3,2-g:5,6-g']diquinolin-13-ium-6-yl)benzoate | CMTPX |
| Circulating tumour cells | CTCs |
| 4',6-diamidino-2-phenylindole | DAPI |
| diaphanous-related formin 3 | DIAPH3 |
| Dulbecco's modified eagle's medium | DMEM |
| Deoxyribonucleic acid | DNA |
| Deoxynucleotide triphosphate | dNTP |
| Deoxyuridine triphosphate | dUTP |
| Deep vein thrombosis | DVT |
| Ethylene-diamine-tetra-acetic acid | EDTA |
| Epithelial growth factor receptor | EGFR |
| Epithelial mesenchymal transition | EMT |
| Extracellular vesicles | EV |
| Fetal bovine serum | FBS |
| Glutaraldehyde | GAD |
| Guanosine diphosphate | GDP |
| Green fluorescent protein | GFP |
| Guanosine triphosphate | GTP |
| Immunoglobulin-G | IgG |
| Infrared | IR |
| Large oncosomes | LO |
| Lox-Stop-Lox | LSL |
| Metastasis associated macrophages | MAMs |

| | |
|---|---|
| Myeloid derived stem cells | MDSCs |
| Minimal essential medium | MEM |
| Microvesicles | MVs |
| Natural killer | NK |
| Pancreatic intraepithelial neoplasia | PanIN |
| Phosphate buffer saline | PBS |
| Polymerase chain reaction | PCR |
| Pancreatic ductal adenocarcinoma | PDAC |
| Phosphatidylethanolamine | PE |
| Paraformaldehyde | PFA |
| Phosphatidylserine | PS |
| Ribonucleic acid | RNA |
| Roswell Park Memorial Institute | RPMI |
| Room Temperature | RT |
| Reverse transcriptase- polymerase chain reaction | RT-PCR |
| Scanning electron microscopy | SEM |
| Tumour associated macrophages | TAMs |
| Thromboelastography | TEG |
| Tissue factor | TF |
| Tumour growth factor | TGF |
| Tumour microvesicles | TMVs |
| Tissue necrosis factor | TNF |
| Terminal deoxynucleotidyl transferase dUTP nick end labelling | TUNEL |
| Vesicle associated membrane protein | VAMP |
| Vascular endothelial growth factor | VEGF |
| Vascular endothelial growth factor receptor | VGFR |
| White blood cells | WBCs |
| Wild type | WT |

# Index

# 1. Introduction

## 1.1. Pancreatic Carcinoma

Pancreatic cancer is currently the 5th leading cause of death due to cancer with a 5 year survival rate of <5%[1]. The underlying causes of this disease are still obscure. Due to its poor prognosis pancreatic cancer is expected to become the 2nd largest cause of deaths due to cancer in the future[2,3]. Given the lack of disease specific markers and of sensitive screening methods, detection of pancreatic cancer in early stages is difficult[4]. Usually the disease is detected clinically only when distant metastasis has already occurred. Pancreatic cancer metastasises most commonly in the liver (76-94%), peritoneum (41-56%) and the lung[5,6,7,8]. The current treatment regimens for pancreatic cancer include surgical techniques such as curative surgeries (distal pancreatectomy, total pancreatectomy and pancreaticoduodenectomy also known as Whipple method) and palliative surgery (blocking of the common bile duct) as well as chemotherapeutics including gemcitabine, FOLFIRINOX, a combination of gemcitabine and nab-paclitaxel and radiation therapies[9,10]. There are essentially two major types of pancreatic cancer, the endocrine type which accounts for less than 5% of tumours detected in pancreatic cancer patients and the exocrine type constituting 95% of the tumours are[11]. Exocrine pancreatic cancer can be further classified as adenocarcinomas (accounting for 90% of pancreatic cancers), acinar cell carcinoma (rarely occurring), Intraductal Papillary-Mucinous Neoplasm (IPMN; cystic tumour) and Mucinous Cystadenocarcinoma (rarely occurring malignant cystic tumour)[12,13].

### 1.1.1. Pancreatic ductal adenocarcinoma (PDAC)

PDAC is the most frequently occurring form of pancreatic cancer, which is known to be a highly aggressive form of exocrine cancer and is usually accompanied by distant metastasis[14]. These carcinomas are often diagnosed in the advanced stages and show resistance to treatments due to which the median survival period is approximately 4 months at the time of diagnosis[12,15]. PDAC usually progresses with increasing stages of dysplasia and nuclear atypia presented as a series of pancreatic intraepithelial neoplasia (PanINs)[16]. The different stages of PDAC are indicated in Fig. 1a, and are as follows 1) PanIN-1A characterised with flat epithelial lesions made up of tall columnar cells with basal nucleus; 2) PanIN-1B are similar to typa1A except

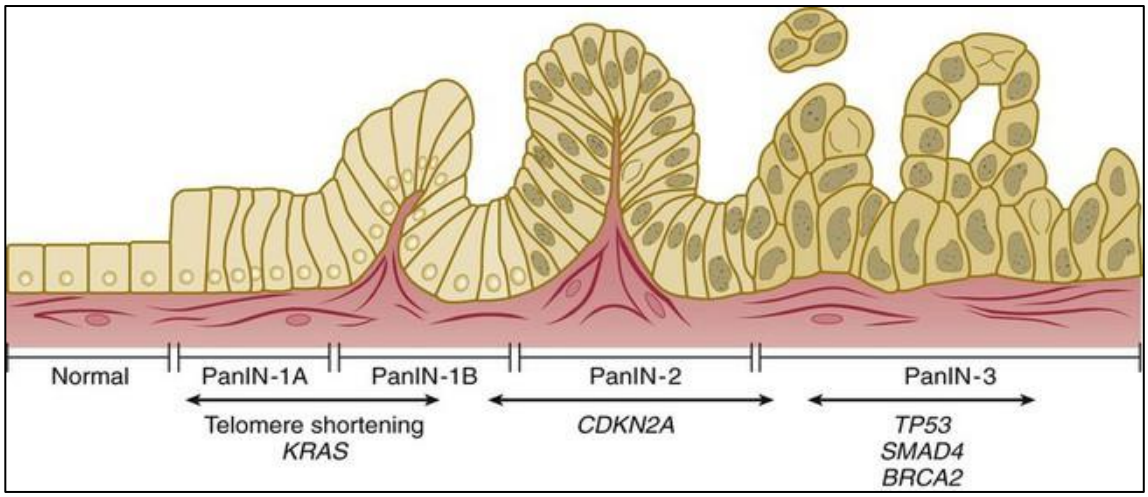


Figure 1: A schematic representation of the progression of PDAC. Genetic mutations triggered with respect to the stages of progression. Adapted from[17].

that they show some papillary or micropapillary architecture of the ducts; 3) PanIN-2 show mucinous epithelial lesions with cells showing nuclear abnormalities; 4) PanIN-3 have papillary lesions with small clusters of epithelial cells budding off in lumen (cribriforming) along with luminal necrosis, nuclear irregularities and faulty mitosis (Fig. 1a)[6,18]. Moreover, the disease shows reproducible genetic mutations which are characteristic of each stage of progression of the disease (Fig. 1)[19]. Genetically engineered mouse models have helped to establish that mutations which lead to constitutively active *KRAS* are the earliest to occur in most cases of PDACs i.e. the first two stages. Further progression of the disease is accompanied by sequential inactivation of various tumour suppressor genes (TSGs) (Fig. 1)[16]. In case of tumorigenesis, the TSGs CDKN2A, TP53 and SMAD4/DPC4 are functionally inactivated[20]. CDKN2A encodes the p16/INK4A protein (cyclin-dependent kinase inhibitor) which is the earliest and most frequently suppressed gene (95% cases of PDACs tumours)[18]. In cells, activation of the *KRAS* oncogene triggers a p16-induced senescence. As a result of which, during early stages of PDACs, CDKN2A suppression is observed as an immediate consequence of *KRAS* activation further inhibiting the senescence response[21,17]. Another important gene, the TP53 gene which encodes for the tumor-suppressor protein p53 is frequently found to display missense mutation leading to inactivation of p53. It is generally observed in advanced PanINs following the inactivation of CDKN2A. As a result of the dysfunctional mutant p53, the expression of downstream genes that promote apoptosis (*CDKN1A/p21, BAX, NOXA and PUMA*) is hindered. Similar to *TP53,* the suppression of *SMAD4* also occurs during advanced stages of PDAC. Some other sporadic mutations in *LKB1, SHH* and *BRACA1/2* genes also have been reported[13].

## 1.2. Immune education

The progression of PDAC is accompanied by the formation of desmoplasia, a significant event convoyed by infiltration of various immune cell populations that are a part of the host immune response[22]. Such immune responses consist of a mixed population of cells that can be both tumour-suppressive as well as tumour-promoting[23]. The concept of immune editing proposes that since the immune system is naturally programmed to recognise and eliminate cancer as a result of which the tumour cells are stressed[24]. Therefore, in order to proliferate and survive, the cancer cells attempt to resist, avoid, or suppress this antitumor immune response, leading to immune-escape and tumour-promotion[25]. The process of immune editing consists of three phases (i) elimination, (ii) equilibrium and (iii) escape (Fig. 2).

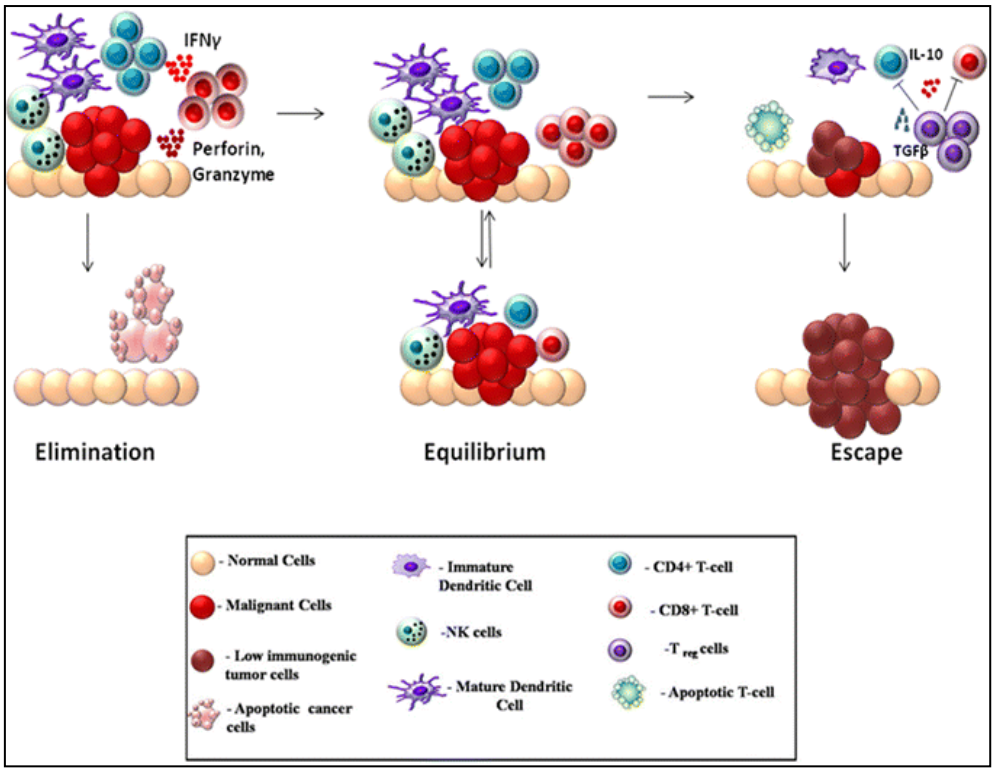


Figure 2: Three stages of immune editing. I) Elimination: cytotoxic immune cells such as CD8+T, CD4+ T cells as well as NK cells along with other immune cells elicit a strong response resulting in tumour cell apoptosis and elimination of the cancer. Ii) Equilibrium: the tumour cells begin to surpass the immune response, but the growth of the cancer remains limited. Escape: Tumour cells escape the immune surveillance and start to disseminate from primary sites progressing towards the development of metastasis. Adapted from[26].

During the first phase, the transformed cells and neoplasia are almost completely and selectively destroyed. This destruction is mainly mediated by cytotoxic T-cells and natural killer cells that are majorly responsible for eliminating cancer cells. In addition, CD8+T cells and NK cells also have the potential to restrict the metastatic growth of cancer cells[27]. The second phase of equilibrium occurs in the case of inefficient elimination of the neoplasia which is mainly due to acquired mutations by the tumour cells that render them resistant to the killing. The tumour cells

and the immune system therefore are in a dynamic equilibrium which keeps the tumour expansion under check further limiting its growth. As a consequence of this selective pressure on the tumour growth some clones might emerge which are completely resistant to the host immune response. These cells exhibit various mechanisms to surpass immune recognition, including various tumour derived factors in its microenvironment, which is seen in most cases of PDACs[28,29]. Therefore, the third phase is where the immune cells are said to escape and survive in distant areas. However, the tumour not only evades the immune surveillance but also engages the immune cells for the development of pre-metastatic niche followed by distant fully blown metastasis. To achieve this the tumour cells engage several processes such as promotion of immunosuppressive cells, induction of T cell apoptosis or hinder immune cell maturation[30].

### 1.3. Pre-metastatic niche formation

The concept of pre-metastatic niche was established in 1889 by Stephan Paget, which concluded that metastasis was not a random event but rather a very selective process where specific tumour cells, "the seed", grow preferentially in a specific microenvironment of certain organs, "the soil". Primary tumour cells can support the initiation of pre-metastatic niche formation at distant sites by secreting various growth factors, cytokines and extracellular vesicles. Overall, these factors promote the infiltration of cells towards future metastatic sites[31]. Tumour-derived secreted factors such as vascular endothelial growth factor (VEGF), tissue necrosis factor α (TNF-α), tumour growth factor β (TGF-β), Lysyl oxidase (LOX) are involved in the formation of a pre-metastatic niche in different tumour types[32,33,34]. The priming of the organ by such factors is thus involved in favouring the tumour cell colonisation of target organ[35]. Due to its unique biology, liver is a major target organ for most cancers namely pancreatic carcinomas, stomach, breast, colon, oesophagus, myelomas and leukaemia[36]. The infiltration of myeloid derived suppressor cells (MDSCs), neutrophils, macrophages and other bone marrow derived cells (BMDCs) into the liver tissue is crucial for the establishment of a pre-metastatic niche. Before the arrival of the metastatic tumour cells, BMDCs expressing vascular endothelial growth factor receptor 1 (VGFR-1) arrive at a distant receptive microenvironment[32]. Hiratsuka et al. provided the first evidence that non-neoplastic cells prime pre-metastatic niche sites[33]. He shows that BMDCs express CD133 and CD4, which are the markers for progenitor cells, along with integrin α4β1, a ligand for fibronectin that is known to be upregulated at distant metastatic sites. Secretion of VEGF-A, TNF-α and TGF-β by primary tumour cells also trigger a pro-inflammatory response, which attracts myeloid cells to the site of premetastasis, thus paving the way for metastasis[37].

### 1.4. Metastasis

Metastasis accounts for the most number of deaths associated with PDAC, even in cases of successful extraction of primary tumour with no clinical detection of spreading of the tumour during the time of surgery[27]. The process of metastasis occurs via sequential events leading to the spread cancer cells from the site of primary tumour to distal sites. First, at the site of the primary tumour, the tumour cells invade neighbouring tissue by escaping the tumouricidal immune response. These tumour cells secrete systemic factors in order to prime distant metastatic sites. The primary tumour microenvironment is altered to aid the egress of the cancer cells into the blood stream, such as by increasing the angiogenesis[38]. The tumour cells intravasate into the blood stream directly or via the lymphatic system. The survival of circulating cancer cells, after intravasation, has been suggested to be supported by the formation of a fibrin clot by platelets and tumour associated macrophages (TAMs)[39]. The cancer cells circulate with the bloodstream and are arrested in a microvascular bed, at a future metastatic site. This tumour cell arrest is termed as micro-circulatory arrest. The arrested cells then extravasate at these metastatic sites escaping the immune surveillance in the blood stream. Extravasation is assisted by metastasis associated macrophages (MAMs), which aid in the increase of vascular permeability. The extravasated cells then proliferate at these sites to initiate the formation of metastatic foci. Eventually the diverse aspects like blood supply, extracellular matrix and immune response are altered so as to promote the progression of metastasis at the metastatic site[40,25]. Especially in PDAC the migratory properties gained by the primary tumour cells is a result of a complex and less understood process called epithelial to mesenchymal transformation (EMT) or vice versa MET[41]. Although the actual involvement of EMT/ MET in PDAC metastasis is still under question this process of rapid transition has been known to be involved to increase the cancer cell motility and dissemination[42].

### 1.5. Extracellular vesicles (EVs)

The term extracellular vesicles (EVs) can be defined as any membrane bound particle carrying complex cargoes, including proteins, lipids and nucleic acids which can be released by any type of cell. They can be classified based on their cellular origin and biogenesis which also defines the type of cargo it might carry. Among the different types of EVs there are the exosomes (50-100 nm) formed via endo-lysosomal pathway, microvesicles (MVs) formed by outward blebbing of the plasma membrane (0.1-1 µm) and oncosomes (1-10 µm) mainly released by rapidly proliferating cancer cells and apoptotic bodies (1-3 µm) (Fig. 3). The main function of extracellular vesicles is to facilitate inter-cellular communication. This exchange

takes place in a pleiotropic manner. For example, the surface proteins from the donor cell can be transferred to recipient cell by membrane fusion and thus delivering respective contents such as transcription factors, oncogenes, small and large non-coding regulatory RNAs such as microRNAs (miRNAs), mRNAs. This transfer is crucial to maintain the physiological functions such as tissue repair, immune surveillance or blood coagulation. In addition, it has recently been identified to play a role in the progression of diseases like cancer by especially being involved in the establishment of pre-metastatic niche[43].

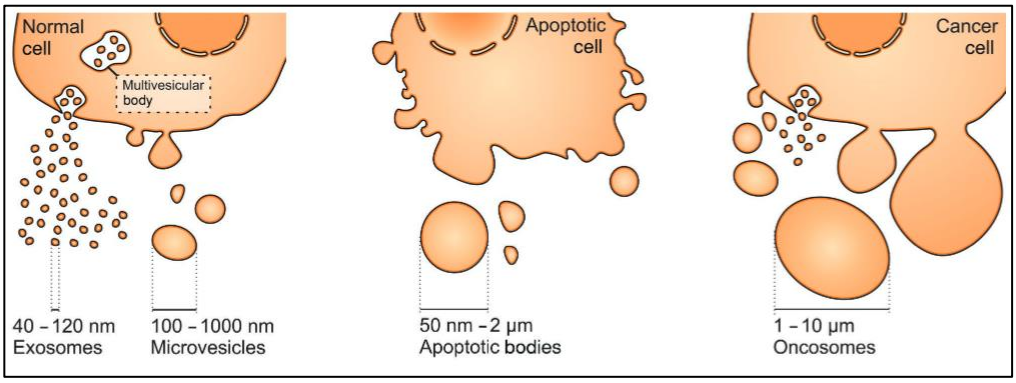


Figure 3: The different types of extracellular vesicles secreted by different cells. Primarily based on their size exosomes (40-120 nm) and microvesicles (100-1000 nm), secreted as membrane blebs, are formed by all types of cells whereas apoptotic bodies are formed from dying cells. Oncosomes (1-10 µm) are secreted by cancerous cells by membrane blebbing. Adapted from[44].

### 1.5.1. Microvesicles

MVs are extracellular membrane bound particles generated by all cell types which are found circulating in the blood, urine and other body fluids[45,46]. Rapidly proliferating cancer cells undergoing EMT also produce MVs. The plasma membrane of cells consists of an asymmetrical lipid bilayer showing the presence of phospholipids like phosphatidylethanolamine (PE) and phosphatidylserine (PS) on the cytoplasmic membrane and phosphatidylcholine (PC) and sphingolipids on the exoplasmic membrane[47]. MVs are known to be highly pro-coagulant due to surface expression of negatively charged PS and the presence of tissue factor (TF), an important initiator protein of the blood coagulation cascade. The shedding of MV is a highly regulated procedure. The various functions of MVs are highly dependent on the type of cargo they carry which in turn depends on the cell where they originate. These particles can travel to distal areas away from their site of origin thus enabling horizontal transfer and deposition of bioactive molecules. For example, MVs from normal endothelial cells play a role in angiogenesis, those from skeletal cells initiate bone mineralisation and delivery of various proteins. Some proteins are selectively incorporated in the MVs such as Vesicle associated membrane protein (VAMP3),

Auxin response factors 6 (ARF6)- regulated proteins, Vascular Endothelial Growth Factor (VEGF), Fibroblast Growth Factor (FGF), Angiopoietin-1 and Ephrin A3[48].

### 1.5.2. Large oncosomes (LO)

The term large oncosomes was first used by J. Rak's group to describe extracellular particles shed from glioma cells containing transferable EGFRvIII on their surface[49]. Following that, V.R. Minciacchi et al reported particles ranging from 1-10μm detected in the supernatants of prostate cancer cells. This was the first time the term large oncosomes was used, based on their atypical large size and cancer specific cargo[43]. Several studies have proven that highly aggressive and invasive tumour cells have a higher rate of oncosome production[50,51]. Especially, the cancer cell types undergoing a transition from the mesenchymal form to a more invasive and metastatic amoeboid phenotype, showed an increased production of LOs[52]. The exact distinction between MVs and LOs is still under investigation. LOs, like MVs, have been reported to carry miRNAs, metalloproteinases, GTPase, ADP-ribosylation factor 6, and caveolin-1. The only protein to be exclusively enriched in large EVs appears to be cytokeratin 18 (CK-18) which can be used as a potential marker to distinguish tumour-derived LOs from other EVs in tissues and plasma[53].

### 1.5.3. Role of EVs in metastasis

Tumour associated microvesicles (TMVs) have been reported to carry effectors which influence various pro-cancerous processes such as angiogenesis, ECM remodelling, immunoediting, transformation of normal cells, tumour invasion, establishment of pre-metastatic niche and finally full-blown metastasis[48]. The host microenvironment evolves along with the progression of cancer which in-turn activates metastasis. Moreover, EVs have been studied extensively for their role in numerous types of cancers, especially in pancreatic cancer. For instance the involvement of exosomes in metastasis, especially pre-metastatic niche formation, is known and discussed extensively for some time now[54]. Exosomes have the potential to promote metastasis by activation of PI3K/AKT and MAPK signalling pathways, matrix-metallo proteinases 2 (MMP-2) and MMP-9, tyrosinase-related-protein-2 (TYRP-2) to mention a few[55]. Exosome-derived factors are actively taken-up by Kupffer cells to generate a fibrin-rich environment increasing the infiltration of tumour associated immune cells[56]. A few studies have also shown that pancreatic cancer-derived exosomes increased migration and non-adhesiveness of cells *in vitro* and were involved in pre-metastatic niche formation in the liver *in vivo*[57]. A high number of procoagulant MVs has been reported in pancreatic and breast cancer

patients[58,52,59]. The term oncosomes itself suggests that these particles are derived predominantly from cancerous cells and hence potentially play an important role in establishment of metastasis. Since LOs can be quantified not only in tissue surrounding the primary tumour but also in the blood, they could help to modify distal microenvironment thereby supporting metastasis[51,53]. In addition to prostate cancer, in a recent report, Headly et al. has been able to visualize, fragmentation of CTCs, that is large oncogenic fragments spontaneously being formed in the lung metastasis model[60].

### 1.6. Coagulation cascade

The coagulation cascade is a necessary process to maintain the integrity of the blood vessel. The process of blood clotting due to blood vessel injury and the subsequent dissolution of the thrombus and fibrinolysis following the repair of the injured vessel wall is termed haemostasis. The coagulation cascade is essentially a series of biochemical reactions involving conversion of a zymogen to the active enzyme ultimately leading to the conversion of soluble fibrinogen to insoluble fibrin (Fig. 4)[61]. The traditional classification of the pathway broadly comprises the intrinsic and the extrinsic (Tissue Factor (TF) dependent) pathways. The intrinsic pathway is initiated by surface-contact activation. An initiation complex comprising of high molecular weight kininogen (HK) is formed that converts pre-kallikrein into kallikrein. This initiation complex in-turn leads to the conversion of the zymogen Hageman factor (Factor XII) to the active enzyme FXIIa (Fig. 4)[62]. Further downstream, activated FXIIA converts FXI to FXIA leading to the activation of FIX to FIXa which is a member of the intrinsic tenase complex involved in the formation of activated FXa[63,64].

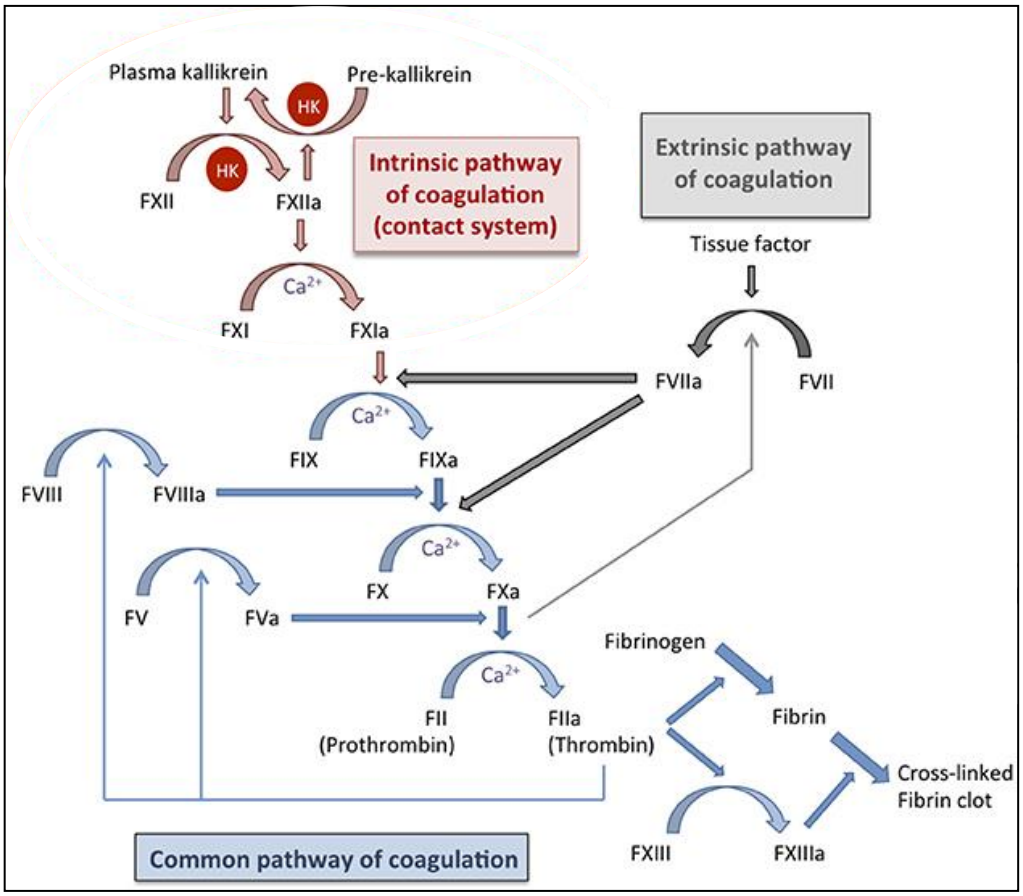


Figure 4: A schematic diagram showing the coagulation cascade. The scheme shows the intrinsic pathway of blood coagulation (thick red arrows), the extrinsic pathway (thick grey arrows) and the common pathway (thick blue arrows). The respective feedback mechanisms are indicated by thinner arrows (blue and grey). Adapted from[61].

The extrinsic pathway triggers the formation of FXa due to exposure of TF as a consequence of vascular injury. TF immediately forms a complex with Factor VII to activate it. The TF-VIIa complex directly or indirectly activates Factor X. The formation of factor Xa triggers the downstream reactions leading to the formation of thrombin from prothrombin (common pathway) in the presence of $Ca^{2+}$ ions and phospholipids, which in-turn leads to the conversion of insoluble fibrin to fibrin polymers (in presence of factor XIII). The resulting clot is formed by of fibrin polymers, platelets, red blood cells (RBCs) and/ or white blood cells (WBCs). The thrombin produced by the extrinsic pathway activates a positive feedback loop for the formation of factor Va and VIIIa which in turn accelerate the upstream production of Xa and IXa respectively[62].

### 1.6.1. Cancer and coagulation

The interdependency of cancer and coagulation has been known now for more than 100 years. In 1865, Armand Trousseau for the first time described the clinical relation between thrombosis and cancer[65]. Cancer patients are susceptible to thrombosis and show several abnormalities related to haemostasis. An example is deep vein thrombosis (DVT) which is the second largest cause of death due to cancer progression[66]. The procoagulant activity of cancer cells is primarily thought to be responsible for the activation of blood coagulation during tumour development. It is particularly associated with haematogenous metastasis[67]. The expression of procoagulant factors on the surface of the cancer cells, like the expression of TF, may contribute to the recruitment of many immune cells and in the activation of platelet aggregation[68]. Most solid tumours in cancer patients and mouse models show presence of cross-linked fibrin[69]. In addition, fibrin degradation products might also aid pro-metastatic processes such as immune-modulation and angiogenesis. The haematogenous, survival, spreading and arrest of cancer cells in the microvasculature is often associated with deposition of fibrin/ fibrinogen and platelets[70]. Taking in account all these facts fibrin might play a very important role in cancer development and metastasis. Therefore, it could be potentially exploited for diagnostic and therapeutic purposes involving early detection as well as prophylactic measures[71]. For example, fibrinogen and fibrin degradation products in numerous cancers can be used as therapeutic targets. In this context, it is important to know how anti-coagulant therapeutic regimes, which are extensively administered, affect metastasis development[72,73,67]. Indeed, the first line of treatment for coagulation-based complications (for e.g. venous thrombosis) usually involves administration of different anticoagulants. Some commonly administered anticoagulants are rivaroxaban, a direct FXa inhibitor and fondaparinux, a synthetic pentasaccharide which is an indirect FXa inhibitor. The lower-molecular-weight heparins such as enoxaparin and dalteparin have better antimetastatic effects in some cases than the widely popular warfarin a vitamin K antagonist[74,75].

### 1.6.2. Cell surface exposure of phosphatidylethanolamine (PE)

As mentioned in section 1.5.1. lipid bilayers typically show a characteristic asymmetrical distribution of phospholipids across the inner and the outer membrane. PE and PS are enriched in the cytoplasmic membrane whereas PC and sphingolipid (SL) are concentrated in the exoplasmic membrane[76] (Fig. 5). This asymmetry is maintained by a group of phospholipid transporters called the flippases which mainly transport lipids (mostly PS and to a lesser extent PE) from outer membrane to the inner membrane and the floppases which transport the

phospholipids (PC and SL) from the inner membrane to the outer membrane at the expense of energy from ATP hydrolysis[77].

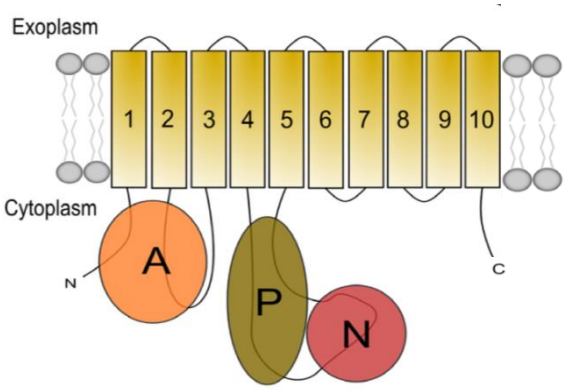


Figure 5: The topological structure of the proteins of the P4-ATPase family comprising 10 transmembrane helices with the N- and C- terminal on the cytoplasmic side. The domains are indicated as follows: large cytoplasmic loop containing (A) actuator, (P) phosphorylation and (N) nucleotide binding sites. Adapted from[78].

The third class of phospholipid transporters comprises of scramblases that transport all kinds of lipids in both directions in an energy-independent manner. Cancer cells have been reported to show an elevated exposure of PS on their surface suggesting a dysregulation of flippases activity[79]. The ATP dependent flippases and floppases primarily belong to the P-type and ATP-binding cassette (ABC) family of transporters[80]. P4- ATPase is one of the largest subtypes, present only in eukaryotes, of a large superfamily P-type ATPases which consists of evolutionarily conserved proteins. They typically consist of a membrane bound protein with ten transmembrane helices and a large cytoplasmic loop harbouring actuator (A), phosphorylation (P), nucleotide binding (N) domains (Fig. 5)[78]. The P4-ATPAses are involved in various physiological processes and deficiencies in these ATPases have been reported to cause liver diseases, neurological disorders, immunological complications and diabetes[81]. The importance of PE exposure, as a tumour promotive measure, is still under investigations. For instance, phosphatidylethanolamine-binding-proteins (PEBPs) are over expressed on the surface of breast cancer cells (also in ovarian and prostate cancer), and knocking down this gene in these cells, induced apoptosis and arrested cell growth by rendering the cells more susceptible to chemotherapeutics[82].

## 2. Objectives of the study

Several different molecular mechanisms influence the metastatic potential of pancreatic cancer cells. The study of the interplay between the pancreatic cancer cells, their extracellular vesicles and the intravascular microenvironment at the site of metastasis will be the main goal of this project. Therefore, the work of this project revolves around three highly interdependent aims.

First, we aimed to examine the pro-coagulant properties of pancreatic cancer cells and their extracellular vesicles in the microcirculation of the liver, the major site of pancreatic cancer metastasis. In particular, the mechanisms enabling pancreatic cancer cells and their microvesicles to stimulate coagulation were examined.

Second, we analysed the exact time line of microvascular fibrin formation as induced by pancreatic cancer cells and their extracellular vesicles to determine their possible role in liver metastasis. We particularly were interested in studying the structure of fibrin-rich thrombi using high-resolution microscopic techniques in various *in vitro* as well as *in vivo* set ups.

Third, the immune surveillance mechanisms triggered upon administration of cancer cells and tumour extracellular vesicles were evaluated. Specifically, we wanted to understand the intravascular immune response to the arrival of tumour material at the metastatic sites. In addition, the different immune cells and their potential roles in the survival or elimination of cancer cells were identified by various techniques including intravital imaging of these tumour entities in the microcirculation.

# 3. Materials and Methods

## 3.1. Materials

### 3.1.1. Equipment

| Items | Company, Type |
|---|---|
| Balance MC1 LC 620 S | Sartorius (Göttingen, D) |
| Cell culture incubator | Köttermann |
| Cell culture microscope | Carl Zeiss |
| Count chamber Neubauer Improved | Brand (Wertheim, D) |
| Culture Hood | Heraeus |
| Electrophoresis power supply | EPS600 Pharmacia |
| Electrophoresis unit | small Bio-Rad Mini-Protean II |
| ELISA Reader Dynatech MR7000 | Dynatech Laboratories |
| Gel Doc system | Vilber Lourmat |
| Heating mantle | Eppendorf |
| Incubator (cell culture) | Heraeus (Hanau, D) |
| Lamin Air flow HLB 2472 | Thermo Scientific (Braunschweig, D) |
| Light microscope Axiovert 100 | Zeiss (Jena, D) |
| LSM 510 Meta | Zeiss (Jena, D) |
| Mega centrifuge | Heraeus, Omnifuge 2.0 RS |
| Micropipettes | Eppendorf (Hamburg, D) |
| Multiphor II blotting device | Amersham Pharmacia Biotech |
| Nano Drop | Thermo Fisher Scientific |
| pH meter | HANNA instruments HI 221 |
| Pipet boy | Integra-Bioscience (Biebertal, D) |
| Pipettes (5ml, 10ml) | Omnilabs |
| Sonicator Bransor | Boston Laboratory Equipment |
| Thermocycler | Biozyme, MiniCyclerTM, MJResearch |
| Thrombelastograph | RoTEG Dynabyte |
| Vortexer | Sartorius (Göttingen, D) |
| Water bath Julabo U3 | Julabo Labortechnik (Allentown, USA) |

### 3.1.2. Antibodies

| Antibody | Company | Catalogue no. | Concentration |
|---|---|---|---|
| anti-CD31 (PECAM-1) | Abcam | ab28364 | 5 µg/ml |
| anti-CD31 (M-20) | Santa Cruz | sc-1506 | 5 µg/ml |
| anti-PECAM-1 (MEM-05) | Santa Cruz | sc-51691 | 5 µg/ml |
| anti-CD335 (NKp46) | Biolegend | 137602 | 20 µg/ml |
| anti-CD8 alpha | Abcam | ab25478 | 2 µg/ml |
| anti-CX3CR1 | Abcam | ab8021 | 10 µg/ml |
| anti-CX3CR1 | Novus | NBP1-76949 | 10 µg/ml |
| anti-CYTOKERATIN 18 | NEB | 4846S | 0.4 µg/ml |
| anti-F4/80 AB [CI:A3-1] | Abcam | ab6640 | 10 µg/ml |
| anti-Fibrin II beta | WAK Chemie | NYBT2G1 | 5 µg/ml |
| anti-hTF | American Diagnostica | AMD 4509 | 50 µg/ml |
| anti-human IgG | American Diagnostica | 4508CJ | 50 µg/ml |
| anti-Ly6C [ER-MP20] | Abcam | AB15627 | 5 µg/ml |
| anti-Ly6G | BD Pharmingen | 551459 | 15 µg/ml |
| anti-Mouse Alexa 488; 546; 594 | Life/Thermo | A11034 | 2 µg/ml |
| anti-Rabbit Alexa488; 546; 594 | Life/Thermo | A11034; A11035; A11037 | 2 µg/ml |
| anti-rat Alexa 488; 546; 594 | Life/Thermo | A21208; A11081; A21211 | 2 µg/ml |
| anti-rat IgG-Dylight488 | Abcam | ab96887 | 2 µg/ml |
| anti-rat IgG-Dylight550 | Abcam | ab96888 | 2 µg/ml |
| Anti-stabillin II STB2 3.1 | Kai Schledzewski | | 5 µg/ml |
| Anti-TMEM16F | Santacruz | sc-136930X | 50 µg/ml |
| Mouse Anti-Biotin (PE) | Biolegend | 409003 | 0.2 µg/ml |
| mouse $IgG_1$, Isotype Control | Life/Thermo | MG100 | 50 µg/ml |
| mouse $IgG_{2a}$, Isotype Control | Life/Thermo | MG2A00 | 50 µg/ml |

### 3.1.3. Kits

| Name | Company | Catalogue no. |
|---|---|---|
| Antibody Labeling Kit Alexa488 | Life/Thermo | A-20181 |
| Antibody Labeling Kit, Alexa555 | Life/Thermo | A20187 |
| Click-it Plus TUNEL 488 Kit | Thermo fisher scientific | C10617 |
| QIAquick Gel Extraction Kit | Qiagen | 28704 |
| RevertAid First Strand cDNA Synthesis Kit | Thermo fisher scientific | K1621 |

### 3.1.4. Buffers

Blocking buffer
1x PBS
0.1 % Tween 20
2% / 5 % / 10% BSA (as per protocol)

$CaCl_2$ (Faktor Xa Formation; 50ml)
225 mg $CaCl_2$ .$2H_2O$
ddH2O

Ca/Hepes (TEG)
10 mM Hepes
100 mM $CaCl_2$,
dd$H_2O$, pH 7,4

PBS (Phosphate Buffered Saline) (1L)
8 g NaCl
0.2 g $KH_2PO_4$
1.42 g $Na_2HPO_4.2H_2O$
0.2 g KCl

Permabilisation/ Blocking-Buffer
0.2 % Fish Skin Gelatin
0.5 % BSA
0.1 % Saponin
Sterile filtered

Tris-EDTA buffer
10 mM Tris pH 8.0
1mM EDTA pH 8.0

TNC (Tri-Nitrium Citrate for blood drawing)
3.68 g TNC
100 ml dd$H_2O$
Sterile filtered

10X Tris-Boric-EDTA Buffer (1 L)
55 g Boric acid
107.8 g Tris-HCl
7.44 g Na-EDTA
pH 8.3

10X-SDS-PAGE running buffer (1 L)
30.25 g Tris
144 g Glycin
50 ml 10% SDS

Resuspension buffer (1 L)
138 mM NaCl
2.7 mM KCl
12 mM $NaHCO_3$
0.4 mM $NaH_2PO_4$
1 mM $MgCl_2.6H_2O$
5 mM D-Glucose
5 mM Hepes
pH 7.35

5X SDS-PAGE Sample buffer (10ml)
1 ml 10X Tris-HCL (3.1 M pH 6.8)
0.25 g SDS
5 ml Glycerol
12.5 mg Bromophenol blue
6% (v/v) ß-Mercaptoethanol

Tryphan Blue in PBS (cell counting)
0.4% Tryphan blue
1 mM Ca++
$ddH_20$

SDS-PAGE transfer buffer (1L)
2.9 g Glycine
5.8 g Tris
100 ml Methanol
3.7 ml 10% SDS

Blocking buffer for WB membrane (1L)
100 ml 10X TBS
1 ml Tween 20
50 g non-fat dry milk (BSA)
900 ml distilled water
Filter with 0.2 mm Whatmann filter paper

Washing buffer for WB membrane (1L)
100 ml 10X TBS
3 ml Tween 20

### 3.1.5. Cell lines

| Type | Origin | |
|---|---|---|
| KPC | Mouse pancreatic cancer cell line | Dr. Hana Algül, II. Medizinische Klinik und Poliklinik, Klinikum rechts der Isar der TU München (München) |
| L3.6pl | Human pancreatic cancer cell line | Prof. Christiane Bruns, Klinik für Allgemein-, Viszeral- und Gefäßchirurgie, Otto-von-Guericke Universität (Magdeburg) |
| PANC-1 | Human pancreatic cancer cell line | ATCC |

### 3.1.6. Mouse models

| Type, Name | |
|---|---|
| C57BL/6 M/F 21-25 G ca.8+ Weeks<br>LysM$^{+}$eGFP<br>CX3CReGFP | Charles River |

### 3.1.7. Chemicals

| Name | Company | Catalogue no. |
|---|---|---|
| Acetone 99,5% | Carl Roth | 9372.2 |
| Acrylamide bis-Acryl | Sigma | A3699 |
| Beriplex | CSL Behring | Apotheke |
| Cell culture Flasks: 175cm$^2$ straight neck | BD Pharmingen | 353112 |
| Cell culture Flasks: 25cm$^2$ straight neck | BD Pharmingen | 353107 |
| Cell TrackerTM Red BODIPY Dye | ThermoFisher Scientific | C2102 |
| Cell TrackerTM Red CMTMR Dye | ThermoFisher Scientific | C2927 |
| Cell TrackerTM Red CMTPX Dye | ThermoFisher Scientific | C34552 |
| Chromogenic Substrate S-2222 | Haemochrom Diagnostic | 41201 |

| | | |
|---|---|---|
| Control siRNA | Santa Cruz | sc-37007 |
| Corn Trypsin Inhibitor (CTI) | Calbiochem | 650345 |
| DAKO Pen for immunohistochemistry | Dako Cytomation | S200230 |
| Desirudin (*S.cerevisiae*) AFl 15 mg | Inresa | REVASC |
| DMSO Hybrid-Max | Sigma | D2650 |
| DNA Ladder 100BP | Life/Thermo | 15628050 |
| DNA Polymerase (*Taq*) | New England Bioloabs | M0273S |
| DNA polymerase (ampli*Taq* 360 gold) | ThermoFisher Scientific | 4398818 |
| dNTP Mix PCR grade | Qiagen | 201900 |
| DRAQ5 | Abcam | ab108410 |
| Duramycin | Sigma | D3168-10MG |
| Duramycin-LC-Biotin | Mol. Targeting Techn. | D-1003 |
| Acetic acid | Carl Roth | 3738.1 |
| Ethanol 99.8% | Carl Roth | K928.3 |
| Fibrinogen from hPlasma | Sigma | F3879-100mg |
| FM 4-64 FX | Life/Thermo | F34653 |
| Gelatin 2% Solution | Sigma | G1393-20ML |
| Generuler 1 KB DNA-Ladder | Fermentas | SMO311 |
| HCl 37% | Carl Roth | 9277.1 |
| Kalium hydroxid; Potassium hydroxide | Carl Roth | 3904.1 |
| Lipofectamine 2000 Reagent | Life/Thermo | 11668027 |
| Mayer´s Hematoxylin | Science Service GmbH | 26381-02 |
| Methanol >99.5% | Carl Roth | CP43.4 |
| Mucin1 shRNA Plasmid (h) | Santa Cruz | SC-35985-SH |
| Multiwell plate: 12-well | BD Pharmingen | 353225 |
| Multiwell plate: 24-well | BD Pharmingen | 353226 |
| Multiwell plate: 6-well | Omnilab | 353046 |
| Multiwell plate: 96-well | BD Pharmingen | 353072 |
| NaCl 1Kg | Carl Roth | P029.2 |
| NaOH Pellets | Roth | 041300 |
| Object glass slides SuperFrost | Omnilab | J1800AMNZ |
| PBS | Sigma | D8537 |

| | | |
|---|---|---|
| Pipette, 10 ml | Omnilab | 4488 5380582 |
| Pipette, 5 ml | Omnilab | 4487 606180 |
| Poly-L-Lysine Solution | Sigma | P8920-100ML |
| Protease Inhibitor | Roche | 11206893001 |
| Protein Assay Reagent A | BioRad | 500-0113 |
| Protein Assay Reagent B | BioRad | 500-0114 |
| Puromycin | VWR | 540411-25MG |
| RacGAP-1 siRNA (m) | Santa Cruz | SC-76336 |
| Reaction cups Safe-Lock (1.5 ml) | Eppendorf | 0030 125.193 |
| Reaction cups Safe-Lock (2 ml) | Eppendorf | 0030 120.094 |
| Roteg-Cuvettes (Cup and Pin pro) | Rotem | 200011 |
| siRNA negative control | Qiagen | 1027284 |
| Sodium Carbonate Anhydrate | Sigma | S7795-500G |
| SYTO 62; SYTO 60; SYTOx-Green | Life/Thermo | S7020 |
| TEMED | Carl Roth | 2367.3 |
| Thromborel S 400T | Siemens Healthscare | OUHP29 |
| Tissue Tek T-TEK | Hartenstein | TTEK |
| Tween20 (Polyoxethylene) | Sigma | P1379-100ML |
| Vecta-shield Hard Set with DAPI | Linaris | H-1500 |
| Vecta-shield with DAPI | Enzo/Life/Thermo | VC-H-1200-L010 |
| Water Tissue culture tested | Sigma | W3500-500ML |

### 3.1.8. Cell Culture Reagents

| Name | Company | Catalogue no. |
|---|---|---|
| DMEM 1 g/l Glucose | Life/Thermo | 31885-023 |
| DMEM 4.5 g/l Glucose | Life/Thermo | 41965-039 |
| FBS | Life/Thermo | 10270106 |
| Freezing Medium | Ibidi | 80023 |
| MEM alpha Medium | Life/Thermo | 22571-020 |
| NEAA (100X) | PAN Biotech | P08-32100 |
| OPTI-MEM (1X) + L-Glucose. | Life/Thermo | 31985-047 |
| Penicillin/Streptomycin (100X) | Invitrogen | 15140-122 |
| RPMI 1640-Medium with L-Glutamine | Life/Thermo | 21875034 |
| Trypan Blue | Carl Roth | CN76.1 |
| Trypsin-EDTA Solution (10X) | Sigma | 59418C |
| Vitamin (MEM-Vitamin Mix; 100X) | Merck/Millipore | K 0373 |

## 3.2. Methods

### 3.2.1. Animal experimentation protocol

All the mice mentioned in section 3.1.6 were obtained from Charles river and were kept under specific pathogen free conditions at the animal facility of Walter Brendel Centrum. The age group of the mice used for the all experiments ranged from 9 weeks to 14 weeks. All the animal experiments were performed as per the guidelines of the local legislation on protection of animals (Regierung von Oberbayern, Munich). Mouse blood was drawn intra-cardially after anesthetisation (isoflurane; Delta Select GmbH), fentanyl i.p. (0.05 mg/kg body weight; CuraMed Pharma GmbH), after which the mouse was sacrificed by strangulating the neck and subsequent the organs were collected and processed as described in section 3.2.4.

### 3.2.2. Injection protocols

The injection scheme for the animal experiments was as described in scheme 1. All the injections of the cancer cells and MVs were i.v. injections via the tail vein. MVs were always injected as two doses (75 µg each), with a gap of 10 min between the two doses. Cancer cells (2 x $10^6$ cells) were injected after 1 h of the second MV injection and the organs (liver, lung, kidney, and heart) and blood were collected after different time points like 0.5 h, 2 h, 6 h, 24 h, 48 h. Scheme 1, part (i) shows the different points after either CMTPX-pre-labelled KPC cancer cells or KPC MVs injection. Long-term experiments were also performed with KPC cancer cells together with KPC MVs as described in scheme 1, part (ii), where the animals were sacrificed after 8 days or 14 days. The CMTPX-labelled MVs were injected first, 1 h after which the BODIPY labelled-cancer cells were injected.

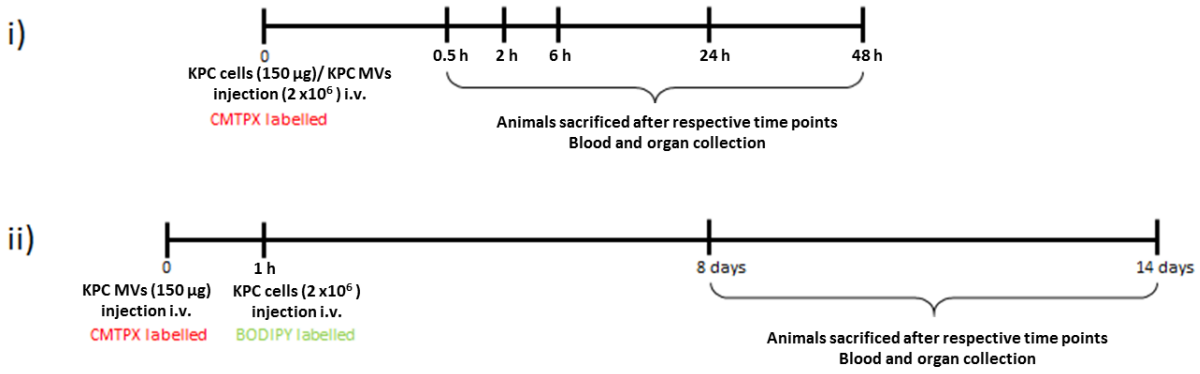


Scheme 1: Injection schemes for KPC cells (2x$10^6$) and KPC MVs (150 µg). All injections were made in the tail vein of the mice. i) only KPC cancer cells or KPC MVs pre-labelled with CMTPX were injected ii) CMTPX-labelled KPC MVs plus BODIPY-labelled KPC cancer cells were injected for long term experiments.

### 3.2.3. Administration of substances

The effects of different substances affecting blood coagulation for e.g. anticoagulants, inhibitors on the various phenomenon like microvascular fibrin formation, microcirculatory arrest of tumour cells, killing of cancer material and extravasation was investigated. In order to achieve this, the mice were either pre-treated before injection of cancer cells and EVs or the cancer cells with EVs were pre-treated before being injected into the mice. The cancer cells and MVs were pre-treated with 10 µm duramycin, for 30 min at room temperature (RT) in a final volume of 100 µl. In order to wash of the duramycin, the cells and vesicles were then washed twice with PBS at 1300 rpm for 5 min and 12600 rpm for 30 min (without break), respectively. In case of biotin labelled duramycin the same procedure as mentioned before was used where the cells were coated with 10 µM biotin-labelled duramycin. To block the TF induced extrinsic pathway of coagulation, the cells and MVs were incubated with respective anti-TF antibodies (50 µg/ml mouse 1h1 anti-TF; or human anti-TF from American diagnostica) for 30 min at RT in a final volume of 100 µl. The antibody in the solution was washed away using PBS by centrifugation at 1300 rpm for 5 min. To block fibrin formation, the mice were administered with factor Xa inhibitor rivaroxaban (3 mg/kg body weight; i.v.) 4 h before the administration of MVs and/ or cancer cells. The effect of PCK, a factor XII inhibitor, was checked by injecting it at a concentration of 10 mg/kg body weight; i.v. few minutes right before the cancer cell and/ or MV injections.

### 3.2.4. Preparation and storage of organs

After organs such as liver, lung, spleen, kidney and heart were harvested from the animals, they were fixed in 2% formalin solution for 2 h. The fixed organs were then transferred to 30% sucrose solution and incubated overnight at 4 ˚C after which the organs were stored at -80 ˚C. The sucrose fixation step was especially essential to preserve the GFP signal from pre-labelled cells.

### 3.2.5. Cryosections

The organs were stored for at the least 24 h at -80 ˚C before being embedded in tissue-tek and subsequent sectioning. The organs were completely covered in tissue-tek to embed them fully at -20 ˚C in the cryotome. The organs were mounted on the apparatus to enable cutting. Sections ranging from 5 µm-10 µm were prepared. The sections were immediately collected on super-frost glass slides, which were pre-labelled with the respective animal number, treatment and other relevant information (time point, type of cell etc.). The slides were stored at -

20 ˚C and remaining organs embedded in tissue-tek and were stored at -80 ˚C until required further to prepared fresh sections.

### 3.2.6. Paraffin embedded section

The organs for the paraffin embedding were first collected in plastic embedding cassettes and incubated overnight in 4% formalin. The cassettes containing the organs were then washed thoroughly (5-15 min) with distilled water. The organs were transferred to a container containing 70% ethanol and incubated for at least 24 h. Thereafter, the organs along with the cassettes were transferred to an embedding apparatus, which dehydrated them by dipping them in increasing concentrations of ethanol and were finally soaked in paraffin. After removing the dehydrated, paraffin soaked organs from the machine, the organs were manually embedded in paraffin at a pouring station to embed the organs in paraffin blocks which facilitates the sectioning of organs. The paraffin sections were made by means of a microtome. The organs were mounted onto the device and 4 μm thick sections were produced. To prevent wrinkles on the sections while cutting, the paraffin embedded organ slices were transferred to a water bath the temperature of which was maintained between 55-65 °C. The uniform sections floating on warm water were carefully transferred on super-frost glass slides. These slides were dried overnight at 37 °C in the drying cabinet and then stored at RT.

### 3.2.7. Cell culture

The KPC cell line was isolated from the pancreas of a genetically modified mouse, KPC (*LSL-KRASG12D/+; LSL-Trp53R172H/+; Pdx-1-Cre*), which developed spontaneous metastasis. The mice carried a point mutation for *KRAS* (G12D) and p53 deletion mutant along with a *Cre* recombinase gene. This cell line was cultured in high glucose DMEM (4.5 g/l) with 2.5% NEAA, 10% FBS and 1% penicillin/ streptomycin. The cell lines were passaged every 8-10 days. The L3.6pl cell line is a human pancreatic cancer cell line which was generated by orthotropic implantation of human cancer cells into the mouse pancreas. This cell line was maintained in low glucose DMEM (1 g/l) with 10% FBS, 2.5% NEAA, 2.5% vitamins and 1% penicillin-streptomycin. The cell line was passaged every 10-12 days. The PANC-1 (ATCC) cell line, is another human pancreatic cancer cell line, was cultured in high glucose DMEM (4.5 g/l), 10% FBS and 1% penicillin-streptomycin. The cell line was passaged every 8-10 days. All the cells were maintained in an incubator with relative humidity, 95%; carbon dioxide ($CO_2$), 5%; temperature, 37 °C. The cells were grown in cell culture flasks of various sizes as per

requirement and maintained with an appropriate amount of culture medium as stated in the catalogue.

### 3.2.8. Maintaining cell lines

The cells were passaged using trysin-EDTA solution. The culture medium was removed and the flask was rinsed with PBS (1 ml-5 ml) to remove of remaining medium. 1 ml of trysin-EDTA solution was added to 175 $cm^2$ flask; 0.5 ml to a 25 $cm^2$ flask and incubated at 37 °C until to allow cell detachment. Detached cells were collected in falcons followed by addition of 1-5 ml PBS. This step was performed twice followed by addition of 5-10 ml complete medium to the flasks to collect all the remaining cells. The cell suspension was centrifuged at 1300 rpm for 5 min. The supernatant was discarded and the cell pellet was resuspended in ≈1 ml PBS/complete medium followed by addition of 10 ml PBS, this being the second wash step. The cells were centrifuged once again as mentioned above and resuspended in 1-2 ml PBS/complete medium. The cells were counted using a Neubauer chamber and further either cultivated in order to maintain them or used for the desired purposes.

### 3.2.9. Preparation of cell stocks

Stocks of cell lines were prepared of all cell lines and stored at -80 ˚C or liquid nitrogen. The cells were passaged as explained in section 3.2.8. Once the cells were washed by subjecting them to centrifugation twice at 1300 rpm for 5 min at RT each time, after which the cells were resuspended in 1 ml freezing medium (Ibdi) and stored at -80 ˚C or in liquid nitrogen.

### 3.2.10. Transient transfection

Cells were seeded in 6 well plates on the day before transfection, to attain a confluency of 50% - 80% at the time of transfection. The medium was removed and optiMEM medium was added and the suspension was incubated at 37 ˚C for 1 h. Cells were transfected using either of the following transfection reagents (Lipofectamine2000, RNAiMax, Ibdi Transfection reagent) according to the manufacturer's protocol. The siRNA and the transfection reagent were diluted in optiMEM. siRNA mix was added to the transfection mix and the mixture was incubated for 30 – 45 min at RT to allow the formation of a complex of siRNA with liposomes. The optiMEM medium from the cells was removed and siRNA plus liposome mixture was added to the cells. The cells were incubated for 4 h-6 h at 37 ˚C to allow the internalisation of siRNA. Medium without antibiotics was added to the cells and incubated overnight without removal of the siRNA complex mixture. The medium was then replaced on

the following day. The transfection efficiency was checked by western blotting and functional assays 48 h/72 h after transfection.

### 3.2.11. Stable transfection

Stable transfection was performed using shRNA. The transfection techniques use the same protocol as described above (section 3.2.10.). After 48 h-72 h of transfection the selection of the transfected cells was started. This step facilitates the elimination of non-transfected cells. Based on the properties of the construct used for transfection of the cells, after transfection, the appropriate antibiotic (ampicillin, puromycin or gentamycin) was added for selection. In order to start the selection process, the cells were subjected to an increasing concentration of the antibiotic (for e.g. puromycin was added in a range between 3 µg/ml to 20 µg/ml) until no more dead cells were seen after at least 24 h of incubating with one particular concentration. The stably transfected cells were always cultured in media containing at least a basal concentration of the antibiotic used for selection (for. e.g. 10 µg/ml puromycin was used).

### 3.2.12. Isolation of extracellular vesicles

Two types of extracellular vesicles were isolated from the supernatants of cells or blood, MVs (ranging between 0.1 µm to 1 µm) and large oncosomes (ranging between 1 µm to 10 µm). The isolation of the vesicles involved a series of centrifugation steps based on the size of the vesicles. The samples were subjected to initial centrifugation at 1300 rpm for 10 min (without break) to remove of large cells and debris. In order to isolate MVs the samples were then centrifuged at 4000 rpm for 20 min (without break) twice to eliminate large vesicles and remaining debris. Next the supernatant was subjected to a centrifugation step of 12600 rpm for 30 min (without break) with a maximum volume of 750 µl in an Eppendorf cup. The pellets obtained after this centrifugation step were pooled and used for various experiments as required. Oncosomes were isolated with the help of vivaspin ultracentrifuge columns or purely centrifugation based techniques. The supernatant obtained after the initial centrifugation step at 1300 rpm for 10 min was added to the top of the vivaspin columns (0.2 µm pore size; PES) and subjected to a short centrifugation step at 8000 g for 30 s. In case of the centrifugation based approach, the oncosomes were pelleted at 10,000 g for 30 min after the initial centrifugation step at 1300 rpm for 10 min with a maximum volume of 750 µl in the Eppendorf cups. The amount of vesicles was estimated as total protein content of the pellet.

### 3.2.13. Protein estimation

The amount of protein present was estimated using Bradford's assay which is an end point, chromogenic assay. The samples were resuspended in a minimum volume of 500 µl PBS. A 1:1 serial dilution ranging from 2 mg/ml to 0.03906 mg/ml was made using a standard protein solution of 2 mg/ml BSA. 5 µl of the standards and samples were added in triplicates to a 96-well plate. 25 µl of copper-alkali-tartrate containing solution A, which forms a complex with the proteins in the suspension, was added to each well. 200 µl of solution B, which reduces the protein complex to generate blue colour from the previous yellow colour of the solution A, was added to each of the wells above. The absorbance was measured at 700 nm in a plate reader. The protein concentration of the samples was calculated from the standard curve using excel scatter graph format.

### 3.2.14. Thromboelastography (TEG)

TEG is a technique used to analyse the various parameters of thrombus formation in whole blood such as the clotting time (fibrin formation), clot strength and other parameters. The procoagulant activity of cancer cells, MVs or oncosomes was tested by this technique using whole blood as a medium. The assay was performed in a specialised TEG pin and cup apparatus. 250 µl of the whole blood with 60 µl of a solution of 30mM $CaCl_2$ with HEPES and 30 µl of sample suspension was added to each TEG cup. The measurements were made using a rotation thromboelastometry device from ROTEG.

### 3.2.15. Factor Xa formation

A chromogenic assay was used to measure the procoagulant activity of the extrinsic pathway of the blood coagulation cascade. Serial dilutions of the standard Thromborel-S were prepared. To each well of a 96-well plate 50 µl of 30 mM solution $CaCl_2$ was added. To these wells 50 µl of standard/samples were added. A master-mix of chromogenic substance S-2222, Beriplex and the respective amount of resuspension buffer was prepared such that 100 µl of this mix was pipetted per well. The absorption was measured at 405 nm using a plate reader (softMAXpro). A cycle of 6 min was repeated for a total of 36 min and the final values were expressed as milliunits (mU)/ ml.

### 3.2.16. Preparation of phospholipid liposomes

Liposomes containing different types of phospholipids were generated using PE, PS and PC (Avanti Polar lipid). For the preparation of the liposomes (100 mol% PC; 30 mol% PE,

70 mol% PC; 30 mol% PS, 70 mol% PC) the phospholipids were dissolved in 1 ml of chloroform. A film of lipids was generated on the walls of the glass tubes by purging with inert gas (nitrogen). To the phospholipids 2 ml PBS was added. To dispose the lipids sterile glass beads were added and the suspensions were rigorously vortexed. Then the suspensions were ultrasonicated for 5 min (40 W) in an ice-bath under inert conditions (continuous flow of nitrogen over the surface). The generated liposomes were pelleted by ultracentrifugation at 100,000 g for 30 min. All the steps after the dissolution of the lipids were carried out at cold temperatures between +2 to +8 ˚C.

### 3.2.17. Immunohistochemistry: Immunostaining of cryo-sections

Immunohistostaining is a procedure to perform imaging by detecting specific antigens by selective antibodies. There are two methods of detection, direct immunostaining wherein the antigen is directly detected by a primary antibody coupled with a fluorophore and indirect immunostaining in which case the antigen is detected by a primary antibody, which is in turn detected by a secondary antibody coupled with a fluorophore.

Cryosections (5-10 µm) were fixed using formalin (2%-4%) for 15 min at RT followed by subsequent washing thrice with PBS for 3 min each. In order to avoid unspecific binding of the primary antibody a blocking step with 2% BSA in PBS was performed for 1 h at RT. After washing once again, the primary antibody with appropriate dilutions was added to the sections and incubated overnight. To retain the primary antibody solution on the sections plastic coverslips were laid on the sections or each section was encircled with DAKO pen to restrict the antibody flowing out of the tissue section. Excess of primary antibody was washed away with PBS as mentioned above. The sections were then incubated with respective secondary antibody for 1 h at 4 ˚C. To stain the nucleus DAPI (1:5000 from stock) was added, after removing the secondary antibody solution, for 5 min at RT followed by subsequent washing with PBS thrice for 3 min each. The sections were then mounted with glycerol and sealed with nail polish or mounting medium. The analysis was performed using Confocal Laser Scanning Microscope (LSM510, Zeiss).

### 3.2.18. Immunostaining of cells in suspension

The cells were harvested and washed with PBS (1300 rpm for 5 min at RT) and counted in a Neubauer chamber with addition of trypan blue to identify dead cells. The viability of the cells was 90%-95%. Cell staining was performed in sterile Eppendorf cups. Usually $8x10^5$ the cells were resuspended in 100 µl PBS. The cells were fixed with 1% formalin for 10 min at

37 ˚C. 200 µl PBS was added to the cells and the cell suspension was centrifuged at 1300 rpm for 5 min. The supernatant was discarded and the cell pellet was resuspended in 300 µl PBS followed by centrifugation at 1300rpm for 5 min. The cells were resuspended in 200 µl PBS with 2% BSA and an appropriate dilution of the antibody was added to the cell suspension. After incubating for 1 h-4 h at 37 ˚C with intermediate vortexing, 200 µl PBS was added to the cells and the suspension was centrifuged at 1300 rpm for 5 min to remove the unbound primary antibody. The cells were washed twice with 300 µl PBS by centrifugation. The appropriate secondary antibody was added at a concentration of 2 µg/ml which was diluted in PBS. The cell suspension with the secondary antibody was incubated for 1 h at 4 ˚C in the dark with intermediate vortexing. The excess secondary antibody was washed off by subjecting the cell suspension to centrifugation at 1300 rpm for 5 min thrice. The cells were stored in a 100 µl suspension with PBS in the dark until microscopic analysis. The immunostaining of the vesicles was performed with the same procedure as used for immunostaining of suspended cells. The washing steps for the EVs differed based on the type of particles. MVs were centrifuged at 12,600 rpm for 30 min at RT whereas large oncosomes were centrifuged at 10,000 rpm for 30 min at RT.

### 3.2.19. Immunostaining of adherent cells

The cells were grown the day before starting the staining procedure in 8-microwell plate or 24-well plate with sterile coverslips, as per the requirement, to attain maximum 70% confluency. The cells were washed thrice with sterile PBS (0.2-1 ml) briefly by pipetting or aspiration. The cells were blocked with 2% BSA for 20-30 min at 37 ºC followed by briefly washing them once with PBS. The primary antibody was added with appropriate dilution in 0.5% BSA solution in PBS for 1 h at 37 ºC. After washing thrice with PBS as mentioned before the respective secondary antibody at a concentration of 2 µg/ml was added to the cells for 1 h at 4 ºC. To stain the nucleus SYTO-green (5 µM) was added for 5 min along with FM 4-64Fx (1 µg/ml) to stain the plasma membrane at RT. This was followed by fixing the cells with 1% formalin for 10 min at RT. The stained cells were then washed thrice with PBS to remove extra formalin. The cells were stored at 4 ºC in PBS until imaging. If the cells were to be stained with SYTOX-green or DAPI these nuclear stains were added after the fixation with formalin because these dyes stain the nucleus of dead cells or cells with perforated outer membrane.

### 3.2.20. Staining with long lived fluorophore

The MVs and cancer cells were stained with long lived fluorophores called CellTrackerTM dyes CMTPX (red), CMTMR (orange) or BODIPY (green). These different dyes were used to label the cells and MVs with the required fluorophore as per the experimental design. The staining was performed as per the guidelines provided by the company. The required numbers of cells or MVs were suspended in 200 µl of PBS. A working solution with a concentration of 40 µM of the dyes, from pre-diluted stock of 10 mM, was prepared in PBS and pre-warmed for 10-30 min at 37 ˚C. To each probe 200 µl of prewarmed working solution of the dye was added such that the final concentration used for staining was 20 µM. This sample was gently mixed by pipetting or vortexing and incubated at 37 ˚C for 10-30 min. The stained sample was subjected to centrifugation to remove the dye in the solution at 1300 rpm for 5 min for cell staining and 12600 rpm for the MVs or 10000 rpm for the oncosomes for 30 min at RT (without break). These steps were repeated once again to wash the sample thoroughly, with 200 µl of PBS as a final wash step. To check if the staining was successful, an aliquot of the stained sample was checked by fluorescent microscopy before injection.

### 3.2.21. TUNEL staining

The killing of cancer cells was calculated by analysing the apoptotic index. The apoptotic index accounts for the number of dead cells plus the number of apoptotic bodies as compared to the total number of cells. In order to identify dead cells and other dead material TUNEL staining (terminal deoxynucleotidyl transferase dUTP nick end labelling) was performed. The principle of the protocol is based on the use of a highly purified TdT enzyme that incorporates fluorophore conjugated nucleotides at the 3'-hydroxyl termini of DNA double strand breaks that are usually generated in the DNA of dying cells. Here for the TUNEL staining the Click-it Plus TUNEL 488 Kit was used (Thermofisher Scientific). Cryosections of livers from mice injected with pre-labelled (long-lived fluorophore) cancer cells or MVs were treated exactly as per the protocol provided by the manufacturer. The TUNEL positive cells were identified by the co-labelling of the cells/vesicles with the long-lived fluorophores (CMTPX/CMTMR), TUNEL staining (green) and DAPI. A cell showing these three labels was considered as dead cell (≥ 5 µm). Dead cancer material for e.g. apoptotic bodies were identified in a similar way by the co-labelling of long lived fluorophore (CMTPX/ CMTMR), signal from TUNEL staining (green) and with but without staining positive for DAPI. These entities largely represented particles smaller than 5 µm.

### 3.2.22. Haematoxylin and eosin staining for paraffin sections

This procedure was performed to visualise cluster of abnormal cells in paraffin sections of liver tissues. Initially glass slides with paraffin sections were prepared (refer to section 3.2.6). To facilitate the staining of the organ sections the slides were first de-paraffinized by incubating them in ROTICLEAR for 3 min at RT under the hood. Thereafter, the hydration of the tissue was performed by subjecting the section to a series of decreasing concentrations of ethanol solution in distilled water. The sections were incubated twice in 100% ethanol for 5 min at RT, while intermittently shaking the slides. This was followed by dipping the slides once in 96% ethanol for 2 min at RT and then in 70% ethanol for 2 min to complete the re-hydration of the tissues. The tissue sections were then stained with Mayer's hemalum solution (Merck)/Haematoxylin solution for 5-6 min and washed by rinsing at least 3-4 times with distilled water. In order to rinse the slides thoroughly and accentuate the staining, slides were washed with distilled water for 10 min with intermittent shaking followed by washing the slides with distilled water once for 10 min. The slides were then briefly washed in 70% ethanol to improve the eosin staining. Next, the tissue sections were stained in eosin solution for 5-6 min. The tissues were then dehydrated again to fix them. Next, the slides were first briefly dipped in distilled water, followed by immersing the slides in ethanol of increasing concentration i.e. 70%, 96% and 100% (in this sequence) and then finally briefly in ROTICLEAR to dehydrate them completely. The slides were briefly rinsed in 100% ethanol before mounting the sections in glycerol.

### 3.2.23. Immunohistochemical image analyses

The analysis of immunohistochemically treated samples was performed using confocal laser scanning microscopy. The Zeiss 510-CLSM system was used with argon lasers to generate lower wavelength light beams and a combination of three helium-neon lasers for wavelengths above 500 nm. The image analysis was based on the use of various versions of the ZEN software (Blue 2009/ 2011; Black 2012; Lite 2.3).

### 3.2.24. Two-photon imaging

Intra-vital imaging was used as a method to image the injected cancer cells pre-labelled with CMTPX/ CMTMR/ BODIPY and EVs pre-labelled with CMTMR/CMTPX in the intra- and extravascular compartments of the mouse liver. The mouse liver was imaged using a multiphoton LaVision Biotech (Bielefeld, Germany) TrimScope II system connected to an upright Olympus microscope, equipped with a Ti:Sa Chameleon Ultra II laser (Coherent)

tuneable in the range of 680 to 1080 nm. Additionally, an OPO (optical parametric oscillator) compact supported the range of 1000 to 1600 nm. The system is equipped with a 16X water immersion objective (numerical aperture 0.8, Nikon). Single images were acquired from a range 80 µm to 100 µm in depth of the liver tissue along with a z-interval of 2 µm. 820 nm was used as an excitation wavelength, with 1024×1024 pixels and detected by photo multiplier tubes (G6780-20, Hamamatsu Photonics, Hamamatsu, Japan). ImSpector Pro (LaVision) was used as acquisition software. An environmental box maintained a stable 37°C environment.

To facilitate the visualisation of vesicles/cancer cells they were pre-stained with long-lived fluorophore (section 3.2.18.). The blood flow was visualised by injecting FITC-Dextran (low molecular weight 10 KDa) or Blue- Dextran (50-100 µg/ml) in a final volume of 200 µl in PBS into the tail vein of the mice. The mice were anaesthetized by isoflurane (Delta Select GmbH) and fentanyl i.p. (0.05 mg/kg body weight; CuraMed Pharma GmbH) and mounted on a custom-built stage connected to a vacuum ring pump device to image the liver for the detection of pre-labelled MVs or cancer cells. In order to restrict the severity of surgery only a small incision to the abdominal cavity was made to expose the liver lobes. The anaesthesia was applied intraperitoneally every 35 min during the entire time of imaging as a reduced dose (1/3 of the afore-mentioned dose). The imaging was performed after various time points, usually after 2 h, 4 h, 6 h, or 24 h.

### 3.2.25. Scanning electron microscopy: Preparation of samples

Scanning electron microscopy was performed to image and identify the structures of the fibrin network along the vessel walls of the microvasculature in the mouse liver. The liver samples of animals previously injection with cancer cells alone or with cancer cells plus MVs were analysed. The liver tissue was fixed in 2.5% GAD for a minimum of 48 h. The sections of the liver were made using the vibratome. In order to mount the liver tissue onto the vibratome, the fixed tissue was embedded in the 4% agar in PBS using a single well of a 24-well plate as a cast. The block of agar with the tissue was mounted onto the vibratome. Sections of the size ranging from 100 µm – 200 µm were made with a blade frequency of 200 vibrations/min. The sections were immediately transferred in PBS and stored at 4 ˚C until they were prepared further for analysis by scanning electron microscopy.

### 3.2.26. Immuno-fluoro-gold labelling for detection of fibrin fibres

The liver tissue was fixed in a mixture of 2% formaldehyde + 1% GAD overnight at 4 °C. The tissue sections were then washed thrice for 5 min each in PBS+glycin (50 µM) with

continuous shaking. Blocking was performed in 2% bovine serum albumin (BSA) solution in PBS to avoid unspecific binding of the antibody followed by washing, thrice, for 5 min in PBS with 0.2% BSA. Rabbit anti-Fibrinogen primary antibody prepared in PBS with 0.2% BSA (Dako; 1:300) and added for 1 h at RT followed by subsequent washing for 5 min, 10 min and 15 min with 0.2% BSA in PBS. The first secondary antibody an anti-rabbit Nano gold-antibody diluted in 0.2% BSA in PBS (1:100) was added for 30 min followed by a single wash step for 5min with 0.2% BSA in PBS. The second secondary antibody, anti-rabbit Alexa 488-labelled antibody (2 µg/ml) was then added for 1 h at 4 °C. The sections were washed for 5 min, 10 min and 15 min with PBS. Bright field images were acquired using different magnifications with the help of the Zeiss LSM510 and fluorescence was detected by the 488 laser. Areas of interest were marked for subsequent analysis and identification by scanning electron microscopy.

### 3.2.27. *In vitro* fibrin clot analysis by scanning electron microscopy

The scanning electron microscopic experiments were performed to take a closer look at the differences in the various properties of clot formation induced by cancer cells as well as host cells (monocytes). The fibrin-rich clots were generated using 25 µl platelet poor plasma, 50 µl of Alexa 488-labelled fibrinogen (1 mg/ml) and 25 µl of sample solution containing 2000/5000 cancer cells/ monocytes. The clotting reacting was started by adding 30 µl of a 20 mM $CaCl_2$ solution and the reaction was stopped after different time points (0, 2, 10, 30, 45, 75 and 105 min) with the use of formalin solution with final concentration of 2% in the reaction mixture. C-LSM analysis of the clot was done to visualise the clot and obtain the parameters to calculate its density. The fixed clot was also processed to be imaged by scanning electron microscopy at Helmholtz Zentrum Muenchen (Abteilung Analytische Pathologie; Dr. Michaela Aichler, AG Walch). The density was calculated by measuring the intensity profile by ZEN 2009 software. For each image, the number of fibres intersecting with a line of 50 µm length were analysed by accounting for the number of intensity peaks per line. A similar line in an area with no fibres was used as blank. The average of the values of the intersecting peaks was used to determine the density of the fibrin-rich clot.

### 3.2.28. Labelling of primary antibody

Primary antibodies raised in mice were labelled with Alexafluor-mAb labelling kit to avoid signals due to unspecific binding of secondary antibody. In co-staining procedures, to facilitate the use of two antibodies raised in the same animal, only one primary-labelled antibody was used. The labelling was performed as per the instructions in the manual. Anti-fibrin, anti-

stab2, anti-CX3CR1, anti-Ly6G, anti-Ly6C primary antibodies were labelled with the kit. The general procedure required 50-100 µg of antibody which was incubated with the labelling reagent for 3 h at RT or overnight at 4 ˚C. To remove the extra dye in the solution the labelled antibody was recovered using Zeba spin columns equilibrated with appropriate buffer as per the instructions of the manufacturer.

### 1.1.1. Statistical analysis

All the values are represented as mean values. Error bars represent standard error of the mean (SEM) The significance was calculated using the Sigma-Stat software and the results were analysed by one-way ANOVA, Mann-Whitney ranks test or unpaired t-tests. Differences in the mean values with $p<0.05$ were considered to be as statistically significant.

# 4. Results

## 4.1. Expression of TF in pancreatic cancer cells

The pancreatic cancer cell lines used for the experiments were immunostained to examine the expression of the coagulation initiator protein, TF. The two cell lines used were L3.6pl, a human pancreatic cancer line, and KPC, a mouse pancreatic cancer cell line (section 3.2.7). The cells were stained with the appropriate anti-TF antibody (anti-mTF antibody or anti-hTF antibody) and the respective Alexa-546-labelled secondary antibody as explained in section 3.2.17. The cell membrane was identified by staining with the FM-64Fx dye and the nucleus was stained with SYTO-Green at the end of the staining procedure. The cells were then fixed with 1% PFA to facilitate imaging via C-LSM. The image in Fig. 6a shows that the human pancreatic cancer cell line L3.6pl strongly expresses TF (orange dotted structures) on the surface of the cells. In contrast, the mouse pancreatic cancer cell line KPC meagrely expressed TF on the surface of the cells (Fig. 6b).

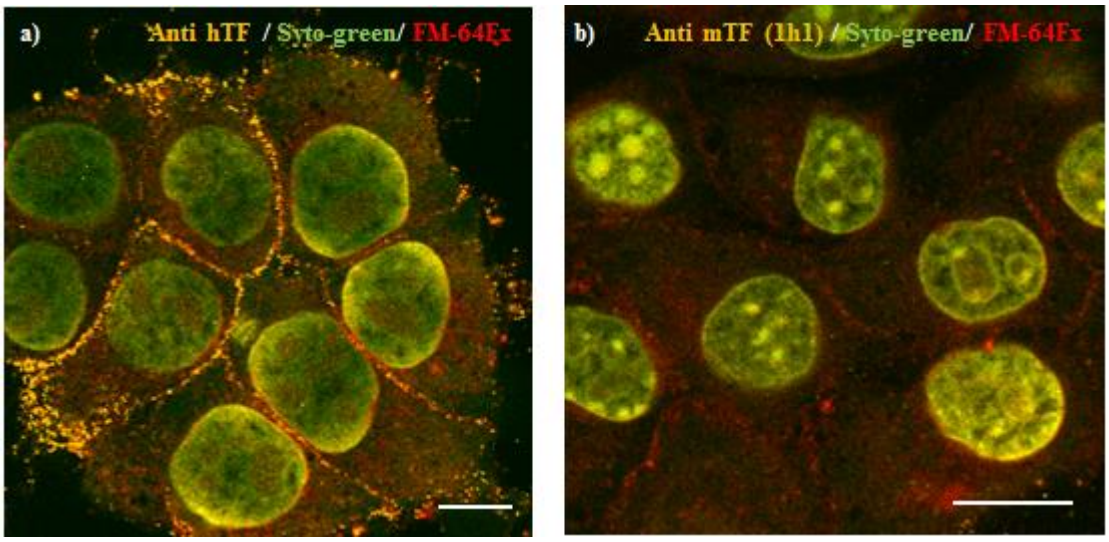


Figure 6: a) L3.6pl cells stained with anti-hTF antibody (50 µg/ml; American Diagnostica) and respective Alexa 546-secondary antibody. b) KPC cells stained with anti-mouseTF antibody (50 µg/ml) and respective Alexa 546-secondary antibody (orange). The cell membrane was stained with FM-64Fx dye (red) and the nucleus with SYTO-Green. Scale bars: 10 µm.

Therefore, it can be hypothesised that the pro-coagulant activity of L3.6pl cell line might be attributed to the surface expression of TF. In contrast the pro-coagulant activity of KPC cells could potentially be due to expression of other pro-coagulant factors on the cell surface.

## 4.2. Procoagulant activities of pancreatic cancer cells

### 4.2.1. *In vitro* analysis

As a next step to test our first hypothesis, to investigate the procoagulant activity of the cancer cells, functional *in vitro* assays were performed. The activation of Factor X, indicating the activation of a central element in the coagulation cascade, was monitored by a chromogenic assay. This chromogenic assay requires the use of S-2222 as substrate to test the extent of formation of Factor Xa (section 3.2.17). L3.6pl cells and KPC cells were tested for FXa formation under different conditions.

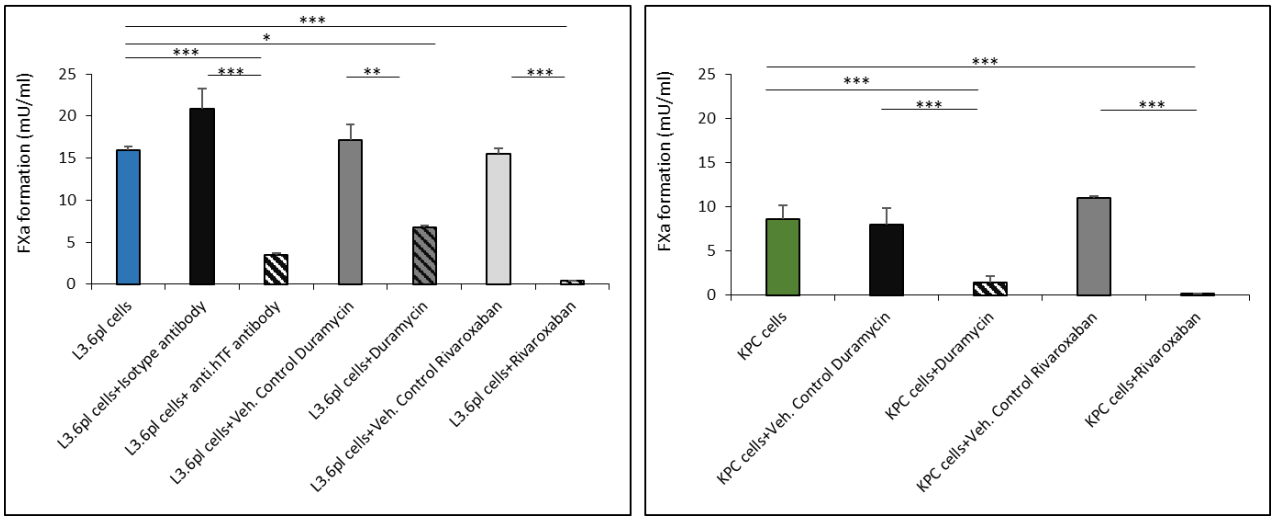


Figure 7: Factor Xa formation with cancer cells. The cells were pre-treated with anti-hTF or anti-mouse1h1 antibodies or appropriate isotype antibody, duramycin (10 µM) or respective vehicle controls. Experiments were performed with 10,000 cancer cells per experiments and the data represents the standard error mean of at least three experiments per condition. * $p < 0.05$; ** $p < 0.01$; *** $p < 0.001$.

In particular the neutralisation of TF by anti-TF antibody and the effects upon pre-treatment with duramycin and rivaroxaban was tested (Fig. 7). Duramycin is a cyclic peptide which specifically binds to PE exposed on the outer membrane of lipid bilayers. The L3.6pl cells stimulated Factor Xa formation to a higher degree than the KPC cells (comparison between Fig. 7a and 7b). The Factor Xa formation by L3.6pl cells was reduced upon pre-treatment with anti-TF antibody. In contrast, no change in Factor X activation was seen after incubation of KPC cells with anti-mTF antibody. This was in accordance with our previous results, indicating that L3.6pl expressed TF on their surface to a much higher extent than the KPC cells (Fig. 6). After treatment with duramycin (10 µm) the Factor X activation of both cell types was strongly reduced (Fig. 7a and b). This indicated that the PE exposure on the plasma membrane played an important role in triggering the pro-coagulant activity of the pancreatic cancer cells under investigated (Fig. 7a

and b). Similarly, pre-treatment with rivaroxaban also showed similar results with decrease in stimulation of FXa formation.

### 4.2.2. Scanning electron microscopic analysis of fibrin fibres *in vitro*

The structure of the fibrin fibres and the overall composition of the fibrin network were further studied by *in vitro* methods. The fibrin clot was generated *in vitro* in the presence/absence of KPC/L3.6pl cancer cells and as a control, by host immune cells (LPS-activated monocytes). To this purpose cancer cells were added to a mixture of labelled fibrinogen and platelet-poor plasma. The clot density, the branching of the fibres and their diameter were analysed as explained in section 3.2.27. Overall the cancer cells formed the clot much faster than the clot generated by the activated monocytes (data not shown). Nevertheless, it was observed that the density of the clot formed by the cancer cells (Fig. 8a and b) appeared not to be strongly different from the one formed by the activated monocytes (Fig. 8c). The images shown below are indicative of a clear association of the fibrin clot with the cancer cell. In addition, the cancer cell also shows some membrane blebs and EVs in its vicinity.

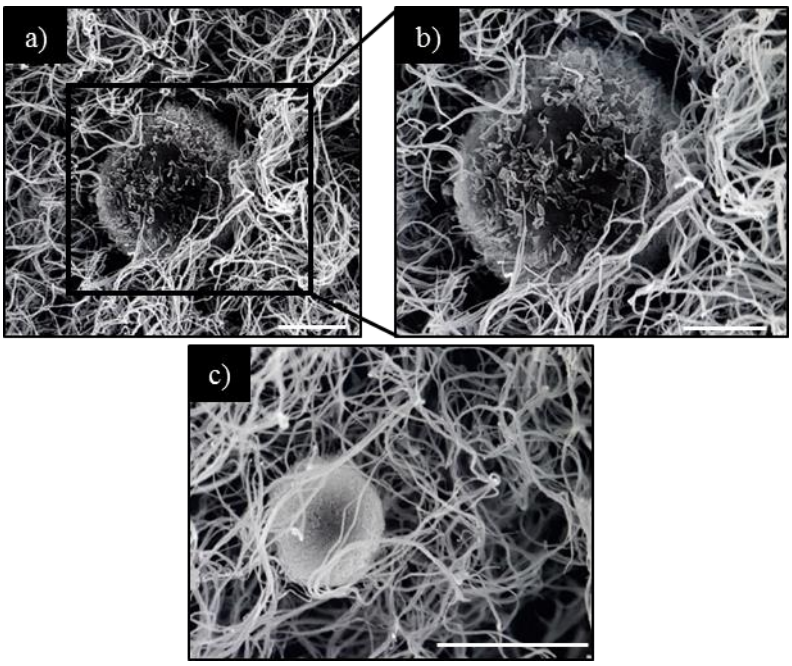


Figure 8: Scanning electron microscopic images of fibrin clots generated *in vitro* as explained in section 3.2.27. (a) Clot generated by L3.6pl cell. (b) Figure inset was magnified to view the cancer cell and the membrane blebbing. (C) Fibrin clot generated by LPS stimulated inflammatory monocytes isolated from human blood samples.
Scale bar 5 µm.

### 4.2.3. Release of EVs by pancreatic cancer cells

The different pancreatic cancer cell lines were tested for oncosome production. The supernatant of KPC and L3.6pl cells was processed for isolation of oncosomes as described in section 3.2.12. The cancer cells were stained with membrane markers (diL 550) and nuclear marker (Syto-62). The oncosomes in this case were detected as spherical membrane blebs of varying sizes at the surface of the cancer cells. These blebs likely represented large oncosomes did not contain any traces of nuclear material and the boundaries of the vesicles were marked by membrane markers (Fig. 9). The particles ranged from a size of 2 µm – 7 µm.

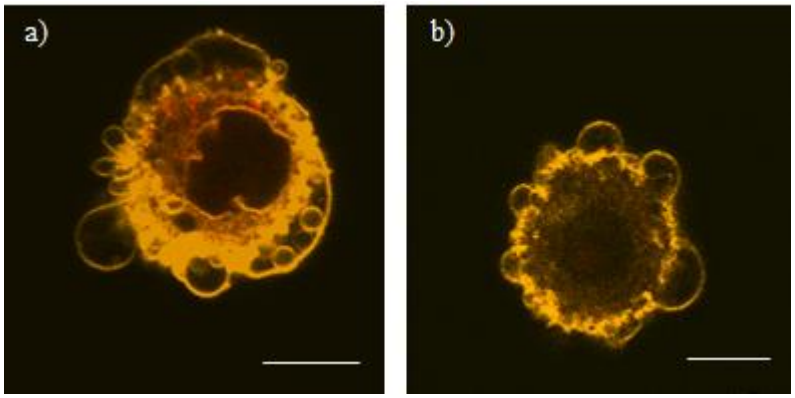


Figure 9: Oncosome production *in vitro*. a) KPC cells and b) L3.6pl cells in suspension showing production of EVs with characteristic of large oncosomes. The membrane was marked by DiL-550 dye which also stained the membrane blebs. Scale bar 10 µm.

The release of EVs, especially oncosomes was also analysed in other pancreatic cancer cell lines too. The extent of oncosome production was analysed as a total protein content of oncosomes which were isolated from the supernatants of different cell lines. Six cell lines with different genotypes were analysed, three of which were isolated from metastatic pancreatic tumours and three from non-metastatic pancreatic tumours. The metastatic cell lines that were used are as follows: 5320 that contained a p48-Cre promoter which is specific for pancreatic cancer, *KRAS* mutation (G12D) by knock-in in the endogenous locus under the control of a stop cassette Lox-Stop-Lox (LSL) along with a reporter gene *PCNA* followed by an internal ribosome entry site (IRES) (p48-Cre +/-, LSL-*KRAS*+/-, LSL-PCNA-IRES +/-); number 53631, which had a p48-Cre promoter with *KRAS* mutation (G12D) (p48-Cre+/-, LSL-*KRAS*+/-), and cell line S134 which contained a Pdx-Flp promoter with *KRAS* mutation (G12D) under the control of Flox-Stop-Flox (FLF) stop cassette with (Pdx-Flp +/+, FSF-*KRAS* +/-). The non-metastatic cell lines used were 8182, which had a p48-Cre promoter and a *KRAS* mutation (G12D) under the control of a stop cassette LSL along with a reporter gene allele Tva (p48-Cre +/-, LSL-*KRAS* +/-, Tva +/+); number 5671 that contained a p48-Cre promoter and a *KRAS* mutation (G12D) along with two reporter gene allele Tva and PCNA-ATG all under the control of a stop cassette LSL(p48-

Cre +/-, LSL-PCNA-ATG +/-, LSL-Tva +/-, LSL-*KRAS* +/-) and number 16990 which had the same genotype as cell line number 53631(p48-Cre+/-, LSL-*KRAS*+/-). The oncosomes from the supernatant of a confluent layer of respective cell lines were isolated as described in section 3.2.12 and were estimated as a total protein content of the oncosome pellet (section 3.2.13.). The metastatic cell lines showed on an average increased production (0.052 µg/ml) of oncosomes accounting to almost double the amount as compared to the average production (0.024 µg/ml) by the non-metastatic cell lines. Nevertheless, one of the non-metastatic cell lines (16990) was seen to produce an amount of oncosomes close to one of the metastatic-cell lines (0.047 µg/ml) which may be attributed to the similarity in genotype to the metastatic cell line 53631. Therefore, these results indicate that the production of oncosomes might be dependent on the metastatic potential of these cell lines.

### 4.2.4. Visualisation of PE exposure *in vitro*

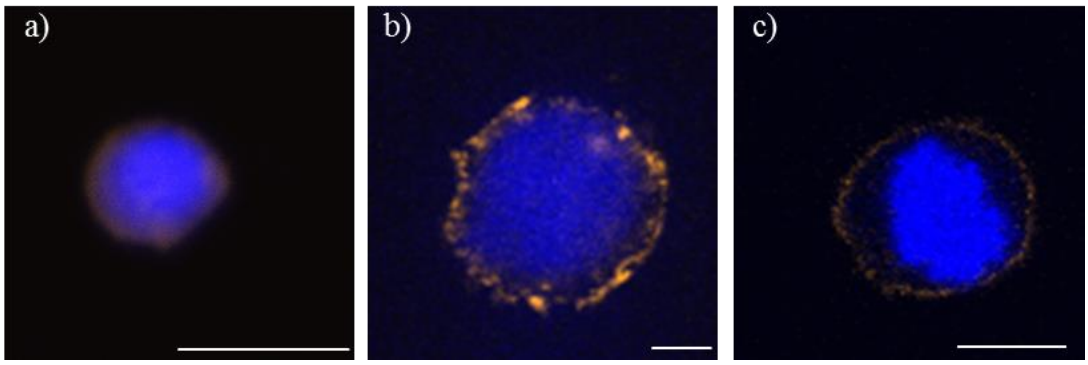


Figure 10: Shows the exposure of PE on the surface of a) unstimulated monocyte b) KPC cancer cell and c) KPC-MUC1 cancer cells. The PE expression was visualised by biotin-labelled duramycin and recognised by anti-biotin secondary antibody as described in section 3.2.16. The pre-coating of cancer cells with biotin labelled duramycin was performed as mentioned in section 3.2.3. followed by immune-staining. A) The monocyte showed reduced PE exposure. b) The KPC cancer cells showed a stronger membrane staining of PE whereas (c) the MUC1 downregulated cell showed a reduced staining of PE on the surface. Scale bar: 10 µm.

The surface exposure of PE was examined by immunostaining procedures as described in section 3.2.18. in both, KPC cells as well as in KPC-MUC-1 downregulated cells. We have seen that downregulation of MUC-1 in KPC cells reduced the procoagulant activity of the cells (data not shown) and therefore might affect the surface exposure PE, especially in the TF-independent mechanism. In the control cells i.e. the unstimulated monocytes a very weak exposure of PE was detected. Whereas the KPC cancer cells, it was seen that PE was distributed over the entire surface of the KPC cells in a rather punctate pattern (Fig.10a). In contrast, PE exposure was strongly reduced in case of the KPC cell with reduced MUC-1 expression (Fig. 10b). Therefore, downregulation of MUC-1 reduced the surface exposure of PE. This in turn might be responsible

for the reduced pro-coagulant activity of the cells with reduced MUC-1 expression seen in our previous work.

To investigate this aspect further the exposure of PE was also analysed via a functional assay by employing artificially synthesised liposomes and MVs. The liposomes containing PE+PC, PE+PS or PC (control) were synthesised as explained in section 3.2.16. Functional assays like chromogenic assay evaluating the FXa stimulation and TEG were performed (Fig. 11).

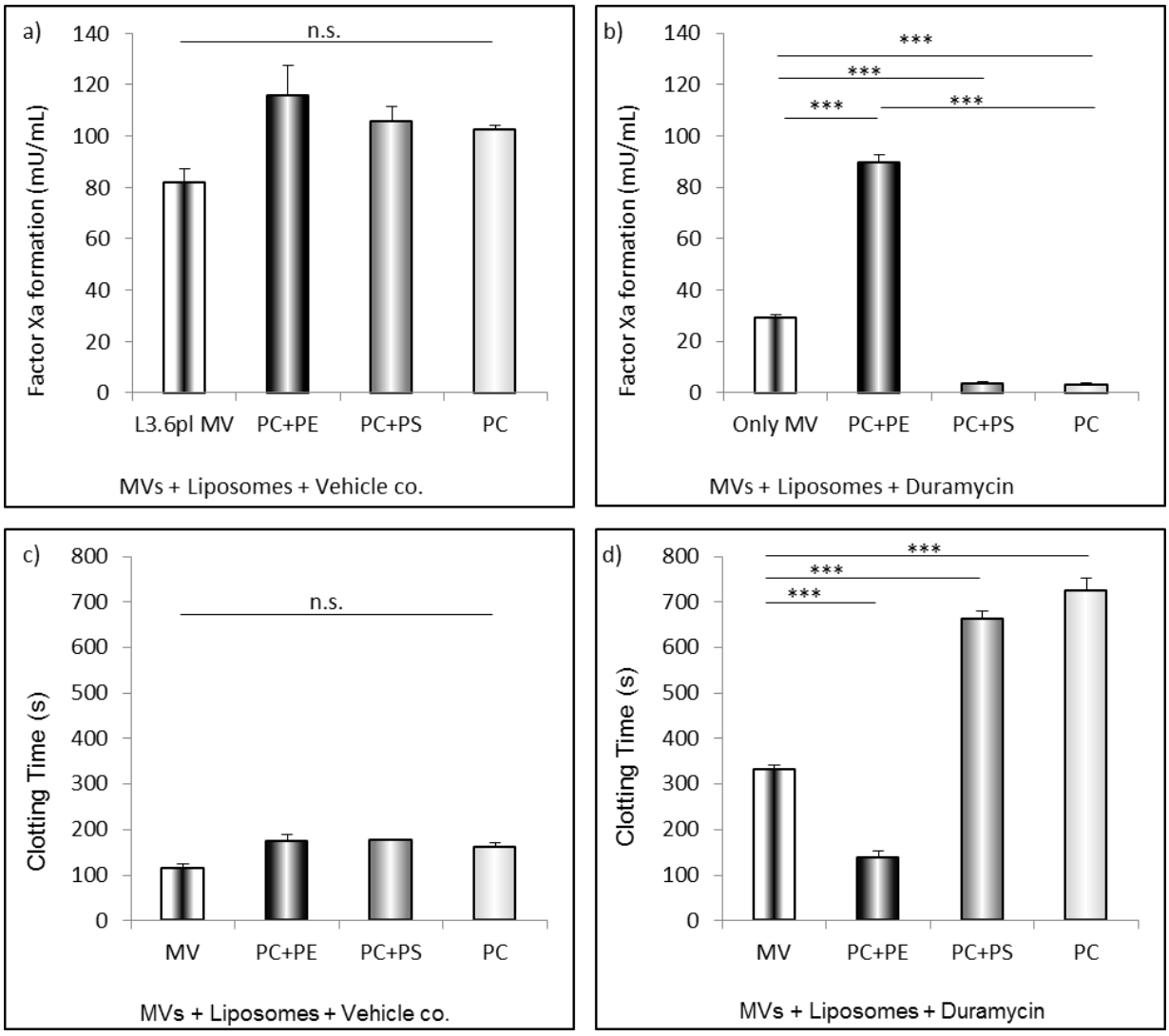


Figure 11: a) and b) Factor Xa formation assay conducted with L3.6pl MVs and different liposomes as indicated below each bar without duramycin (vehicle control) or with duramycin, respectively. c) and d) TEG with whole blood along with L3.6pl MVs and different liposomes as indicated below each bar without duramycin (vehicle control) or with duramycin, respectively. n=3 mean values +/- SEM. *** $p<0.001$; n.s. non-significant.

Highly pro-coagulant L3.6pl MVs were incubated with the liposomes either with or without duramycin. It had already been shown in figure 7a, that duramycin significantly reduced the

procoagulant activity of the MVs. Figure 11b shows that the activation of FXa formation was reduced in the case where MVs and PC+PS or PC containing liposomes were treated with duramycin. In the case of PC+PE containing liposomes and MVs with duramycin the factor Xa formation was partially activated. The clotting time was also reduced. Both, these results suggest that under the conditions analysed duramycin specifically binds to PE.

### 4.3. Bio-informatics analysis of genes involved in phospholipid translocation

The role of altered surface exposure of PE in tumour cells was studied further by examining for potential mutations in genes involved in the translocation of phospholipids across the plasma membrane. First, the exposure of candidate proteins involved in phospholipid transport like ATP11C, TMEM16J and TMEM16F was downregulated by means of siRNA. Anti-TMEM16F antibody was also used to block this protein. Functional analysis by TEG indicated no significant changes in the clotting time under all conditions (Fig. 12).

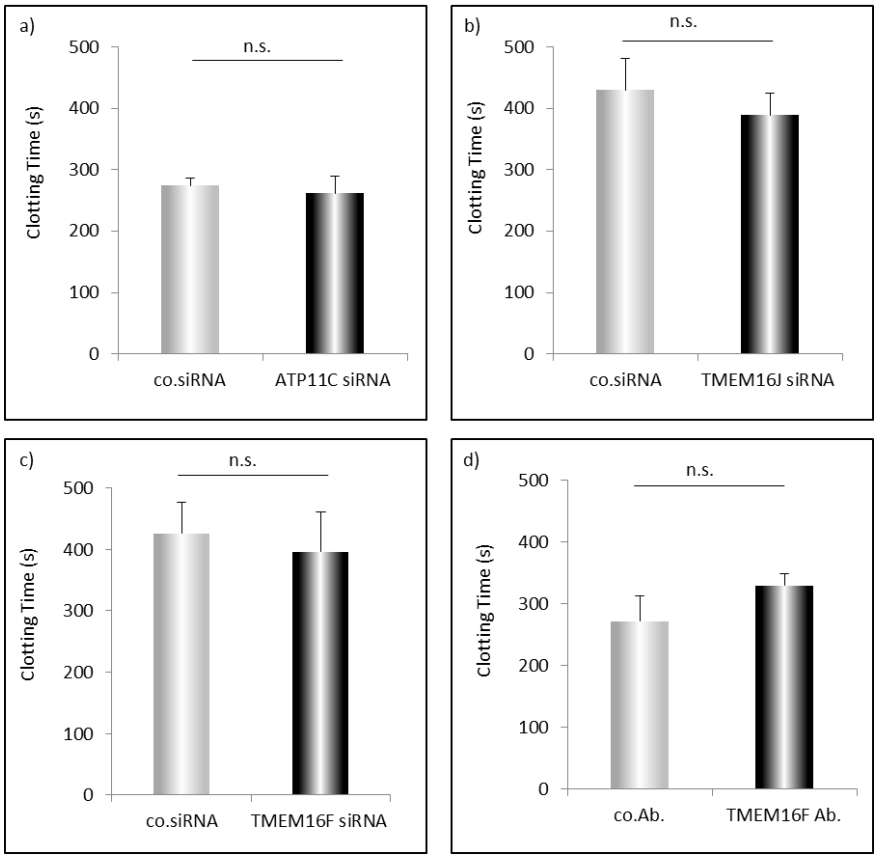


Figure 12: KPC cells were transiently transfected with siRNAs for a) ATP11C b) TMEM 16J c) TMEM16F and d) anti-TMEM16F antibody. The clotting time was analysed by TEG. n=3 mean values +/- SEM. n.s.: not significant.

Therefore, to broaden the search for potential candidate genes the online database, The Cancer Genome Atlas (TCGA) were used to screen for the occurrence of possible mutations in pancreatic cancer patients. This database contains information from various ongoing genomic

sequencing projects on pancreatic carcinoma. Genes hypothesised to be involved in phospholipid translocation like P4-ATPases, phosphatidylethanolamine binding proteins (PEBP), anoctamins to mention a few, were included in a list of a test group of 141 genes. A list of entries carrying mutation in any of the 141 genes was compiled and analysed by bioinformatics tools to extract those genes which showed maximum frequency of mutations. The pool of samples contained 178 tumour samples which were compared amongst each other for differences in their protein expression profiles of the genes. Out of the 141 genes, 89 genes were chosen based on the analysis that more than 50% of the samples reported mutations in these 89 genes. After normalising the genes so that they are nearly in the same range (c-score normalisation) the differences in the expression pattern were represented as a heat map. In the Fig. 13 each row represents the protein expression data from a single gene and each column represents a single sample (i.e. data from a single patient).

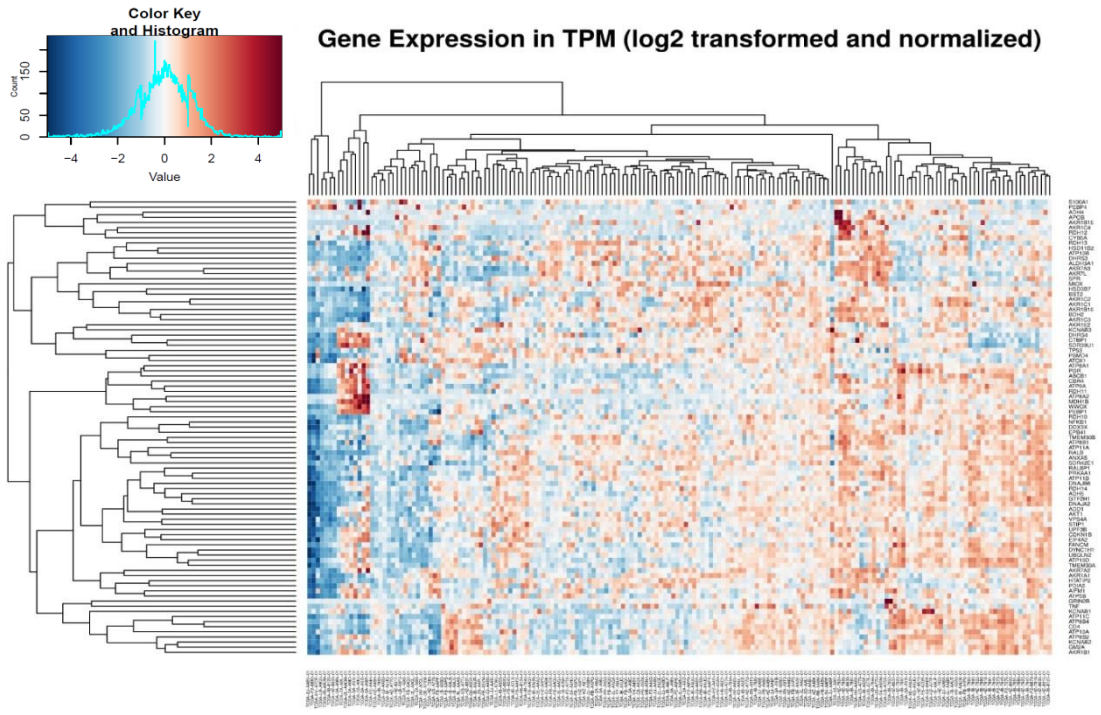


Figure 13: Heat map of protein expression profiles of pancreatic cancer patients (horizontal axis) vs the protein expression profiles of each gene (vertical axis). Each entry on the horizontal axis corresponds to each patient and the vertical axis shows each gene. Blue: indicates low expressed genes; red: highly expressed genes.

The data set was organised such that patient entries and protein expression data of the genes with similar profiles are clustered together. The colour key with the histogram of the data set is shown in the top left corner of Fig. 13 where blue represents low expression of proteins and red represents high expression of the respective protein. The patches (dark red) represent highly

expressed genes in patients. After co-relating each gene from different clusters with the frequency of mutation no significant relation was seen. Nevertheless, *TP*53 was seen to be mutated maximally followed by APOB, DYNC1H1 and ATP10A. Most of the mutations were substitute-missense mutations. Another database COSMIC, was also used to analyse the same group of genes to check for the frequency of mutation. As expected the maximum number of mutations occurred in *TP53.* This was followed by the P4-ATPase ATP8A2 and the P4-ATPase ATP10A which ranked third in this list. Furthermore, upon analysing a subset of the data, we searched for the location of the mutations in the various domains of the P4-ATPases. This sub-set revealed that most of the mutations were present in the cytoplasmic domain close to the phosphorylation and nucleotide binding sites of the protein. Since phosphorylation and protein binding sites are essential for the normal functioning of the protein, mutations in these domains are likely to impair its physiological functions and hence to reduce the transfer of phospholipids such as PE to the inner leaflet of the cell.

### 4.4. *In vivo* analysis of microvascular fibrin formation

The hypothesis that the cancer cells and their MVs support the activation of blood coagulation *in vivo* was investigated further. To pursue this, the pancreatic cancer cells (2 x $10^6$) and MVs (150µg) were injected intravenously via the tail vein in WT mice.

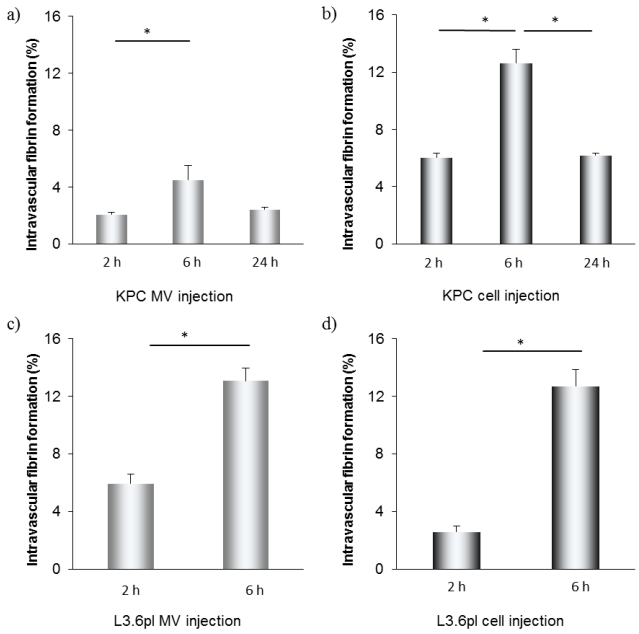


Figure 14: Graphical representation of the fibrin-covered area in the microvasculature a) after KPC MV injection b) KPC cell injection after different time points c) after L3.6pl MV injection d) L3.6pl cell injection after different time points respectively (section 3.2.20). Fibrin covered area was measured encircling the fibrin stained area (stained with primary-labelled anti-fibrin antibody) of the total intravascular area (measured by encircling the vessels stained with anti-Stab2 antibody). The Zen2.3 lite- blue edition program was used to make the calculation. Each bar represents a mean $\pm$ SEM from n=3. * $p < 0.05$.

Subsequently, the fibrin-covered area was measured in the blood vessels of the liver at different time points after administration of the MVs or cells. The injections were made as per the schemes described in section 3.2.2. The fibrin-covered area was calculated as the percentage of intravascular area covered by fibrin in liver microvessels as labelled with anti-stab2 antibody, a specific marker of sinusoidal endothelial cells.

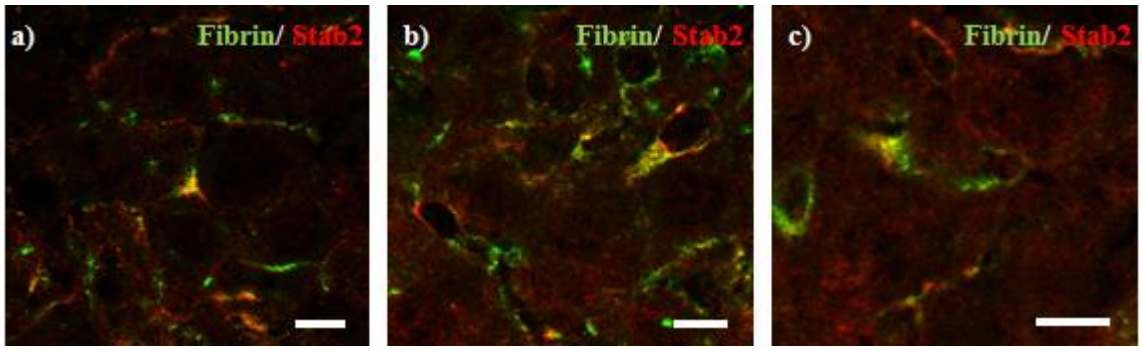


Figure 15: Immuno-histochemical analysis of mouse liver tissue. The mice were injected with KPC cancer cells and were liver samples were analysed after a) 2 h, b) 6 h, and c) 24 h after the injection so as to determine the extent of microvascular fibrin formation. The vessels were stained with anti-stab2 antibody (red) and anti-fibrin antibody (green). Scale bar: 5 µm.

As depicted in Fig. 14a and b fibrin formation was already evident after 2 h of cancer cells' injection or their MVs. In case of both, KPC cells and their MVs, the peak of fibrin formation was observed at 6 h (Fig. 14a and b). The fibrin-formation area was lower at 24 h (Fig. 14a and b), which could be a consequence of fibrinolysis. A similar analysis was also done for the L3.6pl cells and their MVs. Similar to what has been observed with KPC cells, it was also observed that the fibrin formation was higher at 6 h as compared to 2 h (Fig. 14c and d). This indicated that fibrin formation reached a maximum at 6 h, which persisted for a while, and then a reduction in the fibrin formed was detected. Fig. 15 shows IHC images of microvascular fibrin formation in the mouse liver induced after 2 h, 6 h, and 24 h of KPC cancer cell injections, respectively.

## 4.5. Fibrin fibre imaging by scanning electron microscope (SEM)

### 4.5.1. *In vivo* analysis

Based on the results indicating that pancreatic cancer cells and their MVs induced fibrin formation in their liver microvasculature, further structural characterisation of the fibrin-rich aggregates was performed. WT animals were intravenously injected with cancer cells or cancer cells plus their MVs and the liver tissue was harvested 6 h after the injection. Vibratome sections of liver tissue were fixed in 2.5 % GAD and prepared for analysis by scanning electron

microscopy. The vessels which were exposed on the surface of the thick vibratome sections were more closely inspected. Microvessels with diameters ranging between 5 µm and 30 µm were analysed to detect the presence of fibrin network (Fig. 16a). The inset Fig. 16b shows a magnified portion of the microvessel where it was seen that the fibrin fibres were attached closely to the vessel wall. The small openings like structures seen on the wall of the vessels represent fenestrations. Fig. 17a shows a vessel with a diameter of approximately 30 µm that contains a fibrin clot attached to the wall of the vessel. The figure inset clearly shows that the clot is a dense structure composed of fibrin fibres together with RBCs (recognised by their size and concave surfaces with saucer like morphology), leukocytes (recognised by their size and cell extensions) and platelets (detected by their size and irregular surface) along with some type of vesicles. Similar fibrin fibres forming a network over the vessel wall entrapping blood cells could also be seen in Fig. 17b. This indicated that the vessel walls of liver microvessels were indeed covered with fibrin (along with blood cells) as shown by the immune-histochemical analysis in Fig. 15.

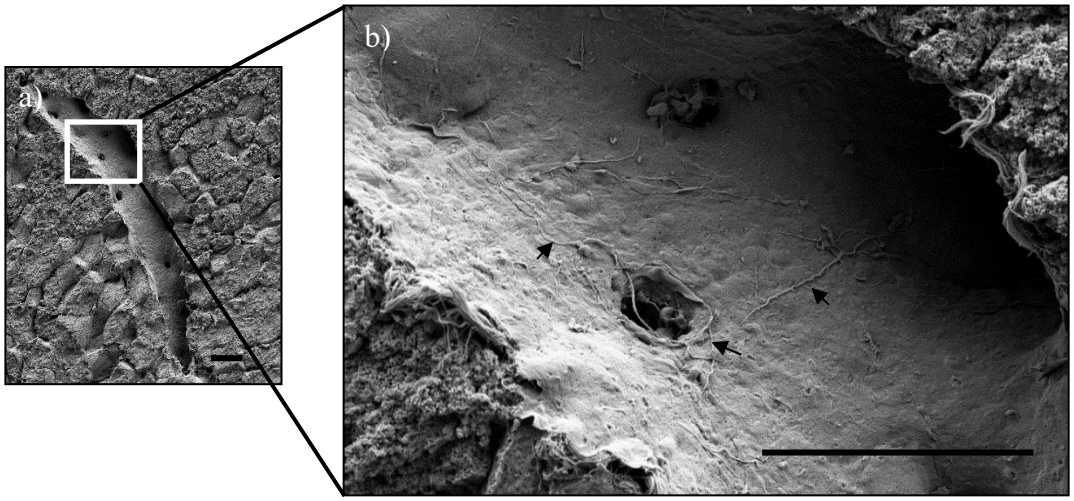


Figure 16: a) The figure shows a liver microvessel (10-12 µm) with fenestrations. The figure inset (b) on the right magnifies the vessel wall covered with single fibrin fibres (indicated with black arrows). The liver tissue was prepared as explained in section 3.2.25. The animal was injected with KPC MVs + KPC cells and the liver was harvested 6 h after injection. The liver tissue was fixed in 2.5% GAD for 2 h and SEM imaging was performed. Scale bar: 10 µm.

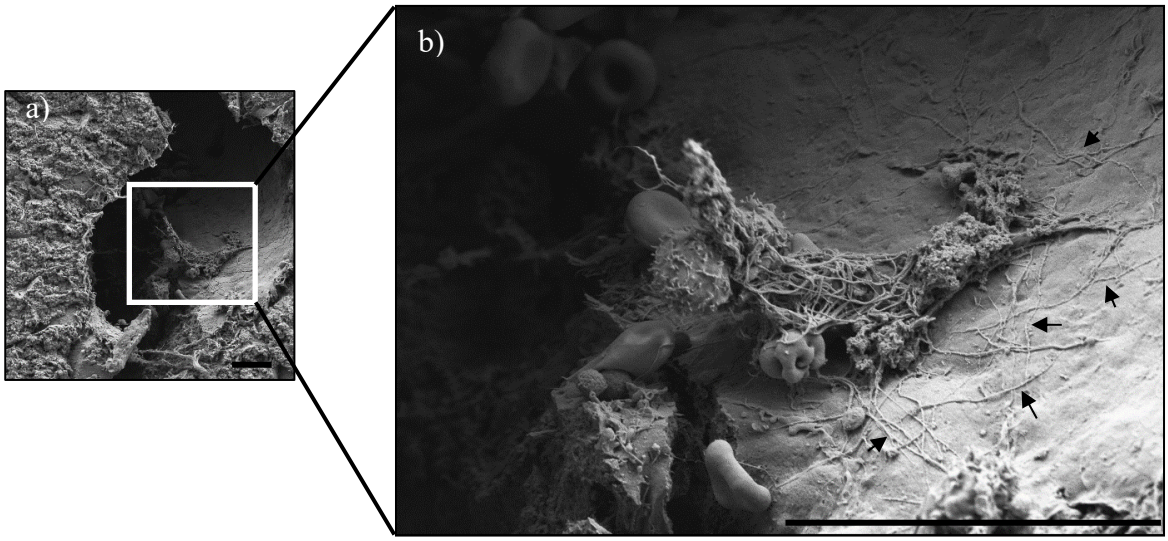


Figure 17: Liver microvessel with a fibrin-rich clot on the vessel wall. This WT mouse was injected with KPC MVs + KPC cells and the liver was harvested 6 h after injection. Single fibrin fibres spanning the vessel wall form a loose network (indicated by black arrows). The liver tissue was fixed in 2.5% GAD for 24 h and SEM imaging was performed. Scale bars: 10 µm.

Microvascular occlusion due to fibrin-rich clots formation was also detected in the sections (Fig. 18). Fig. 18a shows a vessel that is occluded by a fibrin-containing thrombus. The clot is mostly composed of RBCs, leukocytes, platelets and vesicles. It appears that the fibrin network is needed to hold the clot together. A part of the clot was viewed under higher magnification to clearly visualise the fibrin network and the different cell types (Fig. 18b). Thus, these results suggest that the presence of intravascular tumour cells and their MVs induce the formation of fibrin- and RBC-rich microthrombi in the liver microvessels.

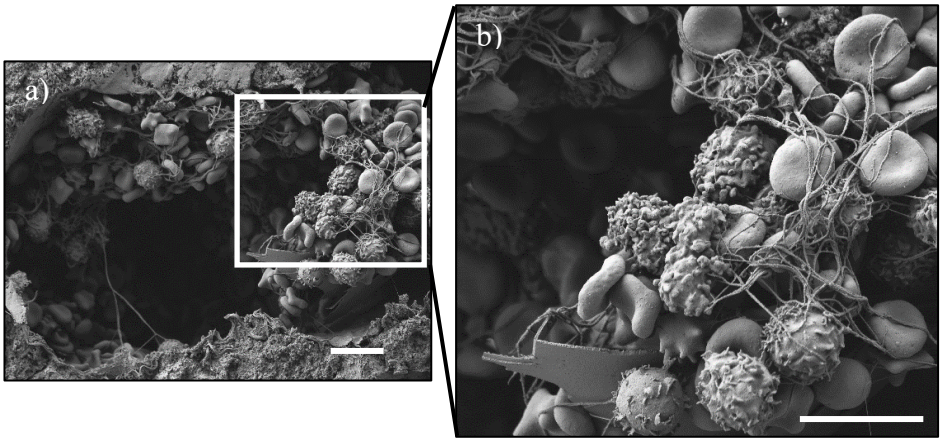


Figure 18: a) Liver microvessel occluded by fibrin clot consisting of RBCs, leukocytes and platelets. The figure inset is magnified (b) to show a part of the clot. The animal was injected with KPC MVs + KPC cells and the liver was harvested 6h after injection. The liver tissue was fixed in 2.5% GAD for 24h and SEM imaging was performed. Scale bars: 5 µm.

### 4.5.2. Immuno-fluoro-gold labelling of fibrin fibres *in vivo*

The fibrin fibres generated by tumour cells *in vivo* were analysed further. The liver sections from mice injected with KPC cancer cells and harvested 6 h after injection were tested for the presence of microvascular fibrin by immune-histochemical procedures before being processed for analysis by scanning electron microscopy. Vibratome-sections of mice livers were stained with primary anti-fibrinogen antibody. The organs were fixed with a mixture of 2% PFA and 1% GAD before immunogold-staining to facilitate parallel analysis by CLSM along with scanning electron microscopy. The staining was performed as per the protocol stated in section 3.2.26. The staining with anti-rabbit Nano-gold particles was performed to confirm that the fibres detected were indeed fibrin. The fibres were seen to be closely attached to the vessel wall (Fig. 19a). The areas indicated with blue arrows in Fig. 19b clearly show Nano-gold particles on the fibres, confirming that the fibres seen in all the scanning electron microscopy images were fibrin fibres.

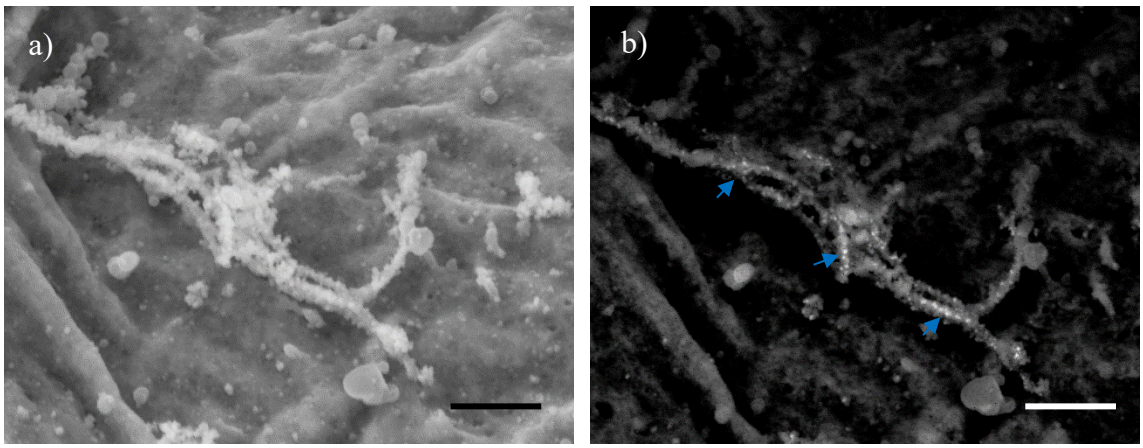


Figure 19: Scanning electron microscopic image of a vessel wall showing a fibrin fibre in the liver microvasculature. a) Shows the structure of the fibres. b) Shows the same fibre to reveal the signal from the nano-gold particles (white bright spots on the fibre). The mouse was injected with KPC cells and the liver was harvested 6 h after injection, fixed with a mixture of GAD and PFA (described in section 3.2.25.). Scale bar: 5 µm.

## 4.6. Extravasation of tumour cells and tumour MVs *in vivo*

### 4.6.1. Intra- vs extravascular localisation of cancer cells and their MVs

The extravasation of MVs from KPC cancer cell line was determined by analysing the localisation of pre-stained MVs (by CMTPX dye) with respect to their localisation being intravascular or extravascular. MVs were injected in WT mice as described in section 3.2.2. where the pre-stained MVs were injected via the tail vein followed by IHC analysis. The liver microvessels were identified by staining the sinusoidal endothelial cells (SEC) with anti-Stab2

antibody. Extravascular MVs were already detected after 6 h of injection of MVs (Fig. 20). Within 48 h 95% of the tumour MVs were detected in the extravascular tissue (Fig. 20).

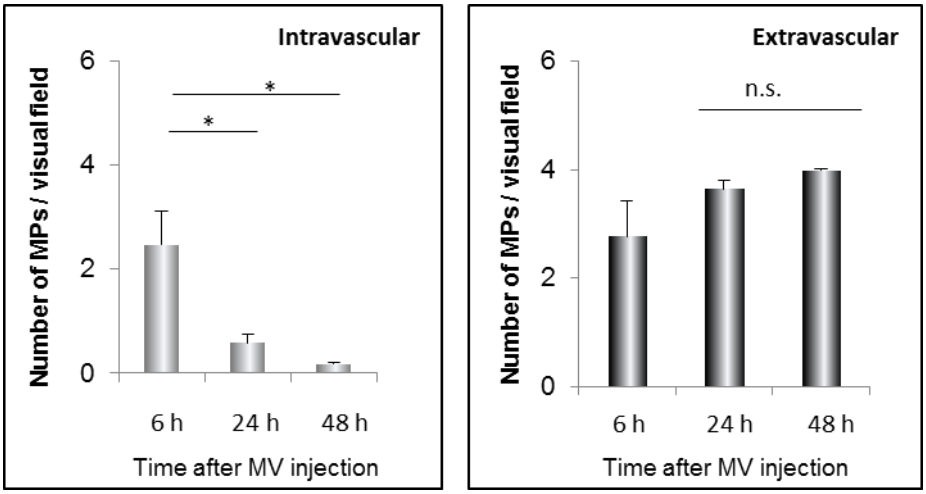


Figure 20: Localisation of tumour MVs labelled with CMTPX detected in the microcirculation of the liver. Shows the analysis of MVs per visual field as an average of 10 visual fields. Results are mean ± SEM. Each bar in the graph represents results from 3 independent experiments. * $p < 0.05$; n.s. not significant.

Further, the extravasation of the cancer cells was studied in the liver microvasculature. Pre-labelled KPC cells, following their injection into WT mice (section 3.2.2.) were detected in the mouse livers, both in the intravascular and extravascular compartments. The extravasation of the cancer cells begins to appear at 6 h and continued until 48 h (Fig. 21 a-d). In order to further follow the fate of the cancer cells in the tissue, long-term experiments with CMTPX-labelled KPC cells were performed. Thus, the localisation of the cancer cells was determined after 8 and 14 days (Fig. 21e and f) of injection. After 14 days all cancer cells were detected to be localised in the tissue (Fig. 21f).

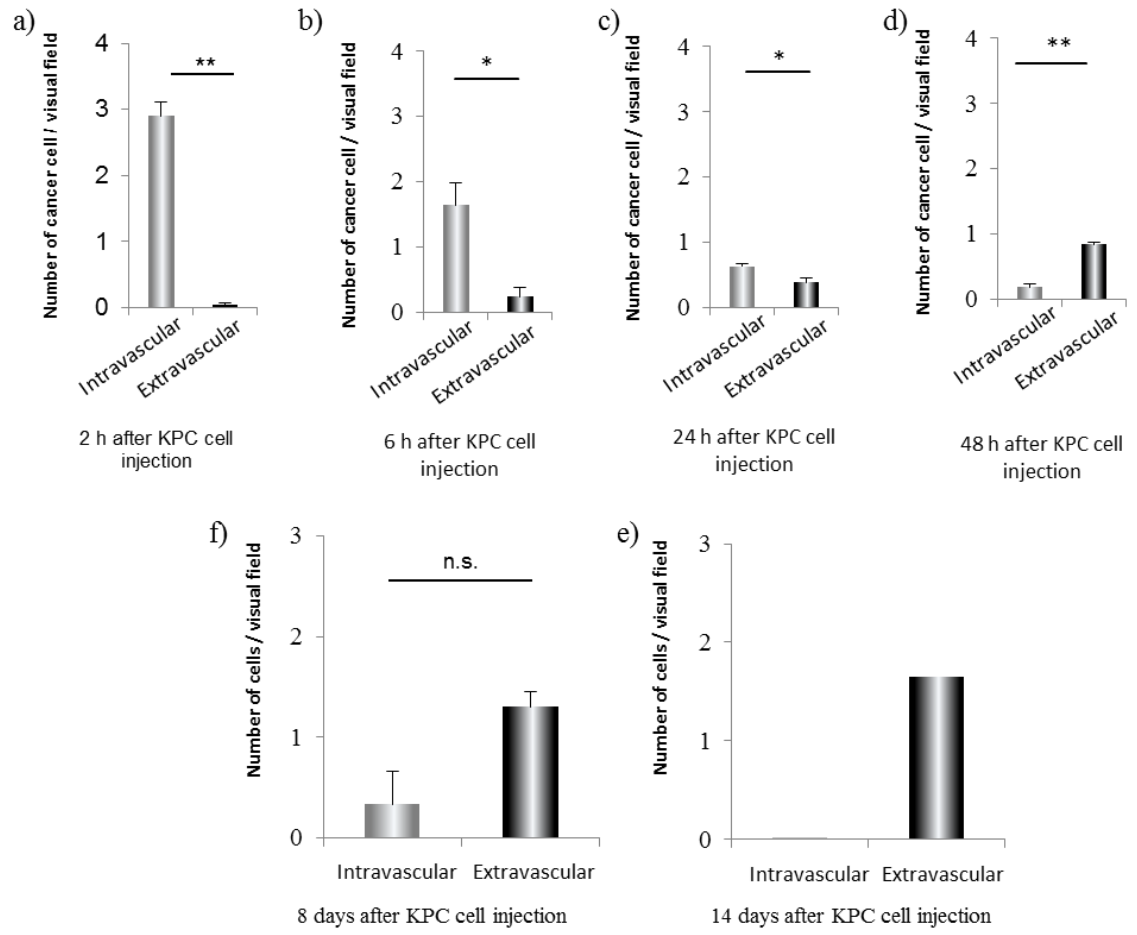


Figure 21: The intra- vs extravascular localisation of KPC cancer cells in the liver microcirculation 2 h to 14 days after administration of CMTPX (red) pre-labelled KPC cells into WT mice (section 3.2.2.). The localisation of the CMTPX-labelled cells in the intravascular vs extravascular compartment of liver tissue. The vascular compartments were identified by staining the SECs with anti-stab2 antibody. a), b), c) d), e) and f) represent graphs after 2 h, 6 h, 24 h, 48 h, 8 days and 14 days of cell injection, respectively. Results are mean +/- SEM of at least n=3. * $p < 0.05$; ** $p < 0.01$.

### 4.6.2. Tracking of cancer cells by intravital 2-photon microscopy

2-photon live imaging technique was implemented to track the movements of the pre-labelled cancer cells in the liver microvessels. The imaging was performed as mentioned in section 3.2.24. KPC cells pre-labeled with CMTPX were injected into the WT mice and blood flow in the vessels was visualised using FITC-dextran. Intravital imaging was performed over a continuous range of time periods beginning from 2 h to 4 h or from 5 h to 9 h after cancer cell injection. It was observed that the cancer cells were already arrested in microvessels at 6 h (Fig. 22). It was also observed that the cancer cells appeared to cause a ‘stop’ in the blood perfusion (as depicted by the vessel marked by yellow dotted line in Fig. 22d).

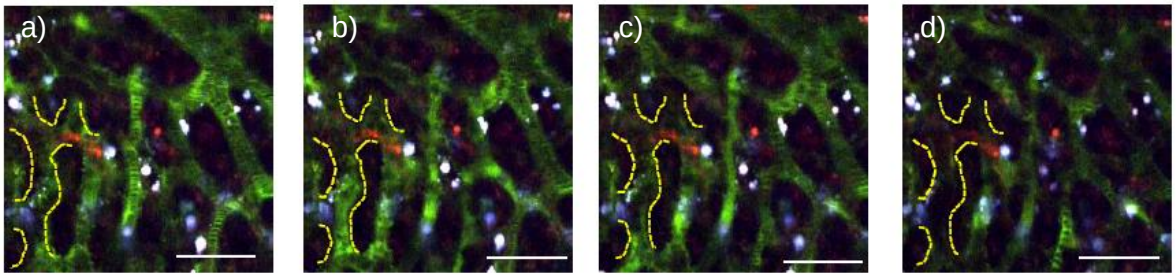


Figure 22: A series of images showing the blood flow 6 h after injection of KPC cells pre-labeled with CMTPX. The blood flow in the liver microcirculation was detected with FITC dextran. The area outlined by yellow dotted lines indicates the area of stop flow, where cancer cells (red) are seen to be arrested. Panels a), b), c), and d) correspond to 6 h, 6.5 h, 7 h, and 7.5 h respectively. Refer to video 1 in section 6. Scale bar: 50 µm.

This obstruction in the blood flow was not seen at the earlier time points until 4 h. Interestingly, as shown in Fig. 23 microvessel outlined in yellow where no reduction or stop in the flow was detected. Particularly the Fig. 23a and 23b corresponding to increasing time 2 h and 2.5 h respectively (imaging period 2 h-4 h), no indications of reduction in the blood flow was observed. However, during the same time period the cancer cells were seen to be arrested in the microvessels already at 2 h post injection.

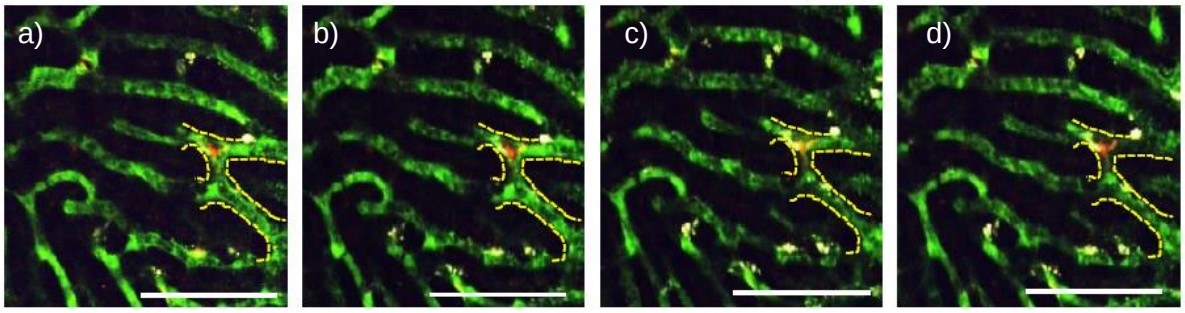


Figure 23: The series of figures showing the blood flow starting 2 h after KPC cell injection (pre-labelled with CMTPX). The blood flow in the microvessels was detected with FITC dextran. The yellow dotted line marks a microvessel. Pre-labelled cancer cell arrested in this vessel could also be clearly seen (red). Panels a), b), c), and d) correspond to 2 h, 2.5 h, 3 h, and 4.5 h respectively. Refer to video 2 in section 6. Scale bar: 50µm.

During the live imaging between time period from 6 h to 9 h, near the area of flow-stop, extravasation of cancer cells in the liver tissue was seen 6 h after injection of pre-labelled cancer cells. One such representative example for cancer cell extravasation is shown in Fig. 24. The encircled area highlights a single cancer cell which was first arrested in the microcirculation (Fig. 24a) was seen to move out from the vessel (Fig. 24b - d) and to travel further within the perivascular tissue (Fig. 24f - h).

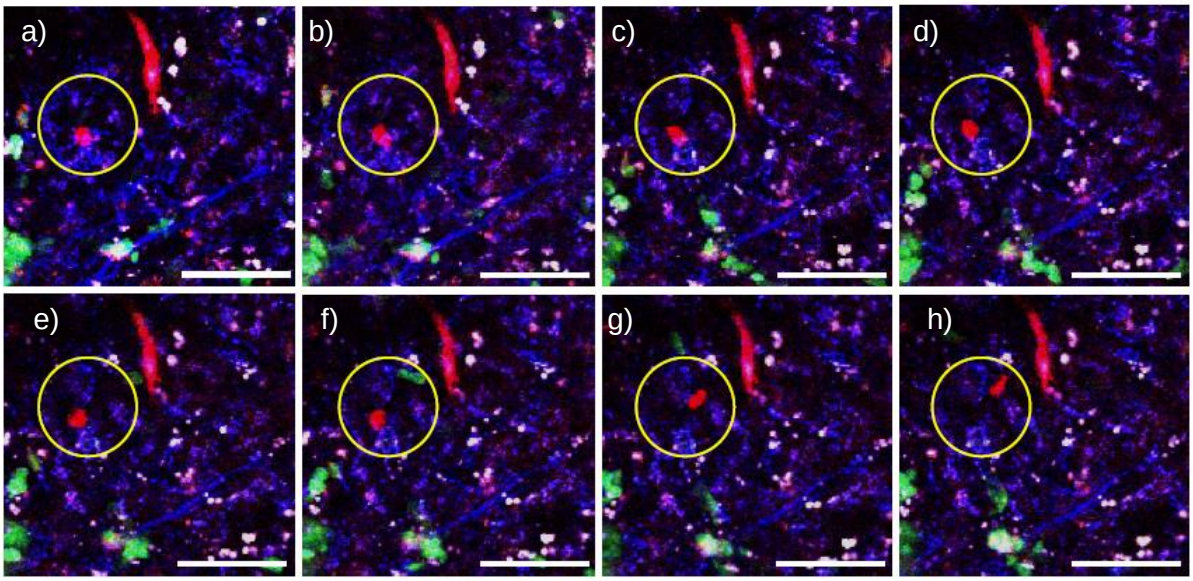


Figure 24: Series of images showing extravasation of a single cancer cell between 6 h-7 h. The KPC cells were injected in LysM$^{+}$eGFP-labelled mouse and the liver was imaged by 2-photon microscopy. The blood flow was visualised by blue dextran. The panels (a)-(h) show images from the video with increase in time from a) 5.5 h; b) 6 h; c) 6.5 h; d) 7 h; e) 7.5 h; f) 8 h; g)8.5 h; h) 9 h. Refer to video 3 section 6. Scale bar: 50 µm.

## 4.7. Immuno-histochemical analysis of EVs

### 4.7.1. Co-localisation of MVs

Cancer cells are known to secrete MVs in addition to large vesicles. The MVs were isolated from tumour cell supernatants (section 3.2.12.). The MVs were pre-labelled with CMTPX (red) and were injected in WT mice as described in section 3.2.2. To address our third hypothesis, we analysed the localisation of the MVs and their association with the immune cells. It was seen that the MVs were engulfed by host cells staining positive for the expression of F4-80 in close proximity to sinusoidal endothelial cells. These results indicated that the MVs strongly associated with the immobilised macrophages of the liver microcirculation (Kupffer cells). Fig. 25a indeed shows MV inside Kupffer cells. The quantification of the association of MVs with macrophages in Fig. 25b shows that 95% of MVs are already associated with Kupffer cells 6 h after MV injection.

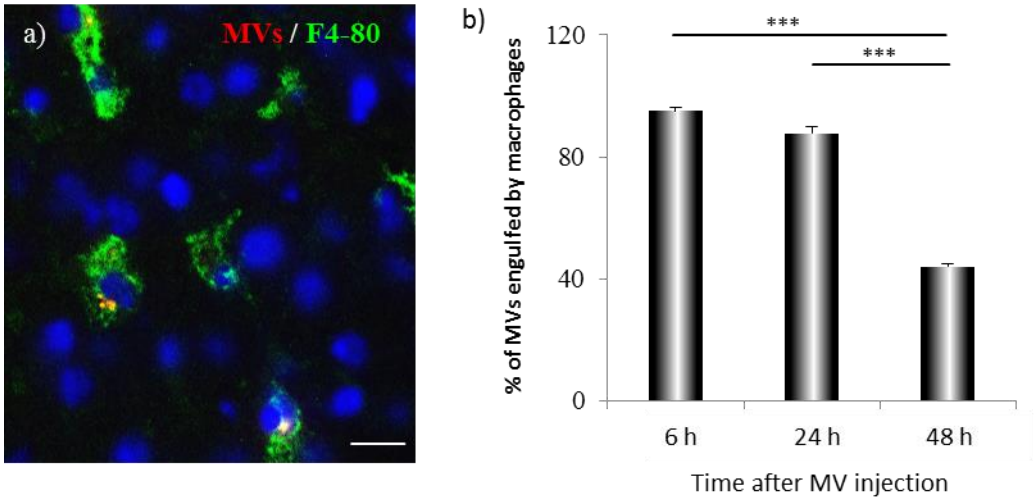


Figure 25: a) Shows KPC MVs (CMTPX) engulfed by macrophages (green) in the liver tissue 6 h after MV injection. b) The graph represents the percentage of MVs, detected in a visual field, that were engulfed by macrophages. Scale bar: 10 µm. n=3; Mean+/- SEM. *** $p < 0.001$.

### 4.7.2. Intravital visualisation of the release of tumour EVs

The release of EVs from pancreatic cancer cells *in vivo* was tracked by 2-photon microscopy. LysM$^+$eGFP-labelled mice were injected with KPC cells pre-labeled with the long-lived fluorophore CMTPX. The imaging was performed beginning from 5 h after the injection until 9 h. During the imaging phase between 7 h to 8 h after injection, the release of a large EV most likely signifying a large oncosome was observed (Fig. 26). The large vesicle was secreted by cancer cells previously arrested in the microcirculation. Fig. 26 shows a series of images captured over a 30 min duration wherein the release of a large vesicle was detected (encircled in white). An oncosome is released by the cluster of arrested cancer cells and eventually moves away from the cancer cells (comparison between Fig. 26a and Fig. 26d). Both, the oncosome which was released and an approaching LysM$^+$GFP-labelled cell are indicated by a dotted circle (Fig. 26a - c). Furthermore, the released oncosome was immediately seen to be engulfed by a LysM$^+$GFP-labelled cell (Fig. 26e and f). The LysM$^+$GFP-labelled cell which engulfs the oncosome was seen to travel away from the arrested cancer cells (Fig. 26h - m). A crude path from the release of the oncosome followed by engulfment by LysM$^+$GFP-labelled cell has been marked by a white dotted arrow in Fig. 26n.

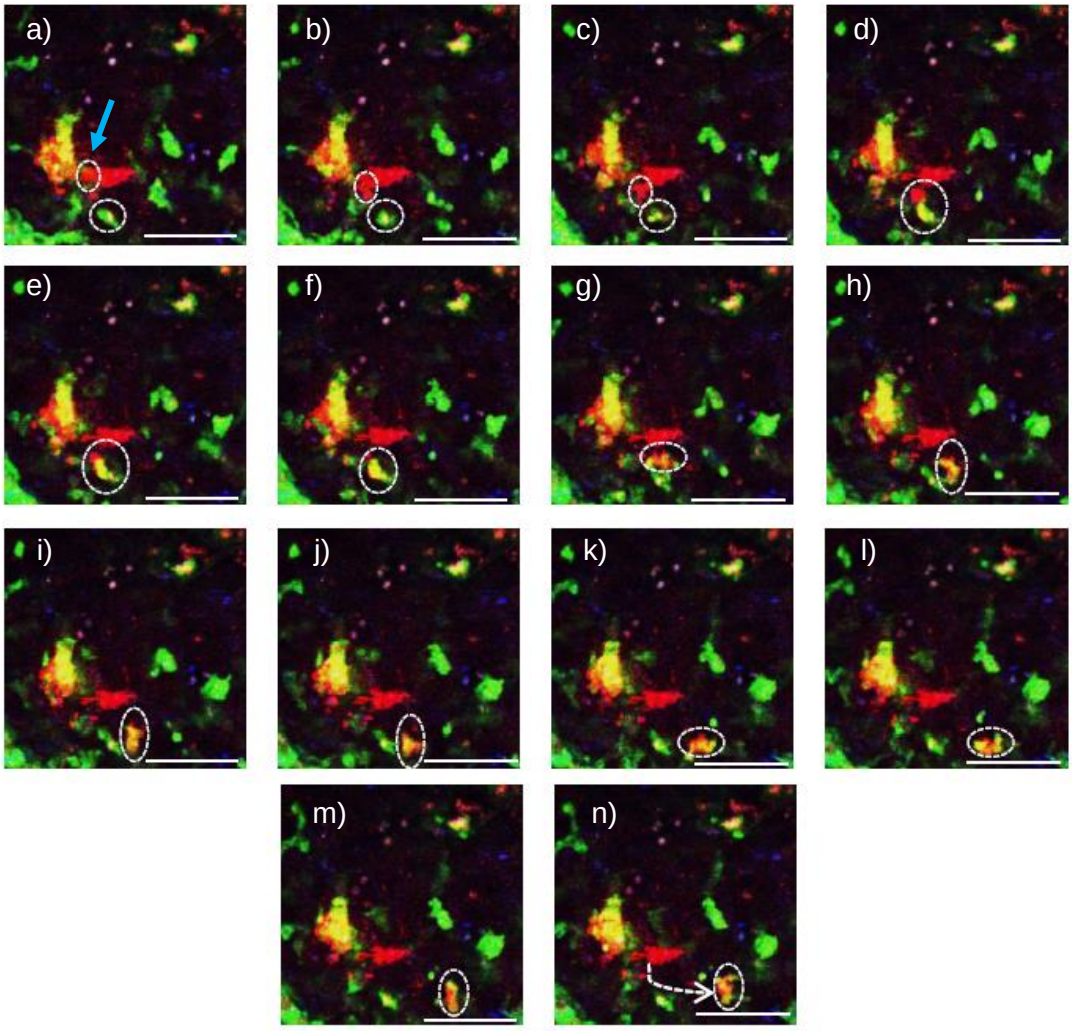


Figure 26: Series of images showing the release of oncosomes from arrested cancer cells (blue arrow in panel a) and immediate engulfment by LysM$^{+}$GFP-labelled cells. Figures a) shows the point of the oncosome was released (blue arrow) and LysM$^{+}$GFP-labelled cell (lower dotted circle) which engulfs the oncosome. b) and c) show release of the oncosome. d) oncosome in contact with the LysM$^{+}$GFP-labelled cell. e) the encircled area now-onwards marks the oncosome which is completely engulfed. (f) the LysM$^{+}$GFP-labelled cell which has engulfed the oncosome starts to move away from the cancer cell cluster. g) to m) show further transport of the engulfed oncosome. The entire path of release until where it was transported is marked by a dotted arrow in figure panel n. Refer to video 4 in section 6. Scale bar: 50 µm.

### 4.8. SEM analysis of EVs *in vivo*

The localisation and interaction of the EVs inside the liver microvessels was further studied by SEM analysis. The mouse liver tissue was analysed 6 h after the injection of KPC cells and MVs. The tissues were fixed in 2.5% GAD as explained in section 3.2.25. It could be seen that the EVs closely interacted with immune cells (Fig. 27a). Indeed, it was observed that an extracellular vesicle (approximate diameter 3 µm) was engulfed by an immune cell (Fig. 27b).

The immune cells were a part of a larger aggregate consisting of EVs, RBCs, leukocytes and fibrin (Fig. 27c). The fibrin fibres appeared to be in close association to the vesicles.

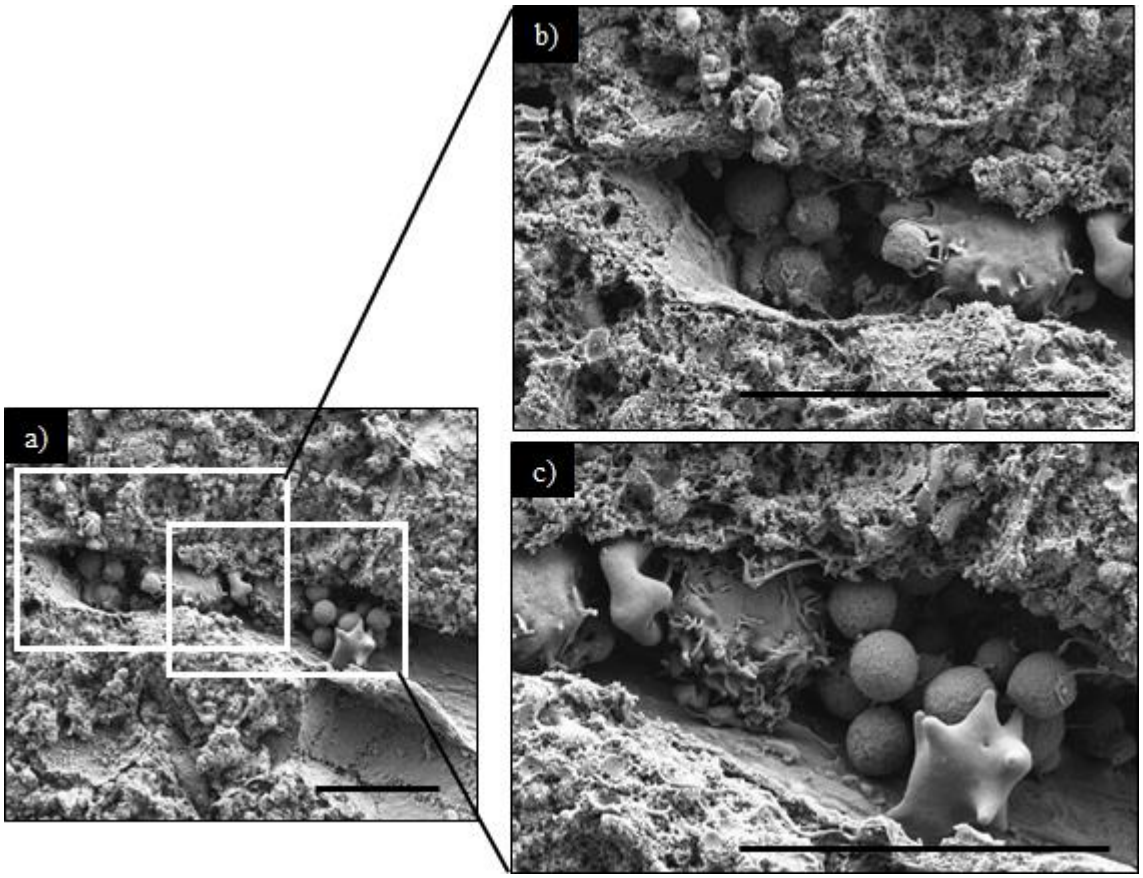


Figure 27: a) The SEM picture shows a microvessel which is occluded by EVs, fibrin and leukocytes. The inset which is magnified as figure (b) shows the part of the microvessel in which the EVs is being engulfed by the leukocyte. The magnified inset figure (c) shows EVs which have an overall size ranging from 2 µm-3 µm. Some EVs are seen to interact with fibrin fibres. Scale bar: 10 µm.

## 4.9. Immune cell recruitment upon tumour cell administration

### 4.9.1. Immunohistochemical analysis

The recruitment of the host immune cells during and after the arrest of KPC cells in the liver microcirculation was analysed. Particularly the identity of the immune cells recruited to the cancer cells and MVs in the liver microcirculation was identified. Overall 6 different immune cell types including NK cells, CD8+ T cells, CD4+ T cells, patrolling monocytes, inflammatory monocytes and neutrophils were identified with cell-specific antigens as marker (see section 3.1.2.). The first cells to arrive in the microcirculation in substantial numbers (at 0.5 h) were NK cells as well as CD8+ T cells and CD4+ T cells. After 2 h, these cells reached a peak (Fig. 28a and Fig. 28b respectively). Recruitment of CD8+ T cells steeply declined after 6 h. Inflammatory monocytes (Fig. 28d) and neutrophils (Fig. 28f) showed an opposite recruitment behaviour. The

former was seen to be decreased with time, while the latter increased within 6 h. Patrolling monocytes only appeared after 6 h (Fig. 28e).

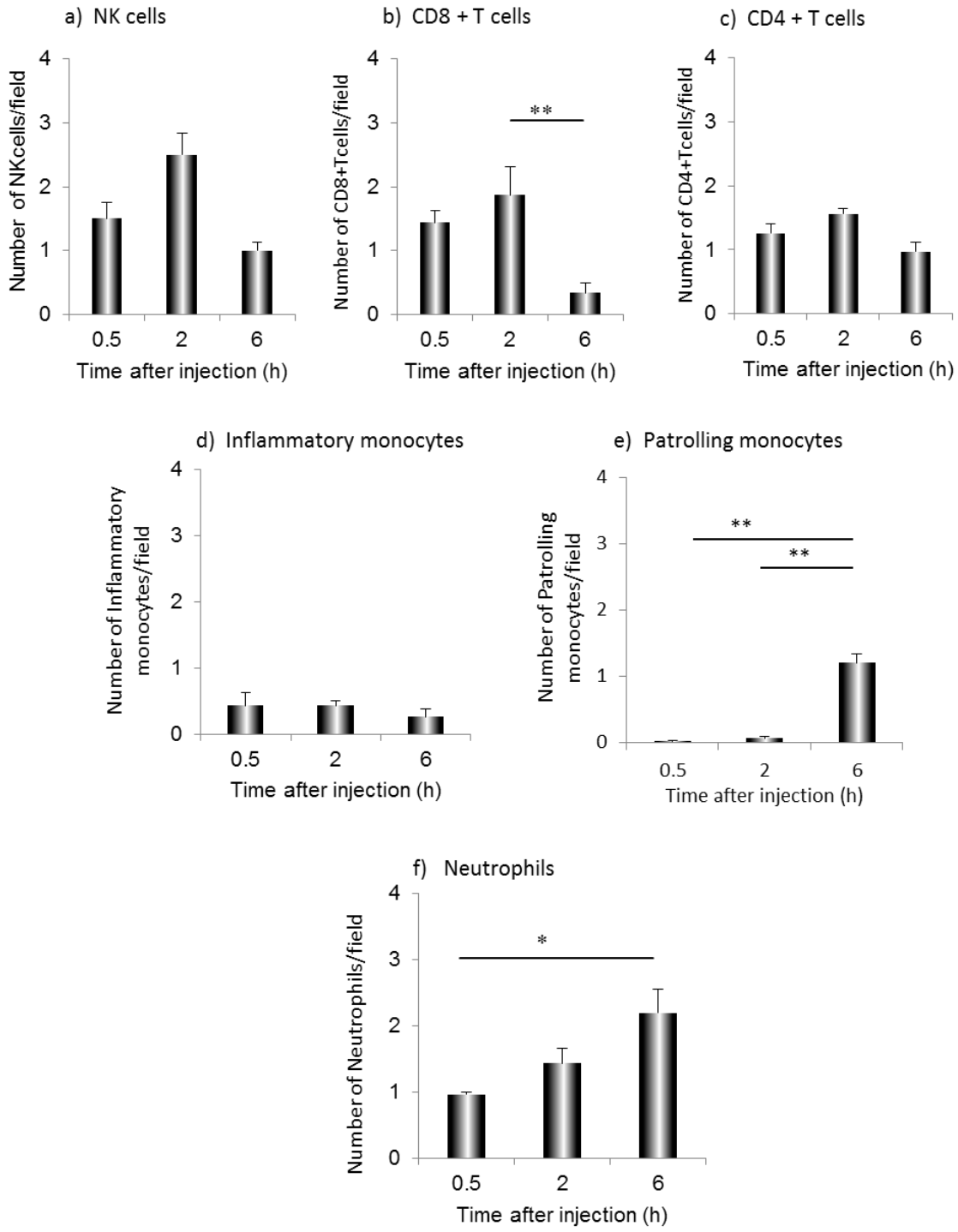


Figure 28: Time dependent recruitment of immune cells in the liver microvasculature of WT mice injected with KPC cancer cells. The graph shows the number of cells per visual fields deduced from an average of 10 visual fields. The y-axis indicates the number of cells and the x-axis indicates the time point at which the mouse liver was harvested after the injection of cancer cells into the mouse. Each column represents the mean of three individual animal experiments with error bars indicating SEM. * $p < 0.05$; ** $p < 0.01$; *** $p < 0.001$.

### 4.9.2. Intravital imaging for immune cell recruitment

The recruitment of neutrophils and their interactions with the cancer cells was further investigated by 2-photon live imaging using the LysM$^+$eGFP-labelled mouse as described in section 3.2.20. In these mice, myeloid cells mostly representing neutrophils are labelled with GFP. In parallel the cancer cells were labelled with CMTPX and the blood flow was visualised by blue dextran. We observed that the GFP-labelled cells interacted extensively with cancer material (Fig. 29). They were seen to infiltrate the liver starting 4 h after KPC cell injection and the number of cells steadily increased until 7.5h (end of imaging shown in Fig. 29c).

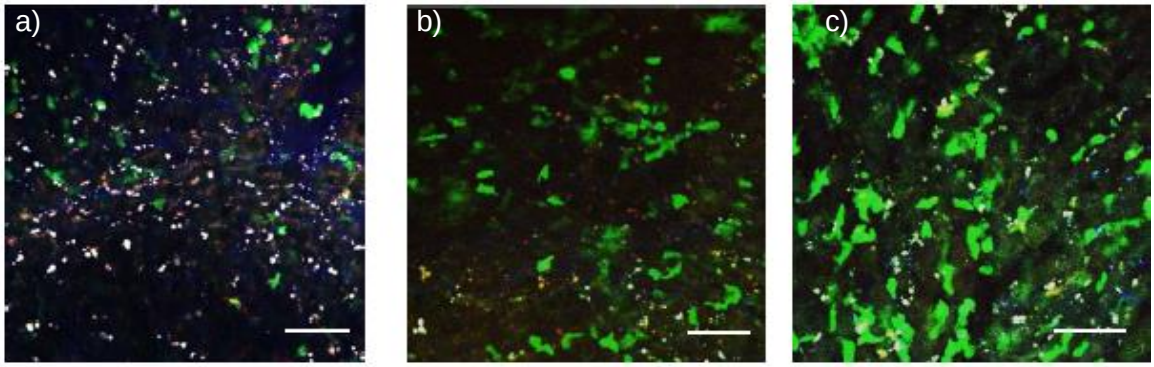


Figure 29: Infiltration of the liver microcirculation by LysM$^+$GFP-labelled cells. Recruitment of myeloid cells strongly increases with time. The figure panels show the images of liver tissue after a) 5.5 h, b) 6.5 h and c) 7.5 h of injection of CMTPX labelled KPC cancer cells. Scale bar: 50 µm.

Moreover, the LysM$^+$GFP-labelled cell formed dense clusters around cancer cell material which, in some instances, were internalised by them (Fig. 30a). However, cell clusters were not engulfed the myeloid cells (Fig. 30b).

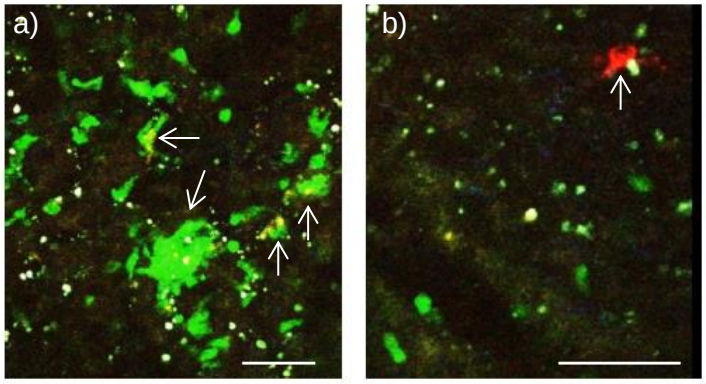


Figure 30: LysM$^+$GFP-labelled cells interacting with cancer cells. a) Shows a cancer cell material completely engulfed by the LysM$^+$GFP-labelled cells forming large clusters (indicated by arrows). b) Large cluster of cancer cells (indicated by arrows) not engulfed by LysM$^+$GFP-labelled cells. Scale bar: 50 µm.

In addition to the mouse model with GFP-tagged myeloid cells, mice with CX3CR1-GFP-tagged cells were used to investigate the interaction of tumour EVs with CX3CR1+ cells (including in particular labelled-patrolling monocytes).

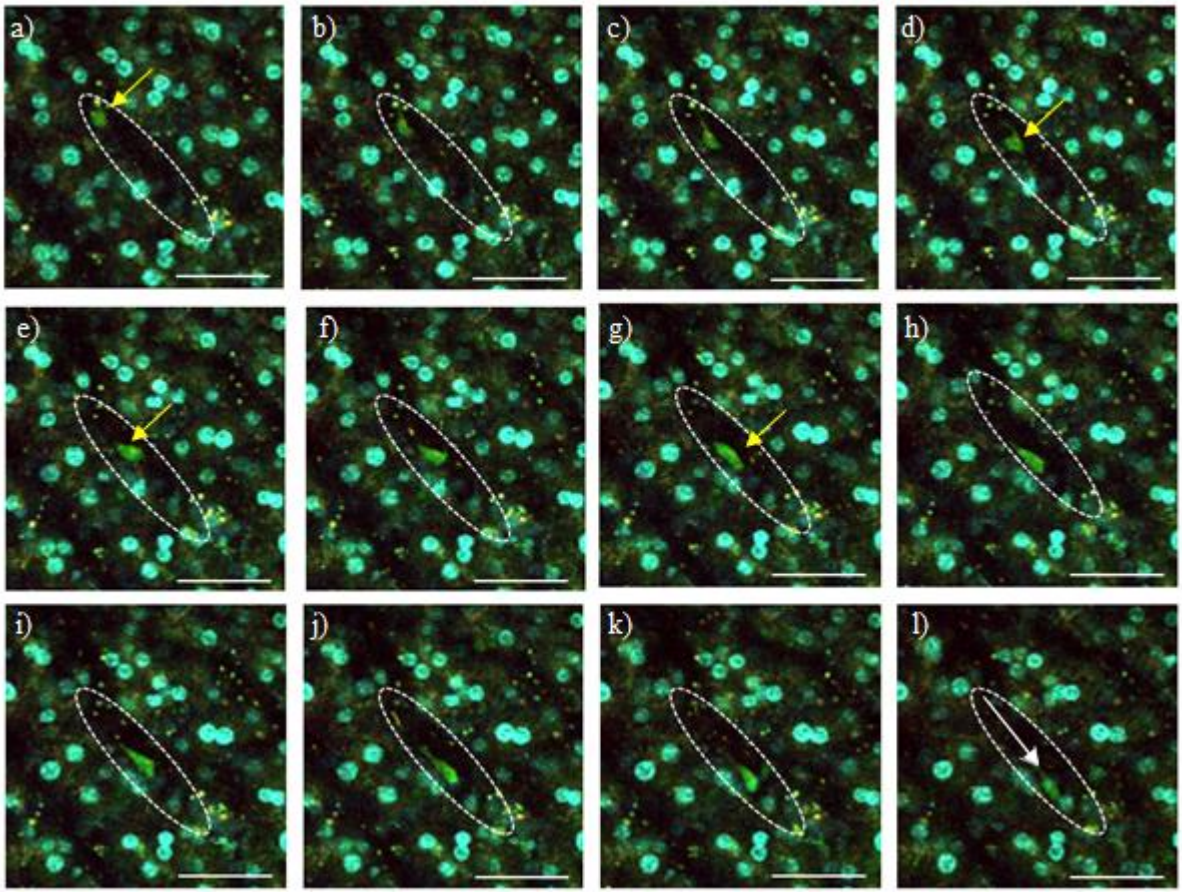


Figure 31: CX3CR1-GFP-labelled cell encircled to visualise its motion along the vessel wall. The GFP- labelled cell contained cancer material (red dots). CX3CR1eGFP mouse was injected with KPC cells labelled with CMTPX and the liver was imaged 6 h after injection. a) The GFP-labelled cell engulfing the EV (CMTPX) in the top of the dotted elliptical shape. b) to e) The cell is seen to travel further downward as marked by the yellow arrow in (d) and (e). g) The GFP-labelled cell has moved further down (centre of the elliptical shape). l) the white arrow indicates the path the GFP-labelled cell traversed. Yellow arrows indicate the position of the GFP-labelled cell. Refer to video 5 in section 6. Scale bar: 50 µm

As shown in the Fig. 31, the CX3CR1-GFP tagged cells appeared to engulf small-sized cancer cell material (red), potentially EV and is seen to crawl along the vessel wall (the path of its movement is marked by a white arrow Fig 31l). Immuno-histochemical analysis of the same liver tissue showed clearly the engulfment of EVs by CX3CR1-GFP labelled cells (Fig. 32). The white arrows indicate EVs engulfed by GFP-labelled CX3CR1 cells.

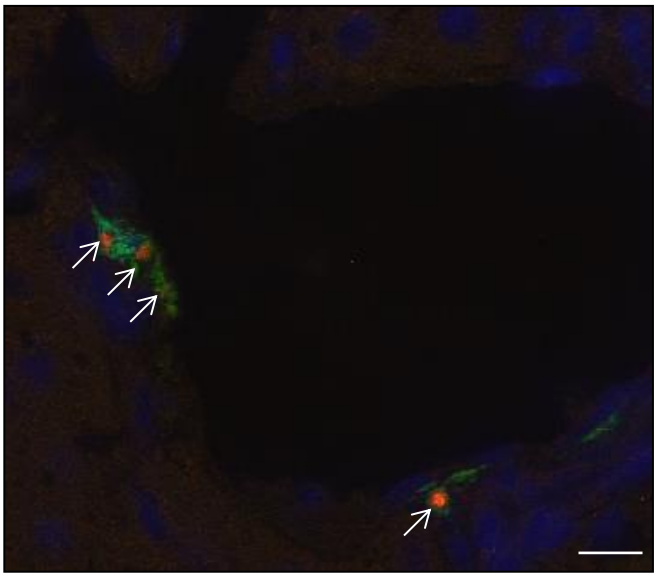

Figure 32: CX3CR1-GFP labelled cell engulfing cancerous EVs (red). Arrows indicate the separate EVs which have been taken up by the GFP labelled cells. Nuclear staining was done by DAPI (blue). Liver tissue was analysed by indirect immunofluorescence technique as explained in section 3.2.1. Scale bar: 10 µm.

## 4.10. Visualisation of cancer cell killing

The apoptotic index, a measure for dead cancer cells, was calculated by accounting for TUNEL stained tumour cells and apoptotic bodies (section 3.2.19.). Dead cancer cells were identified by co-labelling of CMTPX with TUNEL staining and DAPI. Fig. 33(a) shows a TUNEL and CMTPX-positive cancer cell that is additionally positive for DAPI.

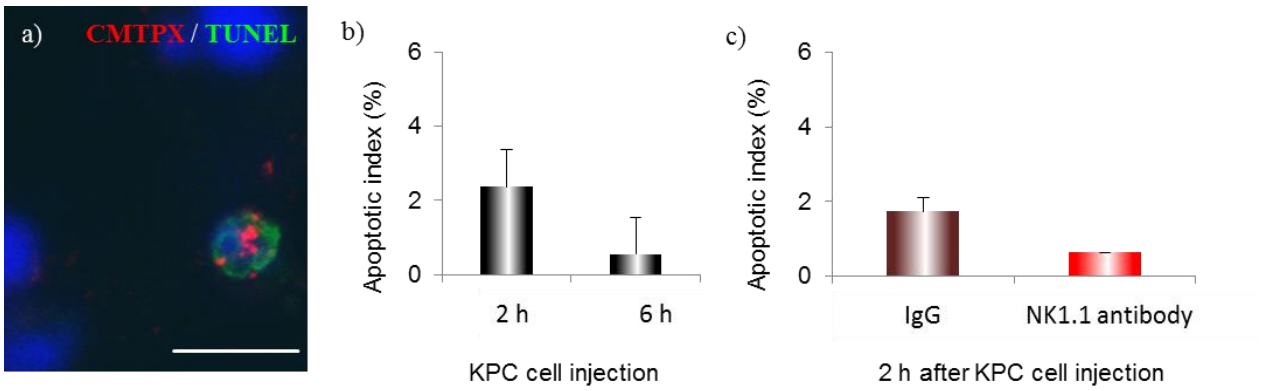


Figure 33: a) Dead cancer cells analysed by TUNEL staining. The cell shows a nucleus (DAPI), cancer cell staining (red) and TUNEL staining (green). b) Quantification of the apoptotic index where the number of dead cancer cells and apoptotic bodies is expressed as the percentage of the total number of cancer cells after KPC cell injection. c) Apoptotic index at 2 h of KPC cell injection after NK cell depletion by NK1.1 antibody as explained in section 2.7.8. n=3, mean values ± SEM. Scale bar: 10 µm.

The apoptotic index was calculated as the sum of dead cancer cells and their apoptotic bodies and expressed as a percentage of total cancer cells. The latter were identified as being TUNEL, CMTPX positive and DAPI negative with a size ranging from 1 µm-5 µm. The apoptotic index was checked after 2 h and after 6 h cancer cell injection. It was seen that the apoptotic index was maximum at 2 h after cell injection (Fig. 33b). The killing of the cancer cells could be a consequence of the attack by the NK cells, specifically since the NK cells are recruited to arrested cancer cells (see Fig. 28a). Therefore, the apoptotic index was also checked after NK cell depletion. The depletion was performed by injection of NK1.1 antibody (blocking antibody) intravenously. NK cell depletion led to a decrease in the apoptotic index (Fig. 33c). This suggested that the elimination of the cancer cells was partly mediated by the NK cells.

## 4.11. Long-term experiments

### 4.11.1. Detection of micro-metastasis

To study the formation of micro-metastasis long term experiments were performed to test the hypothesis that MVs assist in the establishment of pre-metastatic niche. The liver tissues were analysed by H&E staining (refer to section 3.2.22) to identify the micro-metastatic structures. Transgenic mice were injected with KPC MVs (9x200 µg) i.v. over a period of 3 weeks (3 times/ week). Paraffin sections of the mouse liver from five such mice were available. 87% of the cell clusters had a size of <100 µm (Fig. 34a) whereas 6.5% had areas with sizes between 100-200 µm (Fig. 34b) and remaining 6.5% formed areas with sizes >200 µm (Fig.34c). The control mice did not show presence of any structures such abnormal structures.

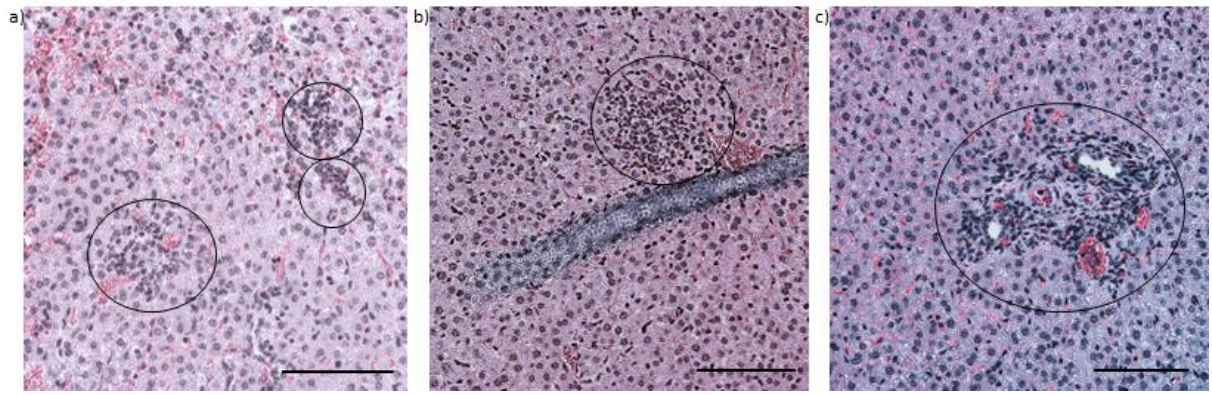


Figure 34: KPC mice were injected with a dose of 9x200 µg KPC MVs over a period of 3 weeks. HandE staining was performed to identify cell clusters in the liver tissue. a) representative picture of a cell cluster with a size of <100 µm; b) representative picture showing a cell cluster with a size range between 100-200 µm; c) representative picture showing a cell cluster with a size of >200 µm. Black circles: indicate the area of close cell clustering indicative of micro-metastasis formation. n=5. Scale bar: 100 µm.

### 4.11.2. Formation of micrometastatic foci with tumour cells and their MVs

In further studies, the fate of the tumour cells and their MVs in the mouse liver tissue was analysed. 8 days after injection of cancer cell (BODIPY) and their MVs (CMTPX), it was seen that the MVs had been engulfed by a host cell (based on their proximity to a nucleus), but did not seem to cluster with cancer cells (Fig. 35a). Instead after 14 days of injection the MVs and cancer cells could be seen to form clusters. Although such events were not frequently detected in the liver tissue, they could be indicative of the beginning of the formation of a pre-metastatic niche.

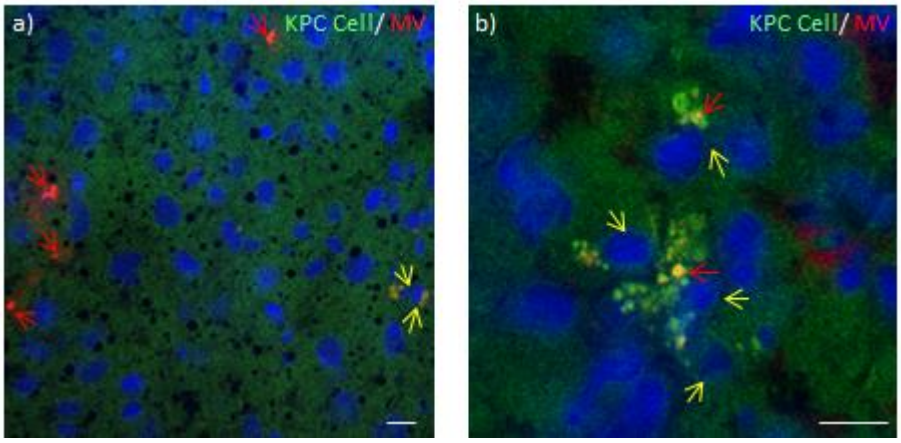


Figure 35: WT mice were injected with BODIPY-labelled KPC cells plus CMTPX-labelled KPC-MVs and analysed after a) 8 days or b) 14 days. The tissue was analysed for localisation of the cancer cells and their MVs. The red arrows indicate MVs and yellow arrows indicate cancer cells. Scale bar: 10 µm.

# 5. Discussion

The role of pancreatic cancer cells and their EVs in establishing a pre-metastatic niche is highly dependent on the various cancer-derived and host-derived factors[83]. Firstly, the involvement of pancreatic cancer cells and their EVs in promoting blood coagulation was studied. The procoagulant activity was investigated based on the expression of TF which is the initiator protein of fibrin formation on various pancreatic cancer cell lines. The human pancreatic cancer cell line L3.6pl, showed a strong expression of TF on the plasma membrane. Whereas KPC cells, mouse pancreatic cancer cells derived from a transgenic KPC mouse model with a point mutation in the *KRAS* gene (G12D) as well as a *p53* deletion under the control of the *Cre* promoter, showed almost no expression of TF on the plasma membrane. Further investigations were conducted to understand the relevance of these findings in a functional context. L3.6pl cells stimulated the formation of Factor Xa in a TF dependent manner as evidenced by neutralisation with anti-TF antibody which was seen to reduce the FX activation. The pro-coagulant activity of KPC cells was due to unknown pro-coagulant factors. These cells stimulated Factor X activation without the involvement of TF as seen from the FXa formation assay. Involvement of phospholipids in activation of FX is now known for more than a decade[84,62] and given the role of the aminophospholipids[85], the exposure of PE on the cell surface of the tumour cells was studied. Pre-treatment of both cancer cell types with the cyclic peptide duramycin,, markedly decreased FXa formation thus, supporting the hypothesis that the pro-coagulant activity of these cells could depend on an altered exposure of PE on the surface of the cells. The specificity of duramycin was determined by functional assays using amino-phospholipid containing liposomes which showed that duramycin specifically bound, in the experimental conditions applied, to PE but not to the other aminophospholipids.

An altered exposure of PE on the surface of cancer cells and their MVs has been reported for instance in case of breast cancer cells PE. It has been postulated that PE potentially plays a pivotal role in recruitment of certain membrane-proteins[84]. Surface exposure of PE was also seen to increase in tumour vascular endothelium especially under hypoxic conditions[85]. Therefore, we hypothesised that the increased PE exposure of the cancer cells was due to the mutations in the genes that translocate phospholipids between the outer and the inner leaflet of the plasma membrane. Several different proteins control the surface exposure of PE, in particular the P4-ATPases, PEBP, anoctamins and some adlo-keto reductases[80,78]. First, a few known candidates like the P4-ATPases ATP11C as well as scramblases like TMEM16J and TMEM16F were down-regulated by specific siRNA in pancreatic cancer cell lines. No significant change in the

pro-coagulant activity was seen after suppressing the expression of these proteins. Therefore, we performed a wider search was conducted for which we performed a bio-informatic analysis to screen online databases reporting information on the gene mutations in pancreatic cancer patients. Overall, we found several mutations in the genes potentially involved in phospholipid transport. The genes which most frequently showed mutations in these patients, apart from *TP53*, were *DYNC1H1*, *APOB* and *ATP10a*. In addition, another database search revealed slightly different results but confirmed *ATP8A2* as a frequently mutated gene together with *ATP10A.* Our hypothesis was that the pro-coagulant activity of the cancer cells could be due to an increased constitutive exposure of PE on the outer leaflet of the plasma membrane. This could be a consequence of functional impairment of P4-ATPases (flippases) which maintain the asymmetric distribution of PE and PS by especially transporting the PE to the inner surface. In P4-ATPases ATP8A2 and ATP10A most of the mutations detected were present in cytoplasmic loop which harbours the ATP binding and phosphorylation domains. This hints towards the possibility that such mutations could render the flippases dysfunctional which would lead to a constitutive exposure of PE on the outer surface of the cancer cells. Additional results such as the expression profiles of these genes will be needed in future to obtain a more complete understanding of their role in the increased PE exposure in pancreatic cancer cells.

The role of cancer cells as activators of blood coagulation was further studied under *in vivo* conditions. In particular the microvascular fibrin formation was analysed in the liver, which is the main site of pancreatic cancer metastasis. We observed substantial fibrin formation in the microvessels due to the pro-coagulant activity of the cancer cells and their EVs. One of the consequences of intravascular fibrin formation was the occlusion of microvessels by fibrin clots. This occlusion was observed to an extent which could contribute significantly to a ‘stop’ in the vessel perfusion. The microvascular fibrin formation observed in response to the arrest of cancer cells might also be partly due to the coagulation response induced by the host immune cells. It has been shown that during systemic infections immune cells embedded in the fibrin-rich microthrombi indeed trigger a coagulation response that aims to capture the bacteria for efficient elimination[61,86]. In line with this, microthrombi formed by the host immune cells could partly help in the entrapment of the tumour cells and thus facilitate their killing. On the other hand, fibrin production by the cancer cells could also be an immune escape mechanism by building a fibrin shield surrounding the cancer cells[40,87]. Our results show that the fibrin formation was triggered already after 2 h of injection of the cancer cells. However, at this time point the fibrin-covered intravascular area was still limited and thus could potentially expose the cancer cells and their EVs to elimination by cytotoxic CD8+T cells or NK cells. At the same time point the

cancer cells were seen to be arrested in the microvessels, but did not cause any occlusion to impede the blood perfusion. Therefore, it is likely that the cancer cells at this time point are more accessible to the killing by NK cells and CD8+T cells. In accordance with the earlier results, the peak of arrival of NK cells and CD8+T cells was also observed 2 h after tumour cell injection. In addition, the apoptotic index was maximum at this same time point and this index was seen to decrease upon NK cell depletion. Overall, these results indicate that cancer cell elimination occurs already after 2 h of injection and that NK cells are eminently involved in the killing of cancer cells. Importantly, these results show that the elimination of the tumour cells occurs inside the blood vessels.

The cancer cells which are arrested in the microcirculation are strongly associated with the microvascular fibrin formation also at the peak of intravascular coagulation activation, 6 h after the injection of the tumour cells. As one of the consequences of co-localisation of the cancer cells with the microthrombi, the microvessels are often occluded as comprehended from the 'stop' in the blood perfusion. It is likely that this results in the formation of hypoxic areas in the vicinity of the blockage. Such hypoxic conditions are known to favour the survival and extravasation of cancer cells[31,88]. The role of immune cells that are rapidly recruited to the tumour cells arrested in the microcirculation needs to be further elucidated. Interestingly, we have seen that the extravasation of tumour MVs can already occur relatively early (2 h time point) although to a very limited extent. This suggests that MVs escape the immune surveillance and extravasate in the tissue probably to the areas of pre-metastatic niche formation. The exact mechanisms of the extravasation of MVs are not known. We observed that Kupffer cells engulfed most of the tumour cell-derived EVs. Besides this, other immune cells for example neutrophils and patrolling monocytes also engulfed tumour derived-EVs and transported them to the perivascular tissue. In general, the release of EVs from pancreatic cancer cells might contribute to their metastatic potential. This is indicated by the preliminary data on the release of oncosomes in the supernatants, of different pancreatic cancer cell lines.

Moreover, the survival of the cancer cells and their EVs was also studied in long term experiments in which the livers were analysed, by immunohistochemical procedures, 14 days after the injection of the cancer cells and their MVs. It was seen that the cancer cells and the cancer MVs formed discrete foci in the perivascular space. These foci could be the starting point of the formation of pre-metastatic niches where the tissue could be remodelled to facilitate metastasis. In line with our previous results, we also saw that long-term experiments (3 weeks) with high doses of MVs showed the initiation of niche-like structures in transgenic mice models

of pancreatic cancer metastasis. Future experiments with longer incubation periods will be needed to give more information about the dynamics of the development of such foci as induced by injected cancer cell derived EVs.

An important aspect of the present project was the identification of the immune cells that were rapidly recruited to the arrested cancer cells. We found that the first cells to arrive were CD8+T cells and NK cells (2 h after cancer cell injection). This suggested that the intravascular immune surveillance immediately aims at the killing of cancer cells. After the cytotoxic immune cells, inflammatory (classical) monocytes and a few hours later neutrophils were seen to be arriving. At the same time point the tumour MVs had already been engulfed by the Kupffer cells. The time line of the arrival of myeloid immune cells was confirmed in videos obtained from the intravital imaging. Beginning from 4 h after experimental tumour cell intravasation a strong increase in the arrival of GFP-labelled myeloid cells into the liver microvasculature was seen. The infiltrating myeloid cells showed varied behaviour upon encountering cancerous entities. Indeed, the myeloid cells interacted to a lesser extent with cancer cell clusters but extensively with small tumour cell fragments. These small tumour cell fragments were seen to be engulfed by the increasingly infiltrating GFP-labelled myeloid cells. This was especially evident in the CX3CR1-GFP-labelled mice where the labelled immune cells (mainly representing patrolling monocytes) appeared to patrol the walls of the microvessels and engulf the tumour EVs. This could either lead to the clearance of the tumour EVs or facilitate their extravasation, after being internalised by the immune cells, to distant potentially metastatic site[40]. Nevertheless, preliminary experiments indicate that at least a part of the cancer cells present in the microcirculation were propidium iodide (PI)-positive indicating that these had been killed. Therefore, NK cells might be majorly responsible for the killing of cancer cells in this model whereas the other myeloid cells might play a role in numerous other functions such as clearance of cancer EVs.

Figure 37 summarises the principal findings of this thesis in relation to what is known about the haematogenic spreading of pancreatic cancer cells and their EVs. Pancreatic cancer cells disseminate from the site of primary tumour, escaping the immune-attack to intravasate into the blood circulation. In the microcirculation of organs such as the liver, which is the most preferred organ for pancreatic cancer metastasis, the cancer cells and their EVs are seen to be arrested. The arrested cancer cells locally activate fibrin formation by the blood coagulation system via PE-dependent as well as TF-dependent or -independent mechanisms. Thereby, they can promote the occlusion of microvessels which may result in the formation of hypoxic areas. This in turn might

help to promote the extravasation of the cancer cells. In parallel, the arrested cancer cells release EVs, especially oncosome-like vesicles. Based on some previous and new findings the cancer cells and EVs which extravasate into the perivascular space contribute to develop metastatic foci.

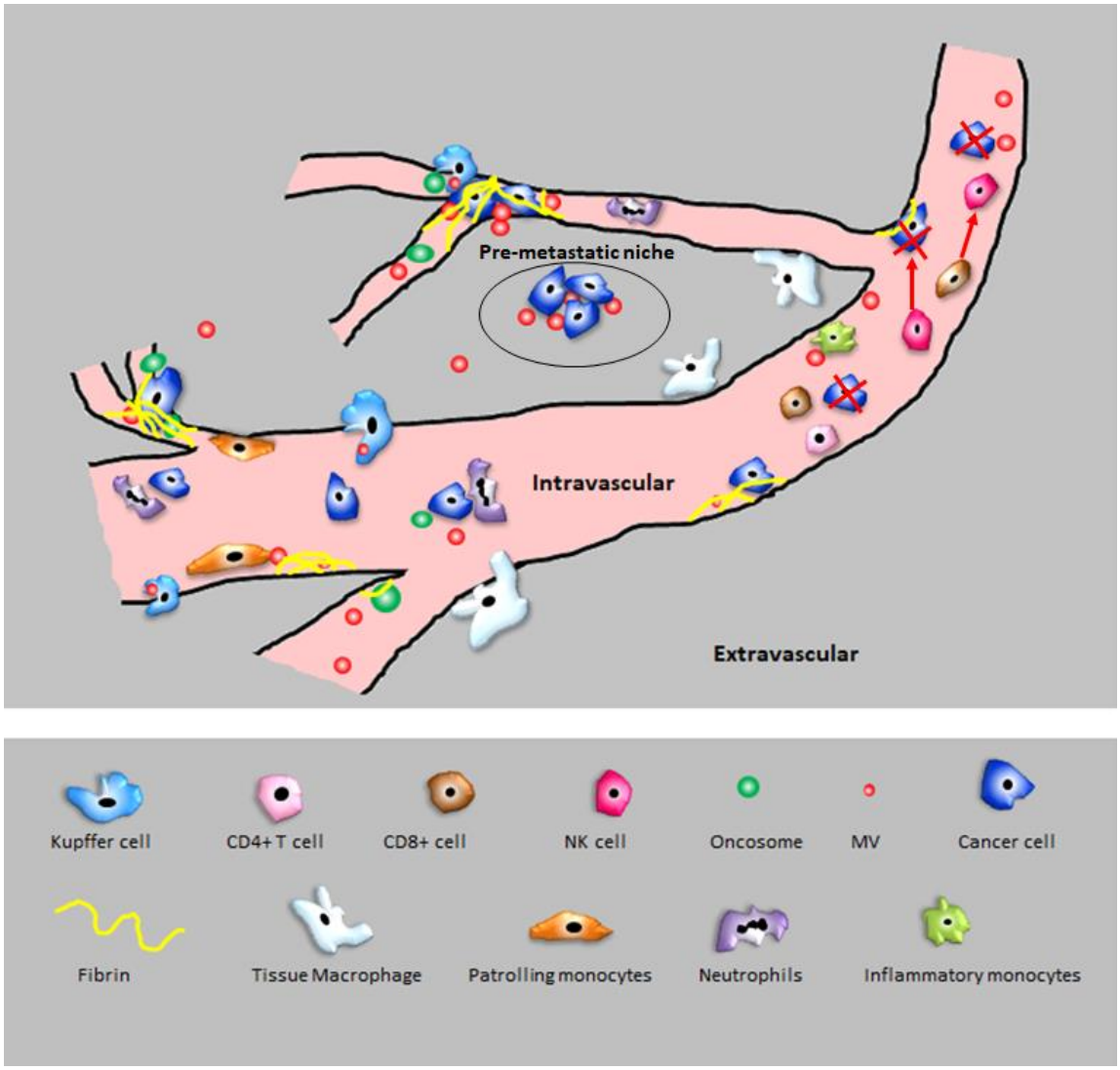


Figure 37: Schematic representation of the process of the intravascular events during pancreatic cancer metastasis depicting the role of EVs, microvascular fibrin formation and immune cells. The metastatic cancer cells and EVs (MVs and oncosomes) are seen to disseminate from the primary tumour and intravasate into the blood stream. Once they are arrested in the microcirculation of the organ where metastasis occurs the cancer cells start to locally promote fibrin formation. Consecutively, they are immediately attacked by NK cells and CD+8T cells. Other immune cells recruited to the arrested cancer cells are inflammatory monocytes, neutrophils and later patrolling monocytes. Most of the EVs are engulfed by intra- and extravascular macrophages. Arrested cancer cells extravasate and traverse towards the pre-metastatic niche area where the EVs have already remodelled the niche to promote cancer cell growth. The extravasated cancer cells settle in these areas, proliferate and begin the process of metastasis.

## 6. Videos

Video 1:

Thesis video links\6. Videos_ video 1.pptx

Video 2:

Thesis video links\6. Videos_ video 2.pptx

Video 3:

Thesis video links\6. Videos_ video 3.pptx

Video 4:

Thesis video links\6. Videos_ video 4.pptx

Video 5:

Thesis video links\6. Videos_ video 5.pptx

# 7. Summary

Metastasis is the most frequent cause of death in patients suffering from PDAC. In the present project, we focused on understanding the mechanisms promoting and counteracting metastasis of PDAC in the microcirculation of the liver, the main site of pancreatic cancer metastasis. In particular, the microvascular thrombus formation was studied with a focus on the procoagulant activity and localisation of cancer cells and their MVs. It was seen that KPC cells, a mouse pancreatic cancer cell line, and their EVs stimulate coagulation in a TF-independent manner. In contrast L3.6pl cells, a human pancreatic cancer cell line, and their EVs stimulated coagulation in a TF-dependent way. Yet both cell lines were shown to promote fibrin formation by presenting PE on their surface. This surface exposure of PE could be mediated by loss-of-function mutations in P4-ATPases, which transfer PE to the inner leaflet of the plasma membrane since patients with PDAC show mutations in such P4-ATPases.

To understand the consequence of stimulation of the coagulation cascade *in vivo* microvascular fibrin formation in the liver was analysed. Intravascular fibrin formation attained a peak 6 h after the administration of pre-labelled KPC cancer cells or their EVs. Fibrin formation was also analysed *in vivo* and *in vitro* by scanning electron microscopy. The results show that fibrin rich clots in the microcirculation of the liver indeed occlude the microvessels thus hindering the blood flow which may in turn deprive the surrounding tissue of nutrients.

Cancer cells and their EVs were detected both in the intra- and extravascular areas of the liver microcirculation. A small proportion of KPC MVs are seen to extravasate early at 2 h. Yet most of the tumour MVs were rapidly engulfed by Kupffer cells. On the other hand, the KPC cancer cells were seen to be arrested in the liver microcirculation at 2 h and started to extravasate into the perivascular areas 6 h after administration. The extravasated EVs were immediately engulfed by tissue-localised myeloid immune cells. Other immune cells such as the NK cells, CD8+T cells, CD4+T cells and inflammatory monocytes were recruited to the intravascular cancer cell material 2 h after injection of cancer cells. At the same time point, apoptosis of cancer cells was maximal which appeared to be potentially related to the arrival of NK cells. Neutrophils, patrolling monocytes and other myeloid cells arrived in the circulation 6 h after injection of cancer cells and their EVs. Long term experiments with tumour cells and their EVs indicated that the tumour cells and their EVs clustered to form micro-metastatic foci in the perivascular tissue of the liver.

# 8. Zusammenfassung

Metastasen bilden die häufigste Todesursache bei Patienten mit PDAC. Daher lag der Fokus in der vorliegenden Arbeit darauf, die Mechanismen zu verstehen, die die Metastasierung des Pankreas-Karzinoms in der Mikrozirkulation der Leber regulieren. Insbesondere wurde das Entstehen von mikrovaskulären Thromben untersucht, wobei ein besonderer Schwerpunkt auf die prokoagulatorische Aktivität und Lokalisation von Krebszellen und deren MVs in den mikrovaskulären und perivaskulären Kompartimenten der Leber gelegt wurde. Es konnte gezeigt werden, dass KPC-Zellen (eine murine Pankreaskrebszelllinie) und ihre EVs, im Gegensatz zu humanen L3.6pl Zellen und ihren EVs, die Koagulation TF-unabhängig stimulieren. Hingegen wurde für beide Zellen nachgewiesen, dass die Stimulierung der Koagulation über die Präsentation des Phospholipids PE auf der Zelloberfläche gefördert wird. Dies könnte durch Mutationen in P4-ATPasen vermittelt werden, die PE in das innere Blatt der Zellmembran transferieren, da Patienten Mutationen in P4-ATPasen aufweisen.

Um die Konsequenzen der *in vivo* Stimulation der Koagulationskaskade während der Metastasierung zu verstehen, wurde die mikrovaskuläre Fibrinbildung in der Leber analysiert. Nach Infusion von markierten KPC-Zellen bzw. ihren EVs erreichte die Fibrinbildung ihr Maximum nach 6h. Zusätzlich wurden durch SEM Experimente *in vivo* und *in vitro* die mikrovaskuläre Fibrinbildung visualisiert. Die Untersuchungen zeigen, dass fibrinreiche Gerinnsel in den Mikrogefäßen der Leber zur Okklusion der Gefäße führen können. Dadurch könnte die Versorgung mit Nährstoffen in den von den Mikrogefäßen versorgten Gewebsarealen beeinträchtigt werden.

Weitergehende Analysen zur Lokalisation der KPC-Krebszellen und ihrer EVs in intra- bzw. extravaskulären Kompartimenten könnten dazu beitragen, die Vorgänge beim Entstehen einer prämetastatischen Nische besser zu verstehen. Ein kleiner Teil der MVs extravasierte bereits nach 2h. Jedoch wurden zum selben Zeitpunkt 95% der MVs von Kupffer-Zellen aufgenommen. Krebszellen adhärierten an das Endothel der Mikrozirkulation ebenfalls bereits nach 2h. Später begannen die Karzninomzellen in die perivaskulären Areale zu emigrieren und dort Cluster zu bilden. Extravasierte EVs wurden sofort von myeloiden Immunzellen des extravaskulären Gewebes aufgenommen. In den mikrovaskulären Gefäßen beobachteten wir eine ebenfalls schnelle Rekrutierung von Immunzellen zu den adhärenten Karzinomzellen, so z.B. von NK-Zellen, CD8+T-Zellen, CD4+T-Zellen und inflammatorischen Monozyten. Zu demselben Zeitpunkt war die Tumorzellapoptose maximal, was möglicherweise durch die rekrutierten NK-Zellen induziert wurde. Neutrophile, patrouillierende Monozyten und andere myeloide Zellen

erschienen erst 6h nach Injektion der Krebszellen und ihrer EVs in der Mikrozirkulation. Langzeitexperimente mit den Krebszellen und ihren EVs zeigten, dass beide Tumor-Strukturen mikrometastatische Foci in der Leber bilden.

# 9. References


1. Sa, B. *et al.* The role of surgery for pancreatic cancer: a 12-year review of patient outcome. *Ulster Med J* **79,** 70–75 (2010).

2. Rahib, L. *et al.* Projecting Cancer Incidence and Deaths to 2030: The Unexpected Burden of Thyroid, Liver, and Pancreas Cancers in the United States. *Cancer Res* **1,** 2913–21 (2014).

3. Siegel R, Miller K, J. A. Cancer statistics. *CA Cancer J Clin* **65,** 29 (2015).

4. Giovannetti, E. *et al.* Never let it go_ Stopping key mechanisms underlying metastasis to fight pancreatic cancer. *Semin. Cancer Biol.* **44,** 43–59 (2017).

5. Le Large, T. Y. S. *et al.* Key biological processes driving metastatic spread of pancreatic cancer as identified by multi-omics studies. *Semin. Cancer Biol.* **44,** 153–169 (2017).

6. Hingorani, S. R. *et al.* Preinvasive and invasive ductal pancreatic cancer and its early detection in the mouse. *Cancer Cell* **4,** 437–450 (2003).

7. Imamura, T. *et al.* Liquid biopsy in patients with pancreatic cancer: Circulating tumor cells and cell-free nucleic acids. *World J. Gastroenterol.* **22,** 5627–41 (2016).

8. Zhou, B. *et al.* Early detection of pancreatic cancer: Where are we now and where are we going? *Int. J. Cancer* **141,** 231–241 (2017).

9. Diwakarla, chandra *et al.* Advanced pancreatic ductal adenocarcinoma -Complexities of treatment and emerging therapeutic options. *World J Gastroenterol* **23,** 2276–2285 (2017).

10. Sideras, K. *et al.* Role of the immune system in pancreatic cancer progression and immune modulating treatment strategies. *Cancer Treat. Rev.* **40,** 513–522 (2014).

11. Ilic, M. & Ilic, I. Epidemiology of pancreatic cancer. *World J. Gastroenterol.* **22,** 9694–9705 (2016).

12. Rhim, A. D. & Stanger, B. Z. Molecular Biology of Pancreatic Ductal Adenocarcinoma Progression: Aberrant Activation of Developmental Pathways. *Prog Mol Biol Transl Sci.* **97,** 47–78 (2010).

13. Guo, J., Xie, K. & Zheng, S. Molecular Biomarkers of Pancreatic Intraepithelial Neoplasia and Their Implications in Early Diagnosis and Therapeutic Intervention of Pancreatic

Cancer. *Int. J. Biol. Sci.* **12,** 292–301 (2016).

14. Esposito, I., Konukiewitz, B., Schlitter, A. M. & Klöppel, G. Pathology of pancreatic ductal adenocarcinoma: facts, challenges and future developments. *World J. Gastroenterol.* **20,** 13833–41 (2014).

15. Gulinnaz Ercan, A. K. and B. O. Pancreatic Cancer Stem Cells and Therapeutic Approaches. *Anticancer Res.* **37,** 2761–2775. (2017).

16. Hruban, R. H. *et al.* Progression Model for Pancreatic Cancer. *Clin Cancer Res.* **6,** 2969–72. (2000).

17. Mauro, L. A., Herman, J. M., Jaffee, E. M. & Laheru, D. A. Carcinoma of the Pancreas. *Abeloff's Clin. Oncol.* **5,** 1397–1415.e7. (2013).

18. Gopinathan, A., Morton, J. P., Jodrell, D. I. & Sansom, O. J. GEMMs as preclinical models for testing pancreatic cancer therapies. *Dis. Model. Mech.* **8,** 1185–1120 (2015).

19. Li, D. & Jiao, L. Molecular Epidemiology of Pancreatic Cancer. *Int J Gastrointest Cancer.* **33,** 3–14 (2003).

20. Pruitt, K. *Molecular and cellular changes in the cancer cell*. (Academic Press is an imprint of Elsevier, 2016).

21. Andrew V. Biankin. Pancreatic cancer genomes reveal aberrations in axon guidance pathway genes. *Nature* **491,** 399–405 (2012).

22. Lauren J. Bayne. Tumor-Derived Granulocyte-Macrophage ColonyStimulating Factor Regulates Myeloid Inflammation and T Cell Immunity in Pancreatic Cancer. *Cancer Cell.* **21,** 822–35 (2012).

23. Clark, C. E. *et al.* Dynamics of the Immune Reaction to Pancreatic Cancer from Inception to Invasion. *Cancer Res* **67,** 9518–27 (2007).

24. Carolyn E. Clark, Gregory L. Beatty, R. H. V. Immunosurveillance of pancreatic adenocarcinoma: Insights from genetically engineered mouse models of cancer. *Cancer Lett.* **279,** 1–7 (2009).

25. Steeg, P. S. Targeting metastasis. *Nat. Publ. Gr.* **16,** 201–18 (2016).

26. Bose, S., Panda, A. K., Mukherjee, S. & Sa, G. Curcumin and tumor immune-editing:

resurrecting the immune system. *Cell Div.* **10,** 6 (2015).

27. Aiello, N. M. *et al.* Metastatic progression is associated with dynamic changes in the local microenvironment. *Nat. Commun.* 12819 (2016).

28. Swann, J. B. & Smyth, M. J. Immune surveillance of tumors. *J Clin Invest.* **117,** 1137–1146 (2007).

29. Ryungsa Kim, 1 Manabu Emi2 and & Tanabe, K. Cancer immunoediting from immune surveillance to immune escape. *Immunol. Rev. Artic.* **121,** 1–14 (2007).

30. Bose, S., Panda, A. K., Mukherjee, S. & Sa, G. Curcumin and tumor immune-editing: resurrecting the immune system. *Cell Div* **10,** 1–13 (2015).

31. Sceneay, J., Smyth, M. J. & Möller, A. The pre-metastatic niche: finding common ground. *Cancer Metastasis Rev.* **32,** 449–64 (2013).

32. Peinado, H., Lavotshkin, S. & Lyden, D. The secreted factors responsible for pre-metastatic niche formation: Old sayings and new thoughts. *Semin. Cancer Biol.* **21,** 139–146 (2011).

33. Hiratsuka, S., Watanabe, A., Aburatani, H. & Maru, Y. Tumour-mediated upregulation of chemoattractants and recruitment of myeloid cells predetermines lung metastasis. *Nat. Cell Biol.* **8,** 1369–75 (2006).

34. Kaplan, R. N. *et al.* VEGFR1-positive haematopoietic bone marrow progenitors initiate the pre-metastatic niche. *Nature* **438,** 820–7 (2005).

35. Krüger, A. Premetastatic niche formation in the liver: emerging mechanisms and mouse models. *J. Mol. Med.* **93,** 1193–1201 (2015).

36. Yohei Saito a, b *et al.* The inhibition of pancreatic cancer invasion-metastasis cascade in both cellular signal and blood coagulation cascade of tissue factor by its neutralisation antibody. *Eur J Cancer.* **47,** 2230–9 (2011).

37. Hiratsuka, S., Watanabe, A., Aburatani, H. & Maru, Y. Tumour-mediated upregulation of chemoattractants and recruitment of myeloid cells predetermines lung metastasis. *Nat. Cell Biol.* **8,** 1369–1375 (2006).

38. Fidler, I. The implications of angiogenesis for the biology and therapy of cancer metastasis. *Cell* **79,** 185–188 (1994).

39. Maclean, J. M., Drs, S., Chambers, A. F. & Macdonald, I. C. Metastatic Disease: Interactions Between Tumor Cells and Host Environment During Cancer Cell Spread. (The University of Western Ontario, 2011).

40. Kitamura, T., Qian, B.-Z. & Pollard, J. W. Immune cell promotion of metastasis. *Nat. Rev. Immunol.* **15,** 73–86 (2015).

41. Farid G Khalafalla and Mohammad W Khan. Inflammation and Epithelial-Mesenchymal Transition in Pancreatic Ductal Adenocarcinoma: Fighting Against Multiple Opponents. *Cancer Growth Metastasis.* **10,** 1–13 (2017).

42. Brabletz, T. EMT and MET in Metastasis: Where Are the Cancer Stem Cells? *Cancer Cell* **22,** 699–701 (2012).

43. Minciacchi, V. R., Freeman, M. R. & Di Vizio, D. Extracellular Vesicles in Cancer: Exosomes, Microvesicles and the Emerging Role of Large Oncosomes. *Semin. Cell Dev. Biol.* **40,** 41–51 (2015).

44. Zaborowski, M. P., Balaj, L., Breakefield, X. O. & Lai, C. P. Extracellular Vesicles: Composition, Biological Relevance, and Methods of Study. *Bioscience.* **65,** 783–79 (2015).

45. Geddings, J. E. & Mackman, N. Tumor-derived tissue factor–positive microparticles and venous thrombosis in cancer patients. *Blood.* **122,** 1873–80 (2013).

46. Engelmann, B. Initiation of coagulation by tissue factor carriers in blood. *Blood, cells Mol. Dis.* **36,** 188–190 (2006).

47. Pomorski, T., Hrafnsdóttir, S., Devaux, P. F. & Van Meer, G. Lipid distribution and transport across cellular membranes. *Semin. Cell Dev. Biol.* **12,** 139–148 (2001).

48. Muralidharan-Chari, V., Clancy, J. W., Sedgwick, A. & D'Souza-Schorey, C. Microvesicles: mediators of extracellular communication during cancer progression. *J. Cell Sci.* **123,** 1603–11 (2010).

49. Al-Nedawi, K. *et al.* Intercellular transfer of the oncogenic receptor EGFRvIII by microvesicles derived from tumour cells. *Nat. Cell Biol.* **10,** 619–624 (2008).

50. Brian Meehan *et al.* Oncosomes large and small: what are they, where they came from? *J. Extracell. Vesicles* **5,** 1–2 (2016).

51. Di Vizio, D. *et al.* Large Oncosomes in Human Prostate Cancer Tissues and in the

Circulation of Mice with Metastatic Disease. *Biomarkers Genomics, Proteomics, Gene Regul.* **181,** 1573–84 (2012).

52. Minciacchi, V. R. *et al.* Microenvironment and Immunology MYC Mediates Large Oncosome-Induced Fibroblast Reprogramming in Prostate Cancer. *Cancer Res* **77,** 2306–17 (2017).

53. Minciacchi, V. R. *et al.* Large oncosomes contain distinct protein cargo and represent a separate functional class of tumor-derived extracellular vesicles. *Oncotarget* **6,** 11327–41 (2015).

54. He, M. *et al.* Hepatocellular carcinoma-derived exosomes promote motility of immortalized hepatocyte through transfer of oncogenic proteins and RNAs. *Carcinogenesis* **36,** 1008–1018 (2015).

55. Alderton, G. K. Metastasis: Exosomes drive premetastatic niche formation. *Nat. Rev. Cancer* **12,** 447 (2012).

56. Zhang, Y. & Wang, X.-F. A niche role for cancer exosomes in metastasis. *Nat. Publ. Gr.* **17,** 709–11 (2015).

57. Yu, Z. *et al.* Pancreatic cancer-derived exosomes promote tumor metastasis and liver pre-metastatic niche formation. *Oncotarget* **8,** 63461–63483 (2017).

58. Thaler, J. *et al.* Circulating procoagulant microparticles in cancer patients. *Ann. Hematol.* **90,** 447–53 (2011).

59. Hager, M. H. *et al.* DIAPH3 governs the cellular transition to the amoeboid tumour phenotype. *EMBO Mol Med.* **4,** 743–60 (2012).

60. Headley, M. B. *et al.* Visualization of immediate immune responses to pioneer metastatic cells in the lung. *Nature* **53151,** 3–7 (2016).

61. Loof, T. G., Deicke, C. & Medina, E. The role of coagulation/fibrinolysis during Streptococcus pyogenes infection. *Front. Cell. Infect. Microbiol.* **4,** 1–8 (2014).

62. Palta, S. Overview of the coagulation system. *Indian J. Anaesth.* **58,** 515–523 (2014).

63. Vogler, E. A. & Siedlecki, C. A. Contact Activation of Blood Plasma Coagulation. *Biomaterials.* **30,** 1857–69 (2009).

64. Wu, Y. Contact pathway of coagulation and inflammation. *Thromb. J.* **17,** 1–9 (2015).

65. Tesselaar, M. E. T. *et al.* Microparticle-associated tissue factor activity: A link between cancer and thrombosis? *J. Thromb. Haemost.* **5,** 520–527 (2007).

66. Fei, X., Wang, H., Yuan, W., Wo, M. & Jiang, L. Tissue Factor Pathway Inhibitor-1 Is a Valuable Marker for the Prediction of Deep Venous Thrombosis and Tumor Metastasis in Patients with Lung Cancer. *Biomed Res. Int.* **2017,** 1–8 (2017).

67. Dongmei Diao, Yao Cheng, Yongchun Song, Hao Zhang & Zhangjian Zhou and Chengxue Dang. D-dimer is an essential accompaniment of circulating tumor cells in gastric cancer. *BMC Cancer* **17,** 1–9 (2017).

68. Im, J. H. *et al.* Coagulation Facilitates Tumor Cell Spreading in the Pulmonary Vasculature during Early Metastatic Colony Formation. *Cancer Res.* **64,** 8613–8619 (2004).

69. Obonai, T. *et al.* Tumour imaging by the detection of fibrin clots in tumour stroma using an anti-fibrin Fab fragment. *Sci. Reports - Nat.* **6,** 1–10 (2016).

70. Palumbo, J. S. *et al.* Platelets and fibrin(ogen) increase metastatic potential by impeding natural killer cell–mediated elimination of tumor cells. *Blood.* **105,** 178–85 (2005).

71. Palumbo, J. S. *et al.* Fibrinogen is an important determinant of the metastatic potential of circulating tumor cells. *Blood.* **96,** 3302–9 (2000).

72. Gay, L. J. & Felding-Habermann, B. Contribution of platelets to tumour metastasis. *Nat. Rev. Cancer.* **11,** 123–34 (2011).

73. Yasunaga, M., Manabe, S. & Matsumura, Y. New concept of cytotoxic immunoconjugate therapy targeting cancer-induced fibrin clots. *Cancer Sci.* **102,** 1396–1402 (2011).

74. J.I. Weitz. Rivaroxaban or Aspirin for Extended Treatment of Venous Thromboembolism. *N. Engl. J. Med.* **376,** 1211–22 (2017).

75. Caroline Helwick. Anticoagulation in Patients With Cancer: Understanding the Complexities of Prophylaxis and Management - The ASCO Post. *The ASCO-post* 1 (2016).

76. Rao, L. V. M. & Pendurthi, U. R. Regulation of tissue factor coagulant activity on cell surfaces. *J Thromb Haemost.* **10,** 2242–53 (2012).

77. Rush, J. S. Role of Flippases in Protein Glycosylation in the Endoplasmic Reticulum

Supplementary Issue: Cellular Anatomy of Lipid Traffic. *Lipid Insights* **88,** 45–53 (2015).

78. van der Mark, V., Elferink, R. & Paulusma, C. P4 ATPases: Flippases in Health and Disease. *Int. J. Mol. Sci.* **14,** 7897–7922 (2013).

79. Vallabhapurapu, S. D. *et al.* Variation in human cancer cell external phosphatidylserine is regulated by flippase activity and intracellular calcium. *Oncotarget* **6,** 34375–34388 (2015).

80. Clark, M. R. Flippin' lipids. *Nat. Immunol.* **12,** 373–375 (2011).

81. Lopez-Marques, R. L., Theorin, L., Palmgren, M. G. & Pomorski, T. G. P4-ATPases: lipid flippases in cell membranes. *Pflugers Arch. 2* **466,** 1227–40 (2014).

82. Wang, X. *et al.* Silencing of Human Phosphatidylethanolamine-Binding Protein 4 Sensitizes Breast Cancer Cells toTumor Necrosis Factor-A Induced Apoptosis and Cell Growth Arrest. *Clin Cancer res* **11,** 7545–53 (2005).

83. Aiello NM, Ocean AJ, Singh S, Zhang H, Thakur BK, Becker A, Hoshino A, Mark MT, Molina H, Xiang J, Zhang T, Theilen TM, García-Santos G, Williams C, Ararso Y, Huang Y, Rodrigues G, Shen TL, Labori KJ, Lothe IM, Kure EH, Hernandez J, Doussot A, Ebbesen SH1, L. D. Pancreatic cancer exosomes initiate pre-metastatic niche formation in the liver. *Nat Cell Biol.* **17,** 816–26 (2015).

84. Hou, S. *et al.* Membrane phospholipid redistribution in cancer micro-particles and implications in the recruitment of cationic protein factors. *J. Extracell. vesicles* **3,** 1–10 (2014).

85. Stafford, J. H. & Thorpe, P. E. Increased exposure of phosphatidylethanolamine on the surface of tumor vascular endothelium. *Neoplasia* **13,** 299–308 (2011).

86. Påhlman, L. I. *et al.* Antimicrobial activity of fibrinogen and fibrinogen-derived peptides – a novel link between coagulation and innate immunity. *Thromb. Haemost.* **109,** 930–939 (2013).

87. Amo, L. *et al.* Involvement of platelet-tumor cell interaction in immune evasion. Potential role of podocalyxin-like protein 1. *Front. Oncol.* **4,** 245 (2014).

88. L.Semenza, G. The hypoxic tumor microenvironment: A driving force for breast cancer progression. *Biochim. Biophys. Acta - Mol. Cell Res.* **1863,** 382–391 (2016).

# 10. Acknowledgements

First and fore most I would like to deeply thank Prof. Dr. med. Bernd Engelmann, for giving me this opportunity to work in his group as a PhD on a topic of my utmost interest along with his timely and up-to-date evaluations during the entire course of my experimental work as well for his careful and accurate correction of my written thesis. I am immensely grateful for his expert guidance for my research topic and constant motivation to help me excel in my scientific career.

Next, I would like to thank Prof. Dr. med. Daniel Teupser, the director of the Institut für Laboratoriumsmedizin Klinikum der Universität München, Ludwig-Maximilians-Universität (LMU) for allowing me to conduct my research work.

I am very thankful to all my labmates and colleagues for a wonderful time in the lab: Dr. Susanne Pfeiler for her constant, much needed supervision and advice, a special thanks to Sarah (my German-teacher) and Mano (my Indian-buddy) for all their encouragement and help in matters of lab and otherwise; Lena, Lydia and Raphael for all their hardwork and individual contribution to take the project further and Pia and Tonina especially for constant help with translation matters.

I would further like to thank Prof. Dr. med. Steffen Massberg (Medizinische Klinik und Poliklinik I, Klinikum der Universität München) and his working group especially, Dr. med. Konstantin Stark and Dr. Hellen Ishikawa-Ankerhold for their highly valuable co-operation and for providing their expertise particularly for all *in vivo* and intravital imaging experiments.

Furthermore, I would like to thank our co-operation partners at the working group of Prof. Dr. med. Hana Algül (Klinikum rechts der Isar der TU München), especially Dr. med. Sonja Wörmann for their co-operation to help me with experiments with pancreatic cancer developing mice models and cell lines. Here, I would also like to thank our collaborators Prof. Dr. med. Roland Rad (Klinikum rechts der Isar der TU München) and Sebastian Müller for providing different pancreatic cancer cell lines.

Next, I am extremely thankful to Prof. Dr. Gerhard Wanner and Manja Luckner for a very fruitful collaboration to develop techniques for scanning electron microscopic imaging of liver tissue and for some superb imaging results.

I would also like to thank Prof. Dr. med. Axel Walch and Dr. Michaela Aichler (Helmholtz Zentrum München) for their cooperation to develop *in vitro* scanning electron microscopic methods.
I would also like to extend my thanks to Dr. Bianca Habermann and Annie Yim (Max Planck Institute for Biochemistry, Martinsried) for their very insightful collaboration for bio-informatics analysis of pancreatic cancer patients' databases.

Apart from this I cannot thank enough my family in India for their love, support and above all immense patience for putting up with me throughout this journey. A very special thanks to my father for his understanding and my brother Hrishikesh for his big-brotherly support and all worldly discussions. Finally, I would like to thank my extended family here Shweta, Priyanka, Jyaysi, Tejaswini, Prajakta, Jaydeep, Abhishek and Ashwin who have been there to celebrate the ups and help me through the downs of this journey making it absolutely memorable.

## Publications related to this thesis

Pfeiler S., Thakur M., **Joshi U.**, Vrabcova P., Samara V., Müller-Stoy G., Bruns C., Megens R., Weber C., Stark K., Massberg S., Engelmann B. Cellular internalization of microvesicles: intracellular segregation and in vivo persistence of tumor microvesicles. Distinct pathogenesis of cancer-associated venous thrombosis identifies new antithrombotic targets in vivo. (*Submitted*)

Pfeiler S., Thakur M., **Joshi U.**, Vrabcova P., Megens R., Coletti R., Samara V., Müller-Stoy G., Ishikawa H., Stark K., Klingl A., Friedrich T., Arnold G., Wörmann S., Bruns C., Algül H., Weber C., Engelmann B., Massberg S. Segregation and long-term persistence of metastasis-promoting tumor microvesicles in tissue macrophages.
(*Submitted*)

Joshi U., Stark K., Colletti R., Zhu L., Vrabcova P., Pfeiler S., Bäumer M., Bruns C., Ishikawa H., Wörmann S., Algül H., Massberg S., Engelmann B. Blood coagulation-centered competition between metastatic immune camouflage and anti-metastatic defence.
(*In preparation*)

## Eidesstattliche Versicherung

Joshi Urjita

Name, Vorname

Ich erkläre hiermit an Eides statt,

dass ich die vorliegende Dissertation mit dem Thema

Role of extracellular vesicles, microvascular fibrin formation and immune surveillance in pancreatic cancer metastasis

selbständig verfasst, mich außer der angegebenen keiner weiteren Hilfsmittel bedient und alle Erkenntnisse, die aus dem Schrifttum ganz oder annähernd übernommen sind, als solche kenntlich gemacht und nach ihrer Herkunft unter Bezeichnung der Fundstelle einzeln nachgewiesen habe.

Ich erkläre des Weiteren, dass die hier vorgelegte Dissertation nicht in gleicher oder in ähnlicher Form bei einer anderen Stelle zur Erlangung eines akademischen Grades eingereicht wurde.

Muenchen, 06.07.2018

Ort, Datum

Urjita Joshi

Unterschrift Doktorandin/Doktorand